Doctoral Thesis

Electromagnetic design of light weight and high power density superconducting synchronous machines for 10 MW class wind turbine generators

(10MW級風力発電機のための 軽量・高出力密度超電導同期機の電磁設計)

平成24年12月3日提出

指導教員 大崎 博之 教授

(Supervisor: Prof. OHSAKI Hiroyuki)

寺尾　悠

（TERAO Yutaka）

Abstract

This thesis focuses on the electromagnetic design of light weight and high power density superconducting synchronous machines for 10 MW class wind turbine generators. Wind energy is well known as a clean energy source, and the installation of wind energy turbines is increasing annually worldwide. The size of wind turbines has also increased from an economical point of view. Direct-drive, low speed, and high torque systems are often adopted for multi-MW class wind turbines because higher efficiency and lower maintenance are expected. There are several proposals for generators that deliver over 10 MW of power.

However, a generator's weight and tower cost increase with its power generating capacity. It is important to develop lightweight and high power density generators for large capacity wind turbine generators.

High-temperature superconducting (HTS) technology is one of the key solutions. Superconducting wind turbine generators have the potential to realize compact and high power density generators, and have been actively studied throughout the world. In general, these generator structures are made of superconducting field coils and copper armature windings. Fully superconducting generators that have superconducting field and armature windings have the potential to be more compact, and have higher output density generators than other machines owing to air gap reduction. However, fully superconducting generators have the technically challenging issue of how to reduce AC loss at the superconducting armature windings. If multifilament MgB_2 superconducting wires are applied to the superconducting generators, it is possible to reduce the AC losses.

This research has three main purposes, namely (1) to develop the world's first fully superconducting generator that has YBCO field coils and MgB_2 armature windings, (2) to develop the electromagnetic design of three types of superconducting generator and a permanent magnet-type wind turbine generator and (3) to investigate the electromagnetic characteristics of 10 MW class direct-drive wind turbine generators by using generator size, weight, HTS wire length, generator losses, and so on. The four wind turbine generators that we focused on were investigated using finite-element method (FEM) analysis, a conventional permanent magnet generator, a salient pole superconducting generator, non-salient pole superconducting generator, and a fully superconducting generator.

In Chapter 1, we present the introduction of this study. First, the current status of global wind energy installation and large-scale wind turbine generator systems is described. Next, superconducting wind turbine generators are introduced as a solution to the issues after explaining the challenging technical issues associated with generators in the over 10 MW class.

Chapter 2 refers to design conditions for 10 MW class wind turbine generators. First, we present initial design conditions such as output power and current voltage. Next, four generator structures and their cooling system design schemes are described. Then, the design concepts for generator components are explained.

Chapter 3 describes the electromagnetic design of a permanent magnet type synchronous generator (PMSG). The PMSG characteristics were investigated with 2D finite element method analysis (FEM). The calculation results showed that there are many technical challenges to realizing 10 MW class PMSGs from the perspectives of generator efficiency, weight, and cost.

Chapter 4 shows the electromagnetic design of salient pole-type superconducting generators (S-SCG) with 2D FEM. Two types of generators with different pole numbers and outer diameters were designed and investigated. The results showed that S-SCG can reduce by over 30% of the generator diameter when compared to PMSG. Also, S-SCG was found to be suitable for the design of multiple and larger diameter structures.

Chapter 5 explains the electromagnetic design of non-salient pole-type superconducting generators (NS-SCG) with 2D FEM. Two types of NS-SCG having different diameters were designed. The generator characteristics showed that both NS-SCG structures require over 1000 km of YBCO wires because of its air-cored structure. Their generator characteristics showed that both NS-SCG structures had many technical challenges.

Chapter 6 focuses on the electromagnetic design of fully superconducting generators (FSCG), which is the original work of this study. Electromagnetic design and characteristics of the FSCG have been investigated using 2D FEM. Two types of FSCG were designed. Because of the air gap length reduction, the required length of HTS wire was reduced in spite of its air-cored structure. While the required length of the HTS wire was less than 200 km, the generator diameter was 4.0 m. FSCG is therefore considered to be a good candidate for the 10 MW class wind turbine generator system.

In Chapter 7, we compare the electromagnetic characteristics of four designed wind turbine generators in terms of generator diameter, weight, HTS wire length, generator loss, and so on. The results show that the FSCG and the S-SCG are the best candidates for 10 MW class offshore wind turbine generators from the size and cost perspective.

In Chapter 8, we conclude this paper and discussed future works of this study.

Acknowledgements

Only this part, I would like to write with Japanese to express my real appreciations for everyone around me.

「*本研究室における私の研究への挑戦はもう少し続きます。今回この場を借りて感謝の言葉を述べさせていただいた皆様の更なるご発展・ご多幸を心より願い、 また3年後の博士号取得へ向け、私自身の更なる成長を皆様に約束し、結びの言葉とさせていただきます*」

2010年3月､修士論文の最後に上の言葉を述べてから3年｡そして東京大学大学院への入学から、あっという間に5年が経ってしまいました。そして、また次の段階へ進む時が近づきつつあります。5年間を通して「超電導風力発電機」の研究を行う上で、本当に多くの方々にお世話になりました。ここで、お世話になった皆様への感謝の気持ちを述べさせていただきます。

本研究の指導教員である大崎博之教授には5年間、本当にお世話になりました。2006年に初めて研究室に見学へ訪れた際には､快く研究室を案内して下さいました｡そして大学院へ入学以来、本論文をまとめるまで､研究に関して懇切丁寧に御指導いただきました｡私が研究で行き詰まった際には何度も先生から御助言をいただき､何とか論文のまとめまで辿り着くことができました。また、数多くの国内・国際会議で発表する機会を与えていただき、多くの経験を積むことが出来ました。大崎先生の御人柄、そして何よりも大崎先生に御指導いただけるということが、私が博士課程に進むことを決心する大きなモチベーションとなったことは、揺るぎ無い事実です｡感謝の気持ちは言葉に表しきれません。

関野正樹准教授には、5年間様々な分野で数え切れないほどお世話になりました。御自身の研究分野に止まらず幅広い知識をお持ちで、実験装置の設計に関する相談や、論文及び学振書類の書き方、また博士論文の副査など数多くの面で懇切丁寧に御助言をいただき、学ばせていただきました。本郷に移られる前、柏の研究室にいらっしゃった際には、大崎先生と共に学生が過ごしやすく、本当に居心地の良い雰囲気を作ってくださっていたのだと実感しております。5年間、本当にお世話になりました。

航空宇宙工学専攻より特別研究員としていらっしゃいました稲守孝哉様は､席が隣であったこともあり､様々なお話をさせていただきました。人工衛星に関する幅広い知識に裏打ちされたお話は大変興味深く聞かせていただきました。また稲守様のように、博士号を取得されてから御自身の専門分野とは全く違う分野で新たな研究を立ち上げられていく様子を間近で見させていただけたことは、私自身の今後をイメージする上で大変勉強になりました。心より感謝致します。

現在、関野研究室に特別研究員として在籍されているキム ドンミン様には、入学前から現在に至るまで、数多くの局面で大変お世話になりました。研究室において研究に対する姿勢、研究室のネットワーク管理等を学んだだけでなく､プライベートでも食事や飲み会等をご一緒させて

いただき、充実した時間を過ごさせていただきました。5年間、研究面でも精神面でも私を支えてくださった方の一人です。心より感謝致します。

研究室の秘書である遠藤麻美様には、研究費の事務手続きや出張費など数多くの面で便宜を図っていただきました。また研究室メンバーの誕生日には、昼食時にサプライズ企画でケーキの調達等を快く引き受けて下さいました。研究の合間の楽しい時間を過ごすことが出来たこと、心より感謝致します。

博士課程の同期であるロイキ・ケバル君は、普段は非常に明るい人柄で研究室を盛り上げてくれました。しかし研究分野になると一変、ストイックなまでに自身の研究を突き詰めるその姿勢には、同期として本当に尊敬しています。また、私の書いた英語論文のチェック、研究分野のディスカッションをするなど、彼のお陰で英語力を磨くことが出来ました。更に、一緒に飲みに行ったり、食事をしたり、更にはマルセイユでの学会の際には、彼の自宅に泊めてもらうなどプライベートでも楽しい時間を共に過ごすことが出来ました。心より感謝するとともに、研究室時代のパートナーとして、またある時はライバルとして今後ともよろしく。

修士課程2年の岡島直輝君は同じ電気系工学専攻の所属として、また研究の合間にサッカーをするなど多くの時間を共に過ごしました。「実際に手を動かすことが出来る能力・行動力」や「鋭い考察力」など、彼の身につけているハイレベルな研究能力は本当に尊敬していました。また、研究室OB会の企画等では数多く手助けをしてもらい、心より感謝しています。奇しくも、修了後には同期として同じ会社に入社します。長い付き合いになりますが、これからもよろしく。

同じく、修士課程2年の岸本孝基君は研究に取り組む姿勢だけでなく、研究室のムードメーカーとして、また研究室旅行やオープンキャンパスなどの企画立案、行動力に関して特筆すべきものを感じました。どのようなこともポジティブに、楽しんで取り組もうとする彼の姿勢を尊敬しています。また、研究室OB会の企画等では岡島君と共に数多く手助けをしてもらい、心より感謝しています。そして、社会でのご活躍を祈念致します。

同じく、修士課程2年の武輪知明君は関野研究室のメンバーとして、1年のみ柏で共に過ごしましたが、彼の黙々と実験に取り組み、結果を出していく姿勢は研究者として非常に尊敬していました。本郷に関野研究室が移ってからも時々一緒に楽しく話をさせていただきました。心より感謝致します。そして、社会でのご活躍を祈念致します。

修士課程1年の大浦雄紀君は、研究室に来て早々から「即戦力」として研究、その他の仕事で大活躍してくれています。研究室に所属して数カ月で成果を出し、学会で立派に発表している姿は彼自身の能力の高さを物語っています。研究室で共に楽しく過ごすことが出来たことに感謝すると共に更なるご発展を祈念致します。

同じく修士課程1年の小川雅史君は、卒業研究から私と同じ超電導風力発電機を研究テーマとしていますが、ソフトウェアの使用法等の飲み込みの速さ、データへの考察力、まとめる能力など素晴らしい能力を持っています。研究室で共に楽しく過ごすことが出来たことに感謝すると共に更なるご発展を祈念致します。

同じく修士課程1年の松下通生君は卒論生時代から共に同じ研究室で過ごしていますが、彼の鋭い考察力、また着実に結果を積み上げていく姿勢は、研究者として尊敬していました。研究室で共に楽しく過ごすことが出来たことに感謝すると共に更なるご発展を祈念いたします。

研究室卒論生の北原康匡君、研究生の銭 可楨君には来年度以降の研究室を生活面、研究面の両面から盛り上げて行ってもらいたいと思います。研究室で共に楽しく過ごすことが出来たことに感謝すると共に更なるご発展を祈念致します。

本郷の関野研究室の皆様とは、月1回の定例ミーティングや授業で本郷へ行った際に研究室でお話しさせていただき、有意義な時間を過ごさせていただきました。心より感謝致します。

私が在籍した5年間で、数多くの大崎研究室OB・OG、研究員、秘書の皆様にお世話になりました。上田靖人様、宮副照久様、小見慶樹様、鈴木達矢様、野中壮平君、安田斉史君、クッディス・ムハマッド・ラシド君、山田正博君、池永健君、加藤拓哉君、中西泰章君、蛭川倫行君、ロシンさん、槻木孝亮君、今川昌信様、長妻優子様、岡永美子様には研究、日常生活の両面で大変お世話になりました。皆様のお陰で充実した大学院の生活を送ることが出来ました。そしてOB同士、今後ともどうぞよろしくお願い致します。

博士論文の副査をお引き受けいただいた、先端エネルギー工学専攻の小川雄一先生、電気系工学専攻の古関隆章先生、馬場旬平先生、横山明彦先生には本論文を完成させる上で数多くの貴重な御助言、御指摘をいただきました。心より感謝致します。そして電気系工学専攻及び先端エネルギー工学専攻でお世話になったすべての皆様に心より感謝致します。

学部時代にお世話になった山形大学工学部・電気電子工学科では、四年間で数多くの皆様に支えられ、また御指導いただき東京大学大学院へ進むことが出来ました。山形での1年間及び米沢での3年間があったからこそ、今の私があると感じております。大嶋重利先生、齋藤敦先生、平野悟先生、相澤慶二先生には卒業研究及び学会、OB会等、数多くの局面で大変お世話になりました。そして廣瀬文彦先生、三浦毅先生には、授業だけでなく大学院へ進学する上で数多くの御助言を頂きました。また、山形大学工学部・電気電子工学科のすべての先生方の授業により今の研究を支える基礎力を身につけることが出来ました。心より感謝致します。

新日鐵住金株式会社の手嶋英一様、森田充様、鉄道総合技術研究所の富田優様、福本祐介様、小方正文様、水野克俊様をはじめとした皆様、横浜国立大学の塚本修巳先生、京都大学の中村武恒先生、岩手大学の藤代博之先生、内藤智之先生、新潟大学の福井聡先生、岡徹雄先生、東京海洋大学の牧直樹先生、和泉充先生、東北大学（現・八戸工業大学）の濱島高太郎先生、九州大学の柁川一弘先生、大阪大学の植田浩史先生、関西大学の大橋俊介先生、鹿児島大学の平山斉様、千葉大学の柳澤吉紀様、産業技術総合研究所の山崎裕文様、株式会社日立製作所の和久田毅様、

一木洋太様、堀知新様には、共同研究のミーティングや学会でお会いした際に、本研究に関する数多くの貴重な御意見や御助言をいただきました。心より感謝致します。

オリエンタルモーター株式会社の皆様には、修士課程1年時から博士課程2年時まで約4年間、アルバイトとしてお世話になりました。大学院で解析中心の研究テーマであった私が、実際の回転機を用いて貴社で実験をさせていただけた経験は私の財産です。また、学生の身分であった私が、大学院で培った能力を将来的に仕事としてどのように用いるのか、企業とはどのような場所かを、エンジニアとして活躍されている方々をはじめとした御社の皆様との交流を通じて知ることが出来、本当に勉強になりました。この先、私がエンジニアとして働く上で皆様にお世話になった時間と経験は決して忘れません。

日本学術振興会及び東京大学グローバルCOEオフィスの皆様には、私が博士課程で過ごす3年間を資金面から支えていただきました。皆様から頂いた研究資金、生活費により、この3年間で数多くの貴重な経験を積むことが出来、心より感謝致します。

そして、修士課程時代に進学するか就職するか最後まで迷っていた私に「日本の技術者として、世界に通じる実力を東大で磨きなさい」と背中を押し、精神面で常に励まし、支え続けてくれた両親・祖母に深く感謝致します。

更に、私がこれから一生をかけて追い続ける目標であり、最も尊敬する技術者である、祖父の故・寺尾弘に心より感謝致します。小中学校時代の夏休みに、祖父と共に作った数々の「自由工作」の経験が、私が理系の世界へ進む大きなきっかけの一つでした。

最後になりましたが、今後の大崎研究室、関野研究室の皆様をはじめとして、私がお世話になったすべての皆様の更なる御多幸・御発展を心より祈念致します。また私自身が技術者として成長し、技術立国日本の発展に貢献することを皆様に約束し、結びの言葉とさせていただきます。

5年間、本当にありがとうございました。

2012年12月3日

寺尾悠

Contents

List of Figures

Chapter 1

Chapter 2

Chapter 3

Chapter 4

Chapter 5

Chapter 6

Chapter 7

List of Tables

Chapter 1

Chapter 2

Chapter 3

Chapter 4

Chapter 5

Chapter 6

Chapter 7

Chapter 1

Introduction

1-1. Wind Energy

1-1-1. Global Installation Status

Wind generation is known to be one of the clean energy sources in use. The Global Wind Energy Council (GWEC) reports that the installation of wind energy facilities has increased annually worldwide, as shown in Fig. 1-1. The global wind power market somewhat recovered during 2011 because of improved economic climates in a number of national markets. The market grew by approximately 6% compared to 2010, and the 40.5 GW of new wind power brought on line 2011 represents investments of more than 68 billion dollars [1].

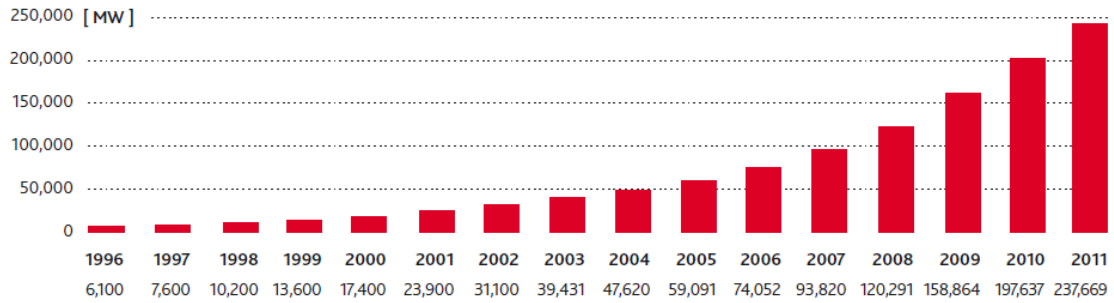

Fig.1-1. Annual world total installation of wind turbines [1].

1-1-2. Increase of Output Capacity

Fig. 1-2 shows the dependence of output on wind turbine size [2]. The unit capacity of a windmill has increased, and the installation of fewer large-scale wind turbines is advantageous from an economic point of view as it leads to reduction in the use of power transmission cables and a more effective use of installation sites. Tsukamoto's group showed that a 10 MW class wind turbine can generate higher output than that of five 2 MW class wind turbines [3]. Also, the ability to implement large wind turbines is one of the major factors behind the decision to install wind turbines offshore as well as onshore.

Fig. 1-3 shows the wind speed distribution at different heights above ground [4]. The wind speed exponentially increases above 50 m because there are usually no obstructions to wind at those heights. In addition, the theoretical output of a wind turbine is found as that shown below.

$$P = \frac{1}{8} C_P \rho \pi D^2 v^3 \qquad (1.1)$$

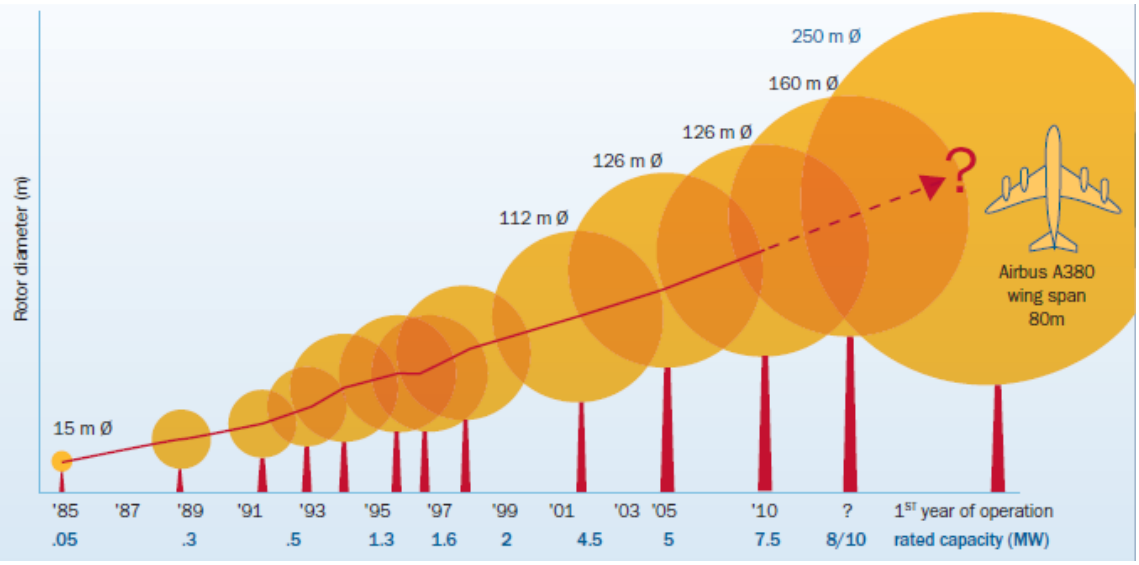

Fig.1-2 Dependence of the output of wind turbine size [2].

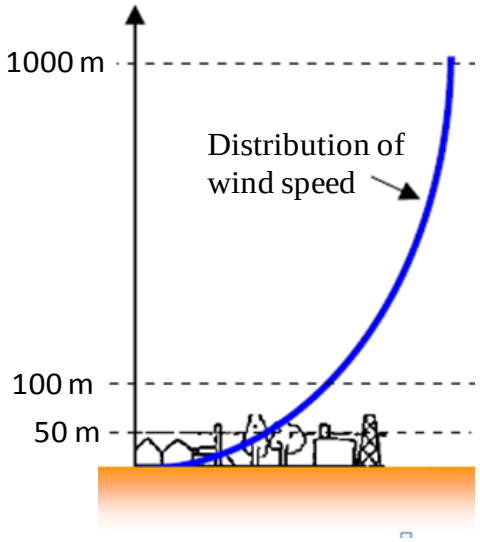

Fig.1-3. Example of wind speed distribution [4].

where C_p (≈ 40–50%), ρ [kg/m^3], D [m], and v [m/s] are the coefficients of the output, air density, rotor diameter, and wind speed, respectively. This equation shows that the output power of a wind turbine is proportional to the square of the rotor diameter and the third power of the wind speed. When installing wind turbines, it is better to place them on “high and windy” places. To date, the targeted output of large-scale wind turbines is 8–10 MW. However, a European project named “UpWind (2006–2011)” is investigating the possibility of realizing 20 MW class wind turbine generators [2].

Tsukamoto's group compared the advantages of 10 MW class wind turbine installation over those of 2.5 MW class generators at the same location [5]. They chose two types of Japanese onshore sites (Fig.1-4). The first one had strong prevailing winds, whereas the other had no prevailing winds. Wind turbines with diameter D [m] were placed at distances of 3D and 10D. Table 1-1 shows the estimated results of the total output of both types of wind turbine. The results show that if both generators are placed at locations with prevailing wind, they can generate higher energy than the location without prevailing winds. Also, some 10 MW class wind turbine generators can generate higher energy than what is realized using several 2.5 MW class wind turbines. If the tower height is also considered, the total output energy of some 10 MW class wind turbines will increase. This report shows that many 10 MW class wind turbines should be installed at sites with prevailing wind.

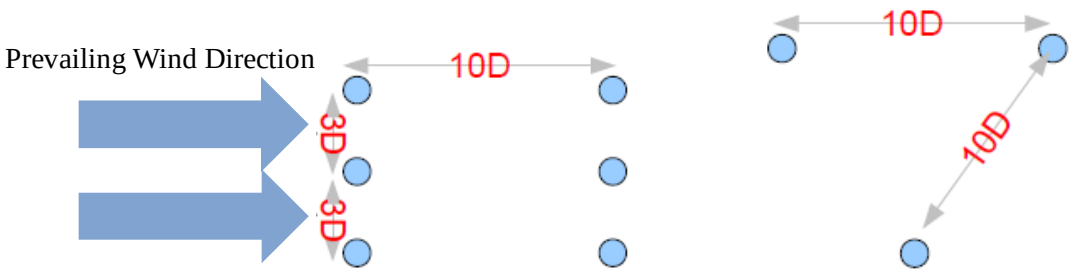

(a) (b)

Fig.1-4.Wind turbine arrangements for two types of sites. (a) site with strong prevailing winds. (b) site without prevailing winds.

Table 1-1 Estimation results after the installation of some 10 MW or 2.5 MW class wind turbines at two types of sites.

Installation Site	Number of Wind Turbines	Total Output (); consideration with turbine height
Prevailing Wind		
A: 7.02 × 3.6 km^2	10 MW × 42	420 MW (567 MW)
	2.5 MW × 135	337.3 MW
B: 7.02 × 7.02 km^2	10 MW × 70	700 MW (945 MW)
	2.5 MW × 243	607.5 MW
No Prevailing Wind		
C: 7.02 × 7.02 km^2	10 MW × 4	40 MW (54 MW)
	2.5 MW × 9	22.5 MW

1-1-3. Wind Power Systems

1-1-3-1. Induction Generator Systems

In Fig. 1-5, there are three types of wind turbine generator systems with induction generators. The squirrel-cage induction generator (SCIG) has some merits from the perspective of cost and simplicity of the structure (Fig. 1-5(a)). However, it is difficult for SCIG to generate electrical energy in the region of low wind speed. Thus, SCIG systems are not applied to large-scale wind generation systems such as those that are 5 MW class. A “wound-rotor induction generator (Wound rotor-type induction generator; WRIG)” is an induction generator with a wound rotor (Fig. 1-5(b)). Its rotation speed is controlled by changing the frequency of the induced current in the rotor winding using the power converter. It enables efficient operations better than SCIG. In recent years, the doubly fed induction generator (DFIG) shown in Fig. 1-5(c) has enabled variable speed operation by the installation of a power converter (rotor side) on the secondary side, and its use has rapidly expanded in the market. In the present market, Repower and Sinovel are the major companies that have adopted the over 5 MW class induction generator wind power system (Table 1-2). All of the generator systems are developed with DFIG.

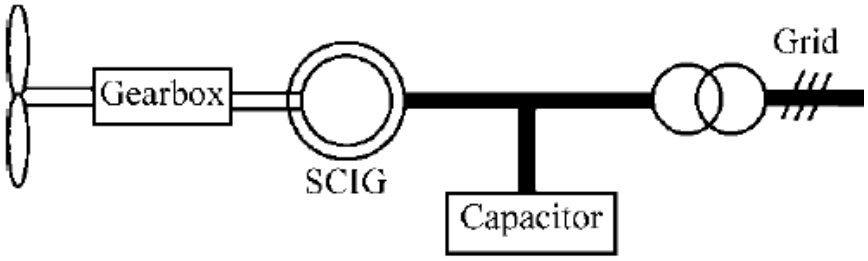

(a) Squirrel-cage induction generator system (SCIG)

(b)

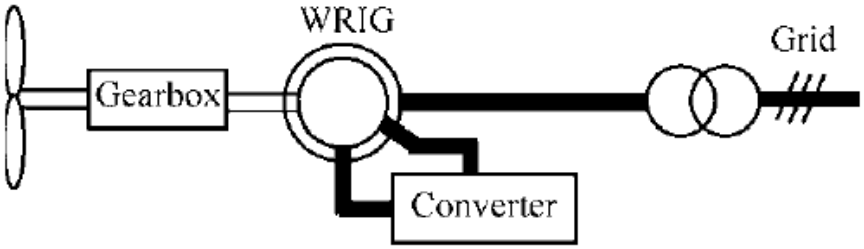

(c) Wound rotor induction generator system (WRIG)

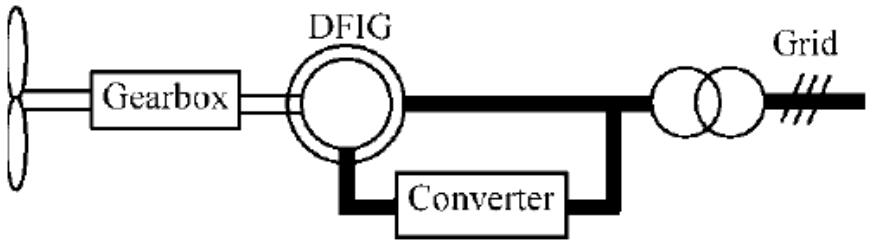

(c) Doubly fed induction generator system (DFIG)

Fig.1-5. Wind turbine generator systems with induction generators [6]

Table 1-2. Over 5 MW class induction generator systems [7]

Manufacturer	Model	Capacity (MW)	Type	Status
Sinovel	SL5000	5.0	DFIG	Prototype installed in 2010
Sinovel	SL6000	6.0	DFIG	Prototype installed in 2011
Repower	5M	5.0	DFIG	Commercially available
Repower	6M	6.15	DFIG	Commercially available

1-1-3-2. Synchronous Generator Systems

Synchronous generators having a DC field rotor induce an AC voltage based on the frequency. The frequency is proportional to the rotational speed of the rotor blade on the armature windings. After generating the output power, its frequency is translated to a system frequency (50 or 60 Hz). As a result, synchronous generator systems have the advantage of being easily acceptable by the power system. The synchronous generators currently used are "synchronous generator wire-wound (electrically excited synchronous generator (EESG))" and "Permanent magnet synchronous generator (PMSG)" shown in Fig. 1-6. The PMSG has the advantage of reducing copper loss on the rotor side. Two types of operation systems currently employ EESG or PMSG. One is the direct-drive system, which is directly connected to the generator and rotor blades. The other is driven with a single-stage gear box between the rotor blades and generators. The direct-drive systems are expected to have high efficiency, low noise, and high reliability by omitting the gearbox. In other words, maintenance for direct-drive systems is easier than that for geared systems. However, the rotational speed tends to be very low (of the order of several tens of rpm), which often results in multipole and high-torque structures. Table 1-3 shows over 5 MW class synchronous generator systems. The synchronous generator system having the highest output capacity is E-126, which was developed by Enercon [8]. Its output capacity is 7.5 MW and the diameter is 12 m. Many companies have been developing synchronous generator systems with PMSG in order to realize higher system efficiency.

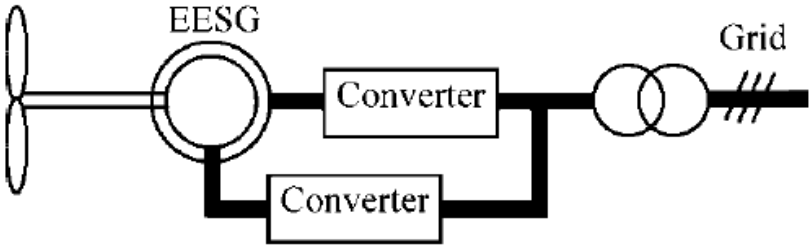

(a) Electrically excited synchronous generator system (EESG)

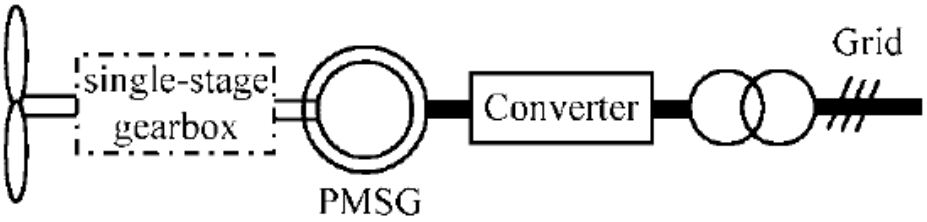

(b) Permanent magnet geared synchronous generator system (Geared PMSG)

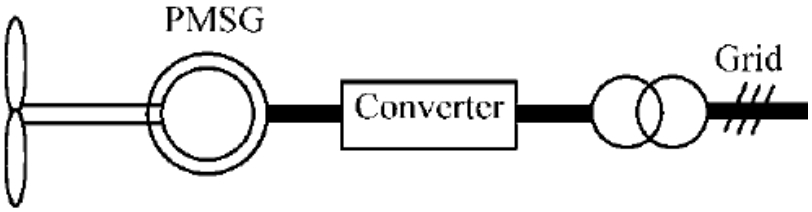

(c) Permanent magnet synchronous generator system(DD-PMSG)
Fig.1-6. Wind turbine generator systems with synchronous generators [6]

Table 1-3. Over 5 MW class synchronous generator systems [7]

Manufacturer	Model	Capacity (MW)	Type	Status
Enercon	E-126-7.5	7.5	EESG	Commercially available
Vestas	V-164-7.0	7.0	PMSG	Prototype expected for 2014
Siemens	SWT-6.0-120	6.0	PMSG	Prototype installed in 2011
Alstom Wind	-	6.0	PMSG	Prototype expected for 2012

1-1-4. Challenging Issues Affecting the Development of Over 8 MW Class Wind Turbine Generator

The installation of 5 MW class systems currently costs approximately 62 billion US dollars (1234 USD/kW) [9]. Fig. 1-7 shows the components of Repower's 5 MW class wind turbine systems with an induction generator, and Table 1-4 shows the cost ratio of the systems. The most expensive component is the tower, which incurs 26.3% of the total cost. The cost of tower enhancements increases with the generator size and weight. Also, there are structural and technical limitations for the tower to support nacelle weight. The technical limitation is currently being worked upon, and one of the challenging issues being faced with over 8 MW wind turbine generators is in determining how to develop generators that have high output and are lightweight at the same time.

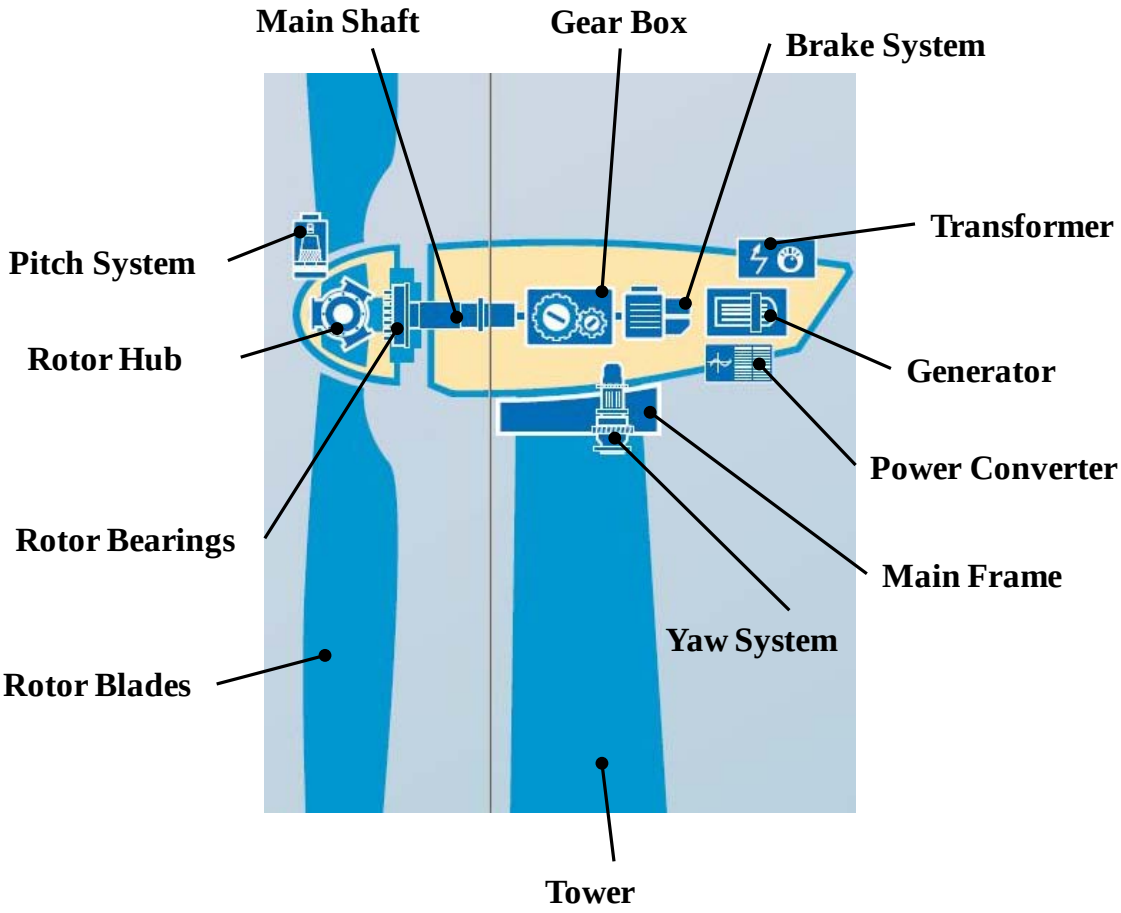

Fig.1-7. Components of 5 MW wind turbine developed by Repower [9]

Table 1-4. The ratios of the 5 MW wind turbine developed by Repower [9]

Components	Ratio (%)
Tower	26.3
Rotor Blades	22.2
Gearbox	12.91
Power Converter	5.01
Transformer	3.59
Generator	3.44
Main Flame	2.8
Pitch System	2.66
Main Shaft	1.91
Rotor Hub	1.37
Nacelle Housing	1.35
Brake System	1.32
Yaw System	1.25
Rotor Bearings	1.22
Cables	0.96

1-2. Superconducting Wind Turbine Generators

High-temperature superconducting (HTS) technology is considered to be a key solution that can mitigate this problem. There are ongoing studies worldwide into the development of wind turbine generators using superconducting magnets, and some merits of superconducting wind turbine generators are as follows:

- It has a more compact and lighter structure than conventional machines
- A generator with higher efficiency is available because there are no joule losses in the superconducting coil.

In general, superconducting wind turbine generators have three structures, namely nonsalient pole-type superconducting generator (NS-SCG), salient pole-type superconducting generator (S-SCG) and fully superconducting generators (FSCG). Usually, the S-SCG and NS-SCG have superconducting field coils and copper armature windings. On the other hand, the FSCG has a superconducting field and armature windings. All of the structures have been applied to direct-drive synchronous generator systems from the perspective of low maintenance cost and higher efficiency. So far, these structures have been globally studied, and the output has been set at 10 MW. The current status of the research and development of the superconducting wind turbine generator is introduced in the next section.

1-2-1. Current Status of Research and Development

1-2-1-1. Non-salient pole type Superconducting Generator (NS-SCG)

Fig. 1-8 shows the scheme of the NS-SCG. This structure as well as superconducting field coils and copper armature windings have been studied in many countries. The structure is often designed as an air-cored structure. In 2010, a research group at the Technical University of Denmark (DTU) published the first paper with a 10 MW class superconducting generator [10]. They used Bi-type HTS wires for the field coils and copper armature windings. While the outer diameter is 4.7 m, the weight is 88 tons. AMSC has also developed a generator with parameters of almost 5.0 m and 188 tons, respectively [11]. On the other hand, Enercon has developed a 7.5 MW class conventional synchronous generator with diameter and weight of 12 m and 220 tons, respectively [12]. These comparisons show that the NS-SCG structure has a significantly smaller generator size and weight even though it has a higher output power than conventional machines. However, this generator requires a large number of HTS wires (length of approximately 1450 km) because of its air-cored structure and larger air gap of 110 mm, as shown in Table 1-5. An air-cored structure implies that large flux leakage occurs in field coils. In order to increase the effective flux to the armature windings, the magnetic motive force should be increased. In other words, long of HTS wire is required. In addition, the larger air gap also results in the increase in the number of HTS field coils. When NS-SCG is designed, the mechanical air gap between HTS field coils and copper armature windings should be considered for the thermal insulation layer and cryostat wall. When compared to conventional generators, the air gap tends to be large, thereby resulting in a large quantity of field coils. The research group of Niigata University and Changwon National University set the air gap to be 80 mm and 70 mm, respectively [13, 14]. They reduced the YBCO wire length to less than 600 km. However, even with this length, the cost of developing and operating the generator remains high.

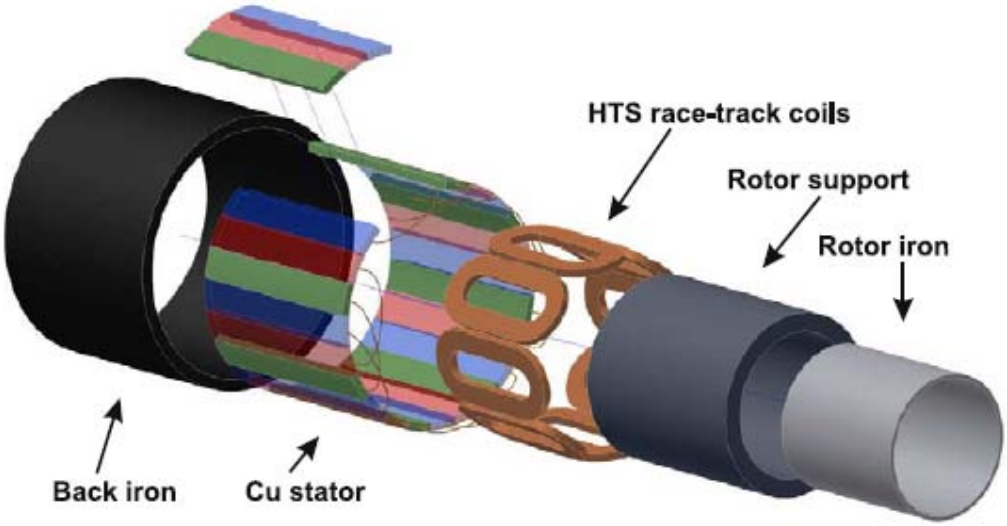

Fig.1-8 Scheme of the NS-SCG [10]

Table 1-5. Specifications of NS-SCG [10, 11, 13, 14]

Groups	DTU	AMSC	Niigata Univ.	Changwon National Univ.
HTS Wires	BSCCO	YBCO	YBCO	YBCO/BSCCO
Operating Temperature [K]	20	30	20	20
Output Power [MW]	10	10	10	10
Poles	16	24	8/12	24
Rated Speed [rpm]	10	-	10	10
Outer Diameter [m]	4.7	4.5–5.0	3.67	5.3/6.7
Length [m]	1.15	-	1.5	0.5/0.2
Gap between field and armature conductors [mm]	110	-	80	70
Max. Magnetic Field [T]	9.1	-	9.59/10.4	8.23/5.46
Length of HTS wires [km]	1450	-	574/770	586/222
Weight [tons]	88	180	60.6/63.7	147/196

1-2-1-2. Salient pole type superconducting generator (S-SCG)

A group at the Tokyo University of Marine Science and Technology has been investigating wind turbine generators with S-SCG [15, 16]. Fig. 1-9 shows the cross section of S-SCG. This structure can effectively use magnetic flux because of a lot of iron presence, and because the air gap length is reduced to approximately 15 mm. This, in turn, results in a reduction of HTS wire length. The YBCO wire length is less than 50 km, as shown in Table 1-6. This result is a significantly lower value than that of NS-SCG. In addition to the reduction of YBCO wire length, S-SCG can operate with higher temperatures such as 30 K or 65 K because the maximum magnetic field generated by field coils is as low as 1.9 T. The cooling power for HTS wind turbine generators can therefore be reduced. Table 1-7 shows the analysis results of generator losses. These results indicate that the iron and copper losses and mechanical losses are the same; however, the cooling system losses are inversely proportional to the increase of operating temperature. In other words, the cooling systems for lower temperatures require higher input power, and affects almost 1% of the generator efficiency. From the perspective of generator size, this structure tends to be larger than that of NS-SCG because of its multipole structure. For the machine using YBCO at 77 K, the diameter becomes 12 m, which is the same as that of E-126, which is manufactured by Enercon. There are also other machines with diameter of 8 m, which is almost one and a half or two times as large as the diameter of NS-SCG. For S-SCG, there is, therefore, a tradeoff between generator cost and size.

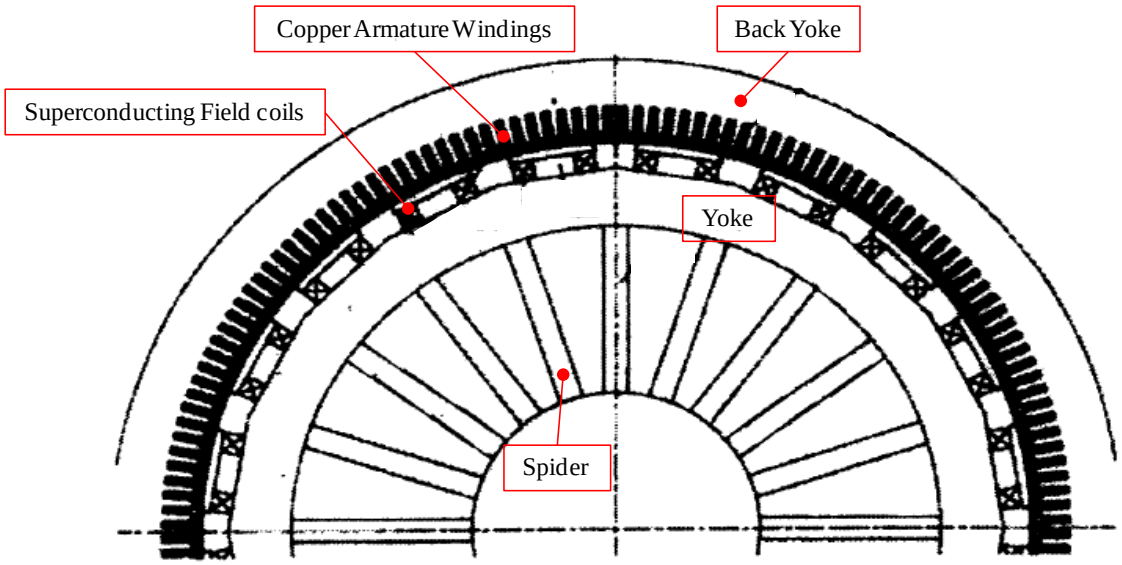

Fig. 1-9 Cross section of S-SCG [15]

Table 1-6 Electrical design results of S-SCG with BSCCO and YBCO [15, 16]

HTS Wires	BSCCO	YBCO	YBCO	YBCO
Operating Temperature [K]	30	65	77	77
Output Power [MW]	10	10	10	10
Poles	60	60	64	96
Rated Speed [rpm]	10	10	10	10
Outer Diameter [m]	8.0	8.0	8.0	12.0
Length [m]	1.19	1.19	1.15	0.5
Max. Magnetic Field [T]	1.9	1.9	1.9	1.9
Length of HTS Wires [km]	22	45	134	109
Weight [tons]	149	151	134	103

Table 1-7 Losses of S-SCG with BSCCO and YBCO [15, 16]

Generator Load	BSCCO	YBCO	YBCO	YBCO
Poles	60	60	64	96
Iron Loss [kW]	31	31	34	34
Copper Loss [kW]	307	307	300	289
Stray Loss [kW]	13	13	13	19
Mechanical Loss [kW]	19	19	19	20
Cooling Power [kW]	89	36	29	29
Efficiency [%]	95.6	96.1	96.2	96.2

1-2-1-3. Other Structures

General Electric (GE) has been involved in the development of superconducting wind turbine generators with low temperature superconducting (LTS) wires (Fig. 1-10) [17]. They have applied MRI coil fabrication techniques into wind turbine generators. The remarkable point of this structure is (1) the use of LTS wires and (2) the outer rotor structure. As mentioned in the previous section, all of the superconducting wind turbine generators are designed with HTS wires, such as YBCO and BSCCO. The use of LTS wires such as Cu-(NbTi) has some advantages from the perspective of reduced cost and the technical know-how of existing technologies. Second, the presence of the outer rotor structure means that LTS field coils are fixed, whereas the armature winding sides are rotating. This structure is derived from MRI magnets, which are operated at 4.2 K. In general, the outer rotor type structure has many challenging issues such as its armature slip ring design, cooling system design for 4.2 K, and so on. Table 1-8 shows some generator specifications. The diameter and armature core length are 4.83 m and 1.88 m, respectively, which means that the 10 MW generator is a more compact structure than S-SCG. Also, the generator's weight is 145 tons. The generator performance has also been investigated at full and partial load. Table 1-9 shows the losses of this generator. According to this data, slip ring losses and cooling system power account for less than 1% of the rated power, and the total efficiency is around 95%. However, this report shows only estimations, but the structure of the cooling system is not clear. The progress of this generator design is as expected.

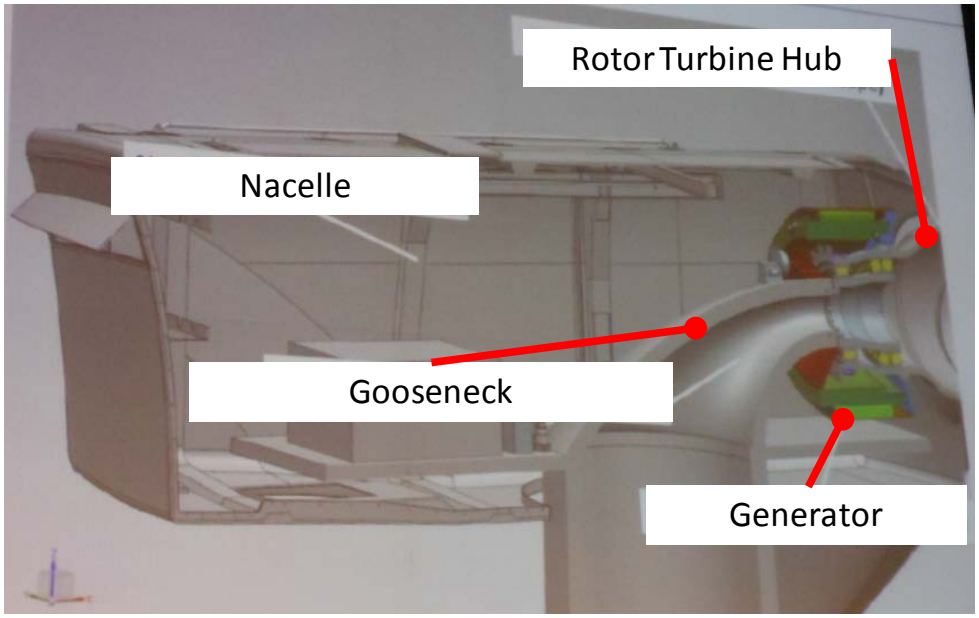

(a)

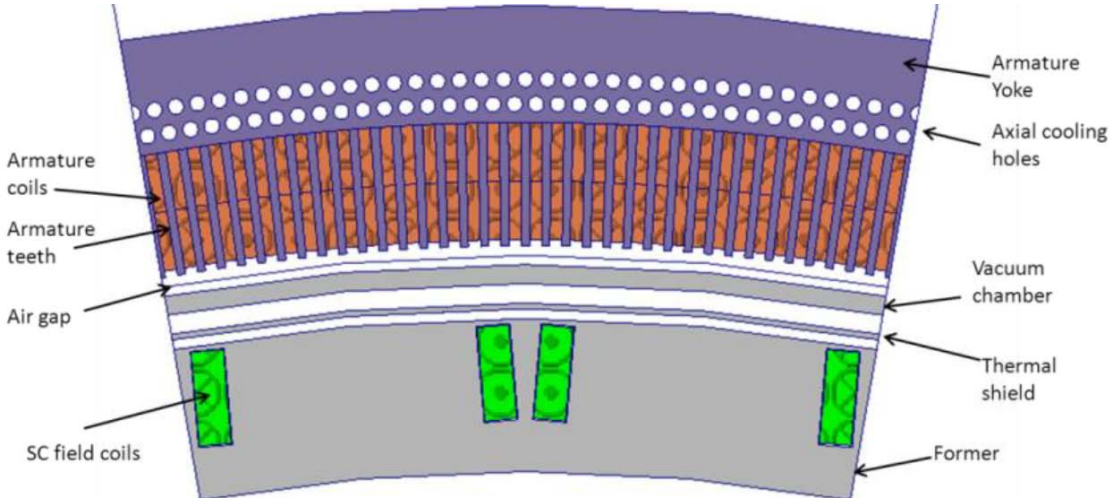

(b)

Fig.1-10. Scheme of superconducting wind turbine generator with LTS wires. (a) the arrangement of generator in nacelle and (b) the cross section of the generator.

Table 1-8 Specifications of GE's generator [17]

Parameter	Value
LTS Wires	Cu-(NbTi)
Operating Temperature [K]	4.3
Rated Power [MW]	10
Rated Speed [MW]	10
Poles	36
Rated Line-Line Voltage [V]	3300
Rated Current [A]	1750
Armature Core Outer Diameter [m]	4.83
Armature Core Length [m]	1.88
Gap between field and armature conductors [mm]	90
Max. Magnetic Field [T]	7.35
Length of LTS Wires [km]	720
Weight [tons]	145

Table 1-9 Breakdown of generator losses [17, modified]

Generator Load	100% - 10MW	50% - 5 MW	25% - 2.5MW
Turbine Speed [rpm]	10	7.9	6.3
Armature winding DC Loss [kW]	363	144	57
Armature AC Loss [kW]	56	35	22
Armature Yoke Loss [kW]	5.7	4.5	3.6
Armature Teeth Loss [kW]	5.6	4.5	3.5
Armature Core Clamp loss [kW]	2.1	1.3	0.8
Field AC Loss [kW]	2.6	2.1	1.6
Armature Slip Ring Loss [kW]	4.6	2.9	1.8
Friction and Windage	Negligible	Negligible	Negligible
Cryocooler Power (3) [kW]	22.5	22.5	22.5
Cooling Air Blowers [kW]	(6) 39	(4) 26	(2) 13
Total Loss [kW]	501	243	126
Efficiency [%]	95.2	95.4	95.2

1-2-2. Challenges for the Future

As shown in the previous sections, NS-SCG and S-SCG are well-known structures used in superconducting wind turbine generators. On the other hand, the FSCG structure, which has a superconducting field and armature windings, is a potential candidate for wind turbines. This air gap of this structure can be reduced, and there is some potential to design a compact generator requiring fewer HTS wires because the superconducting field and armature windings are put into the same cryostat. However, this structure has important challenging issues, such as AC loss, which is proportional to the frequency and the strength of the magnetic field. In general, superconductors have hysteresis characteristics like magnetic materials. If HTS wires are applied into armature windings, its AC loss can be quite high. One of the effective ways used to reduce AC loss is the use of HTS wires with a multifilament structure. MgB_2 is a good candidate for HTS wire that satisfies this requirement. For example, in 2010, MgB_2 wire with 10^5 A/cm^2 at 20 K and 3 T were introduced by NIMS [18]. This wire has 19 filaments and the diameter is almost 1.3 mm. Also, the total cost of MgB_2 wire is somewhat cheaper than that of YBCO and BSCCO. In addition, the direct-drive type synchronous generator system is operated with low frequency. If we use MgB_2 wire for armature windings of FSCG, it will be possible to realize direct-drive synchronous generator systems, which are compact, lightweight, and less costly.

1-3. Aim of This Study

There are many challenging issues involved in the development of large-scale wind turbine generators with superconductors. The aim of this study is summarized as follows:

- We propose the world's first fully superconducting wind turbine generator structure using YBCO field coils and MgB_2 armature windings
- We developed an electromagnetic design of three types of superconducting and permanent magnet-type wind turbine generators.
- We investigated the electromagnetic characteristics of 10 MW class direct-drive wind turbine generators in terms of generator size, weight, HTS wire length, generator loss, and so on.

1-4. Thesis Outline

Fig. 1-11 shows an overview of this thesis. This thesis comprises eight chapters.

Chapter 1 introduces this study. First, the current status of global wind energy installation and large-scale wind turbine generator systems are described. After explaining challenging technical issues regarding the over 10 MW class wind turbine generators, superconducting wind turbine generators are introduced as a solution.

Chapter 2 discusses design conditions for 10 MW class wind turbine generators. Four generator structures and their component design conditions are described in this chapter. To evaluate these generators in uniform conditions, design parameters are defined.

Chapter 3 presents the electromagnetic design of permanent magnet-type synchronous generators (PMSGs). Electromagnetic design with 2D finite element method analysis (FEM) is performed and the generator characteristics are investigated.

Chapter 4 shows the electromagnetic design of salient pole-type superconducting generators (S-SCG). Electromagnetic design with 2D FEM is performed, and the generator characteristics are investigated.

Chapter 5 shows the electromagnetic design of non-salient pole type superconducting generators (NS-SCG). The electromagnetic design is performed using 2D FEM analysis, and the generator characteristics have been investigated.

Chapter 6 shows the electromagnetic design of FSCG. An electromagnetic design was developed with 2D FEM analysis, and the generator characteristics are investigated.

Chapter 7 compares the electromagnetic characteristics of four designed wind turbine generators in terms of generator diameter, weight, HTS wire length, generator loss, and so on.

Chapter 8 concludes the paper and presents future works to be done.

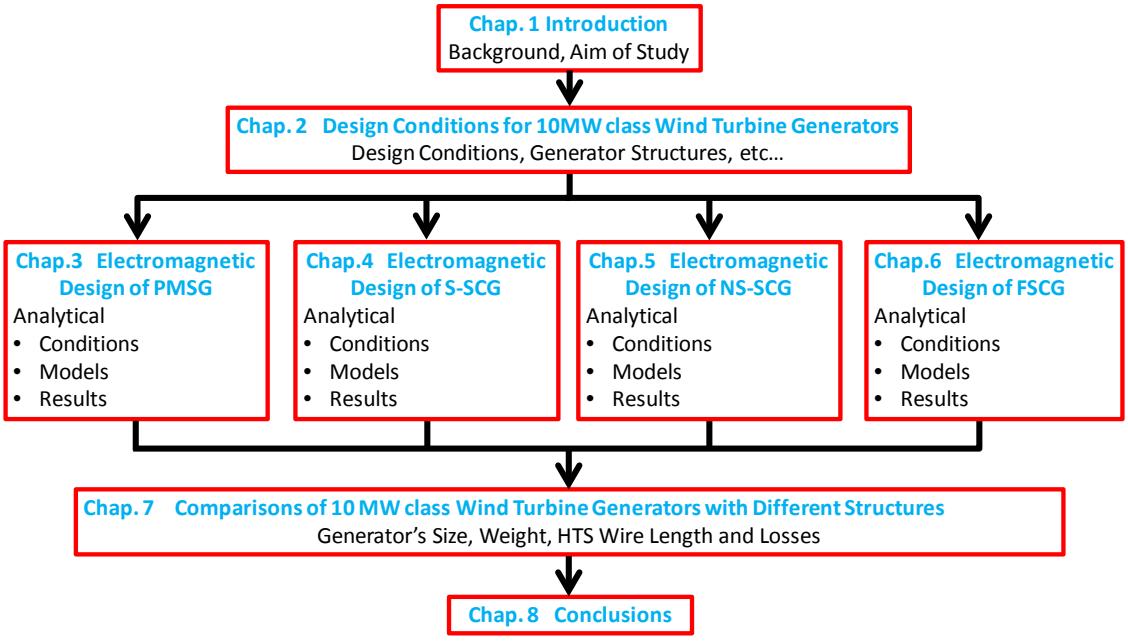

Fig.1-11. Overview of this thesis

Chapter 2

Design Conditions for 10 MW class Wind Turbine Generators

2-1. Basic Characteristics of 10 MW class Wind Turbine Generators

Table 2-1 shows the initial design conditions of 10 MW class wind turbine generators. Four generators: a permanent magnet-type synchronous generator (PMSG), a salient pole-type superconducting generator (S-SCG), a non-salient pole-type superconducting generator (NS-SCG), and a fully superconducting generator (FSCG) have been designed under the initial conditions. PMSG is particularly designed for comparison with superconducting and conventional machine characteristics. These generators are three-phase direct-drive synchronous machines, and result in low-speed and high-torque operation systems (Fig. 2-1). The rotation speed is 10 rpm because of the actual mechanical size of 10 MW class turbine blades. The rated line-to-line voltage and line current are set as 3.3 kV_{rms} and 1.75 kA_{rms}, respectively.

Table 2-1. Initial design conditions of 10 MW class wind turbine generators

Output power	10 MW
Rated voltage	3.3 kV_{rms} as line-to-line voltage
Rated current	1.75 kA_{rms} as line current
Rated revolutions	10 rpm

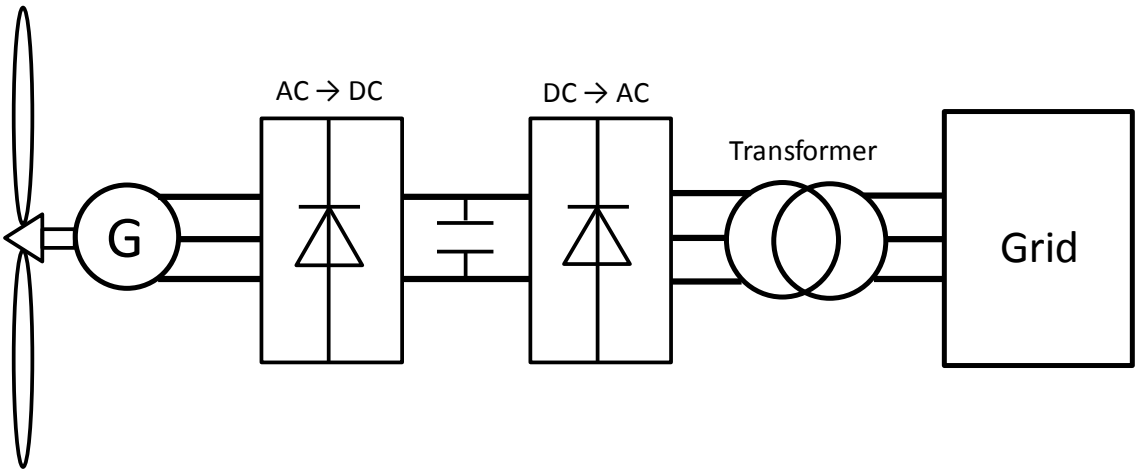

Fig. 2-1. Direct-drive wind turbine system. “G” is the synchronous generator which is directly connected with the rotor blades.

2-2. Fundamental Structures for 10 MW class Wind Turbine Generators

2-2-1. Permanent Magnet Type Synchronous Generators (PMSG)

6 MW class PMSGs have been developed by several research groups of companies and universities worldwide [19]. Fig. 2-2 shows a conceptual illustration of a PMSG having a rotor with permanent magnets. On the other hand, copper distributed armature windings are applied to the stator side. Back and rotor iron are used for magnetic shielding and to ensure the effective use of the magnetic flux. Because of the large quantity of iron, the multipole structure is suitable for this generator. The permanent magnet rotor enables copper-loss reduction, and is expected to have efficiency higher than a machine rotor made of copper windings.

However, the PMSG structure requires a large amount of iron and permanent magnets. It can be still a heavyweight and high-cost machine. In particular, the market price of rare earth materials for PM is not currently stable. Also, the generator size will be over 10 m. Therefore, the development of 10 MW class conventional synchronous generators with high output density is considered to be challenging.

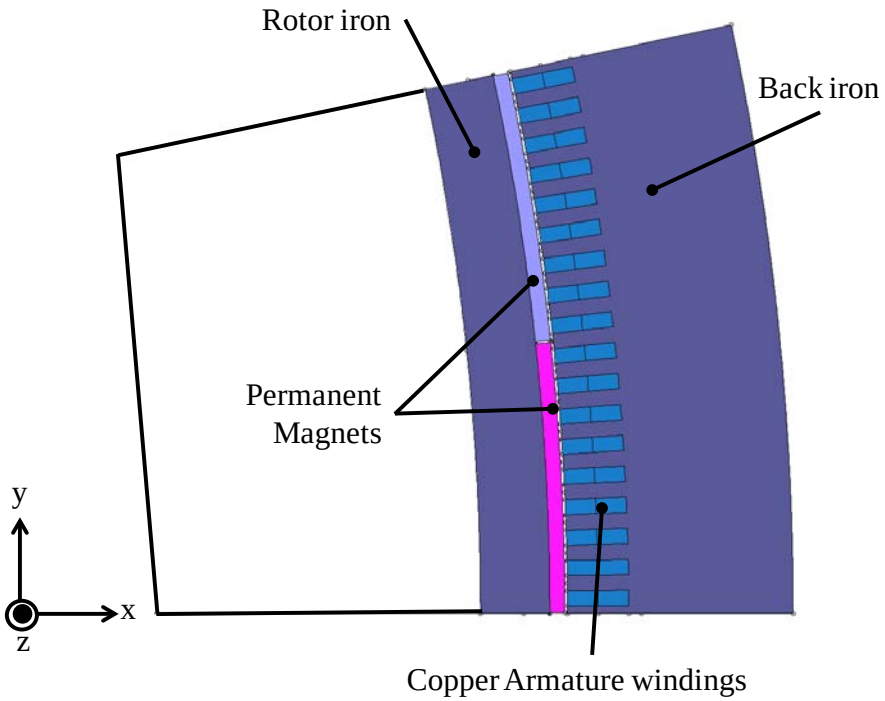

Fig. 2-2. Cross section of a PMSG

2-2-2. Salient Pole Type Superconducting Generators (S-SCG)

The cross section of an S-SCG is shown in Fig. 2-3. The field coil is designed with high-temperature superconducting (HTS) wires, but the armature windings are made of copper and have a distributed structure. The S-SCG structure requires a large quantity of iron to enable the effective use of the magnetic flux, as is the case with PMSG; a multipole structure is therefore suitable for S-SCG. Also, this structure can reduce the air gap between the rotor and stator. In other words, it is possible to use less HTS wire, which will result in reduction in the generator cost. In addition, it is possible to realize a smaller current density, which will lead to it operating at a temperature higher than that of other superconducting generator structures. The cooling system for the superconducting field coils is assumed to be the conduction cooling system shown in Fig. 2-4. The red rectangles indicate the cryostat walls for superconducting field coils.

However, the size of the S-SCG tends to be larger because of its multipole structure. In addition, the generator's weight will increase owing to the greater use of iron. There is, therefore, a tradeoff between the generator size and cost.

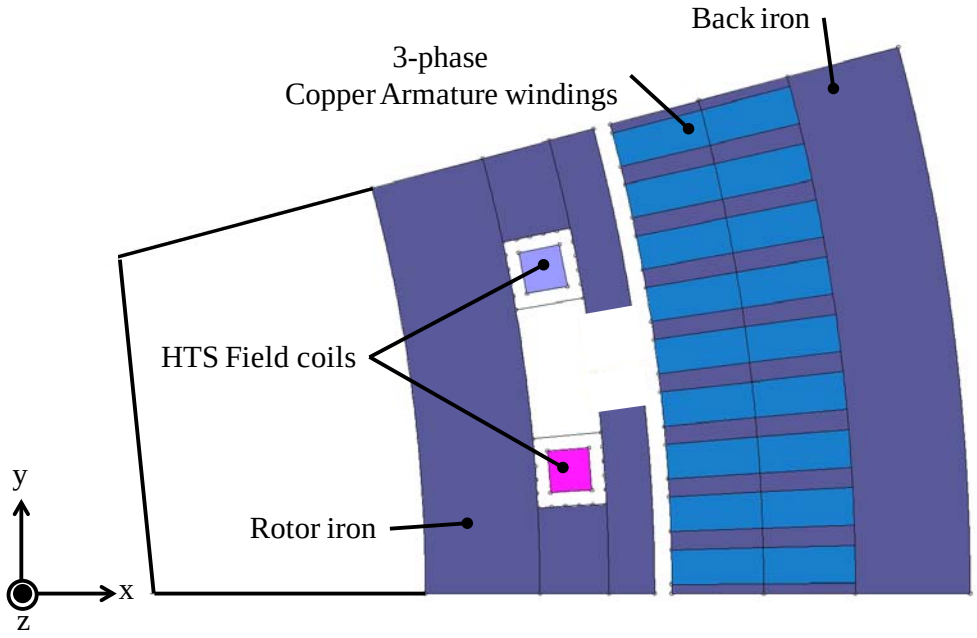

Fig. 2-3. Cross section of an S-SCG

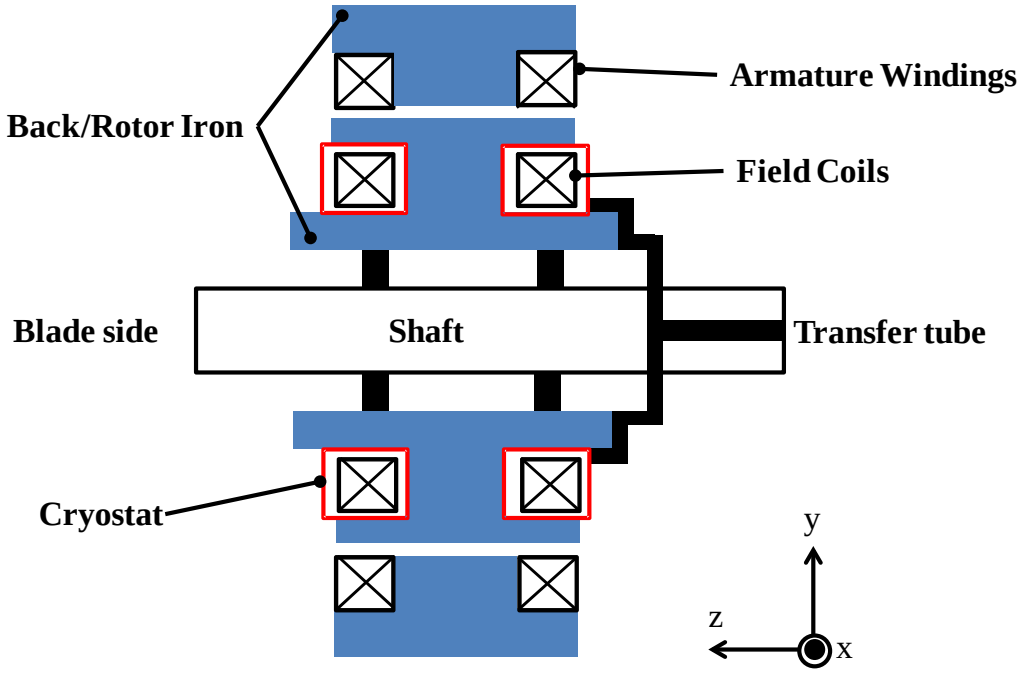

Fig. 2-4. Cooling system of the S-SCG structure. The red rectangles represent the cryostat walls of the superconducting field coils.

2-2-3. Non-salient Pole Type Superconducting Generators (NS-SCG)

Fig. 2-5 shows a nonsalient pole-type superconducting wind turbine generator (NS-SCG). This generator also has HTS field coils and copper distributed armature windings, as with the PMSG and S-SCG structures. To effectively use the magnetic flux generated by the HTS field coils, iron is inserted in the machine rotor side (Rotor iron). The stator of the NS-SCG is an air-cored structure, and it is lighter than that of S-SCG. Back iron covers the stator as magnetic shielding. However, there tends to be a lot of magnetic flux leakage due to the air-cored structure, thereby requiring a large quantity of HTS wire. Therefore, the generator cost will increase. In order to keep the HTS wire length to a minimal, a low pole number is suitable for this generator structure. Also, the use of many HTS wires will generate a higher self-magnetic field. In some cases, the magnetic flux density may exceed 8.0 T, meaning that it is difficult to design a mechanical supporting structure for the HTS field coil. This is one of the challenging issues facing NS-SCG design. With respect to its cooling systems, the field coil is also assumed to be conduction cooling, as shown in Fig. 2-6.

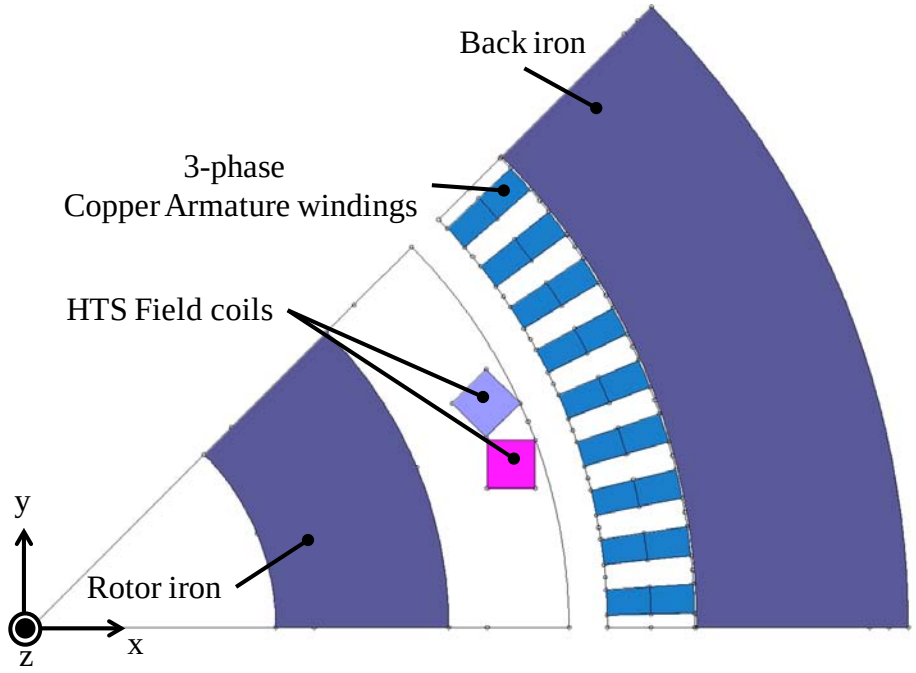

Fig. 2-5. Cross section of an NS-SCG

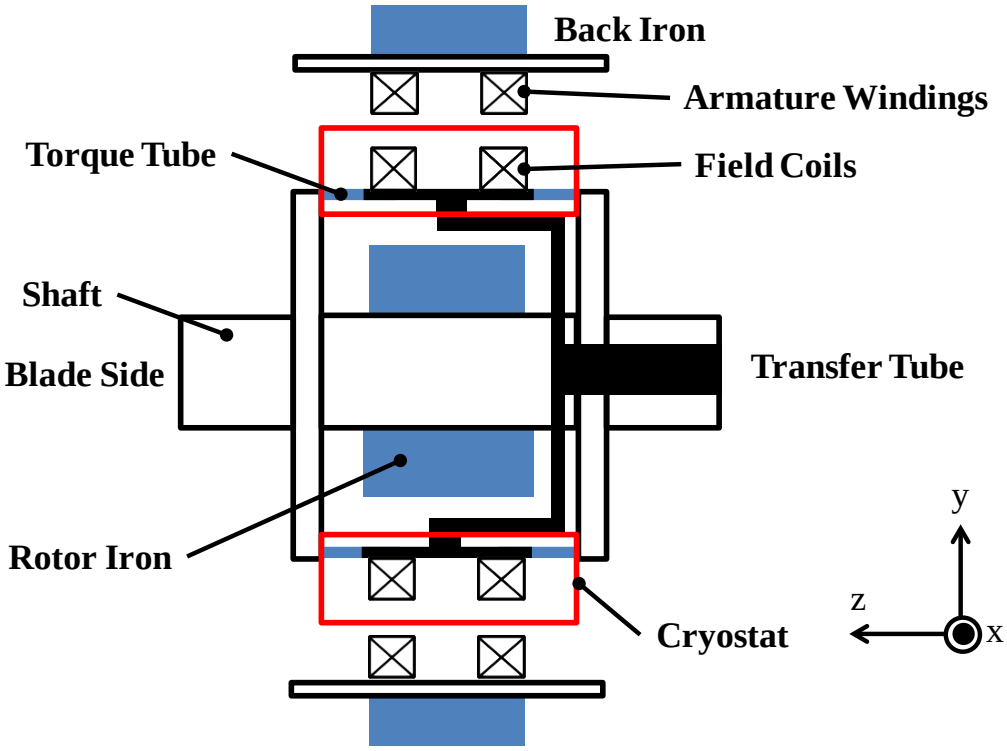

Fig. 2-6. Cooling system of the NS-SCG structure. The red rectangles indicate the cryostat walls of superconducting field coils.

2-2-4. Fully Superconducting Generators (FSCG)

A fully superconducting generator (FSCG) is shown in Fig. 2-7, and is expected to be lightweight and reduced in size. This generator has an air-cored structure, which allows lesser usage of iron, making it more lightweight than iron-cored machines. A small air gap reduction is another advantage of this structure because the field and the armature windings are placed into the same cryostat. A decrease of the total diameter is also possible.

However, the loss of AC is one of the challenging issues affecting this structure. In order to resolve this issue, an FSCG is designed with HTS field coils and MgB_2 concentrated armature windings, as shown in Fig. 2-5. In this structure, concentrated armature windings are used to create a simple cryostat design. The armature windings with MgB_2 can contribute to reduction in AC loss because of its multifilament structures. Also, a lower pole number is suitable for FSCG because the AC loss is proportional to the frequency. In addition to AC loss reduction, the low pole number has another merit of reducing the HTS wire length, thereby resulting in a reduced generator cost. Also, the cooling method for these superconducting coils is assumed to be a conduction cooling structure with refrigerant, as shown in Fig. 2-8.

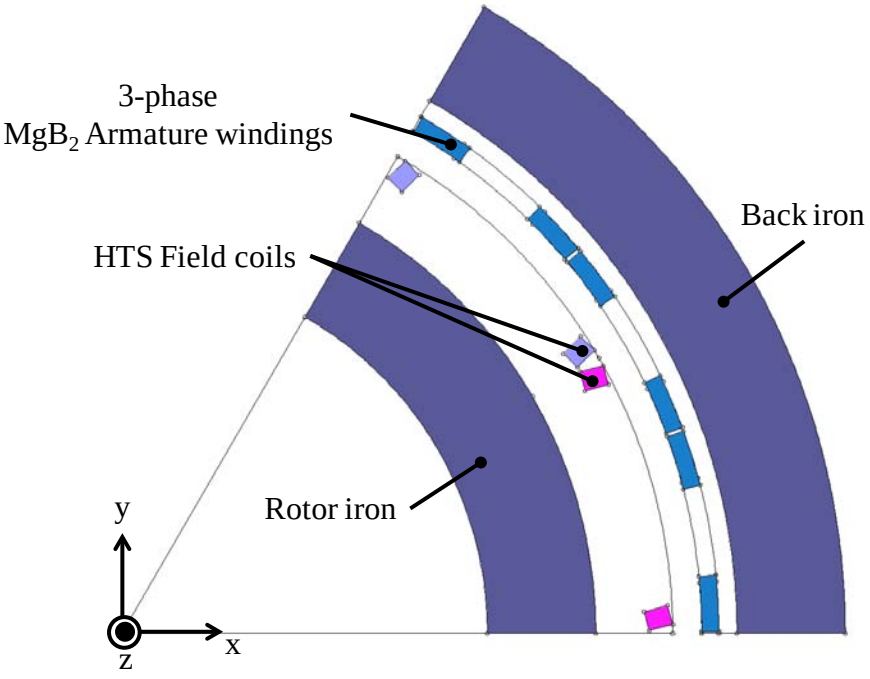

Fig. 2-7. Cross section of an FSCG

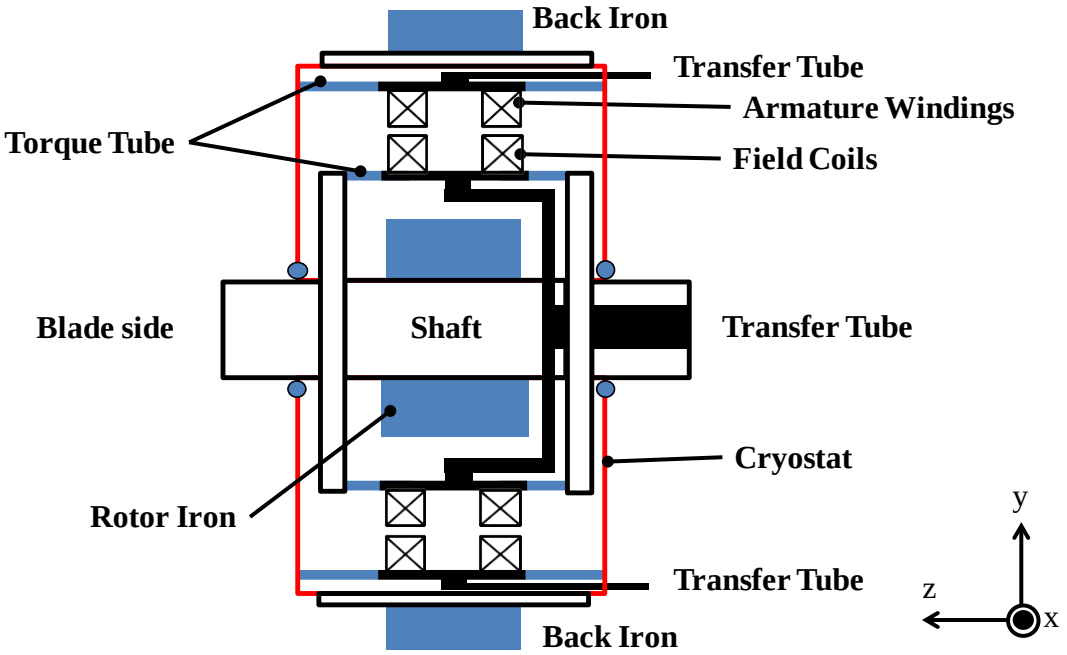

Fig. 2-8. Cooling system of the FSCG structure. The red lines indicate the cryostat walls for superconducting field coils and armature windings.

2-3. Design Conditions for Generator Components

2-3-1. Field Coils

Fig. 2-9 shows the outline of the HTS superconducting field coil for three superconducting wind turbine generators. YBCO superconducting wires are used with this structure because of their good mechanical strength and good *Jc–B* characteristics in stronger magnetic fields. The field coil structure is shaped like a racetrack, and its cross section is assumed to have a square shape. The packing and load factors for YBCO superconducting field coils are set as 0.5 and 0.8, respectively.

The specifications of YBCO were from Superpower, as shown in Fig. 2-10 [20]. The cross section of this wire, $w \times t$, is 4.0×0.1 mm^2. The FSCG will be operated at 22 K because of the *Jc–B* characteristics of the MgB_2 armature windings. The NS-SCG structure is also set at 22 K because a high critical current density is required with the high magnetic field at the field coils. On the other hand, the superconducting field coils of the S-SCG will generate a lower self-magnetic field, and can be operated at a temperature higher than the NS-SCG and FSCG. 33 K was chosen considering the interaction between the *Jc–B* characteristics of the YBCO wires and the cooling system input for the S-SCG.

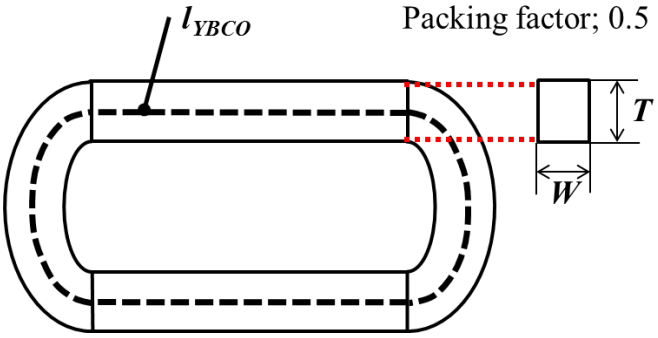

Fig. 2-9. Outline of superconducting field coils

When we estimate the total YBCO wire length for superconducting field coils, L_{YBCO} [m], the following equations are used:

$$L_{YBCO} = P \times l_{YBCO} \times N_{YBCO} \tag{2.1}$$

$$N_{YBCO} = \frac{(T \times W) \times 0.5}{t \times w} \tag{2.2}$$

where P, l_{YBCO}, N_{YBCO}, T [mm], and W [mm] are the pole number, average length, number of YBCO conductor, and height and width of the superconducting field coils, respectively.

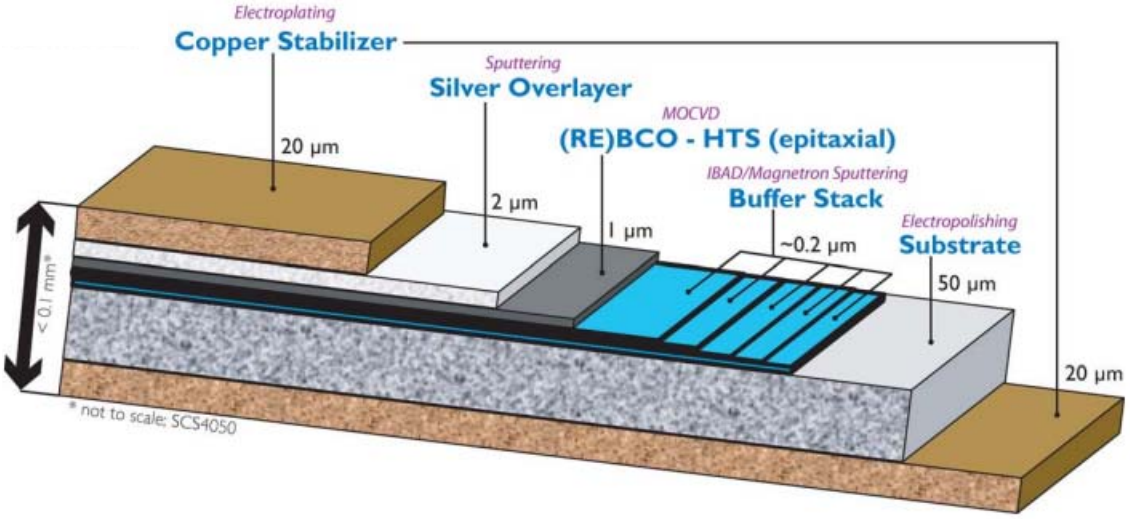

(a)

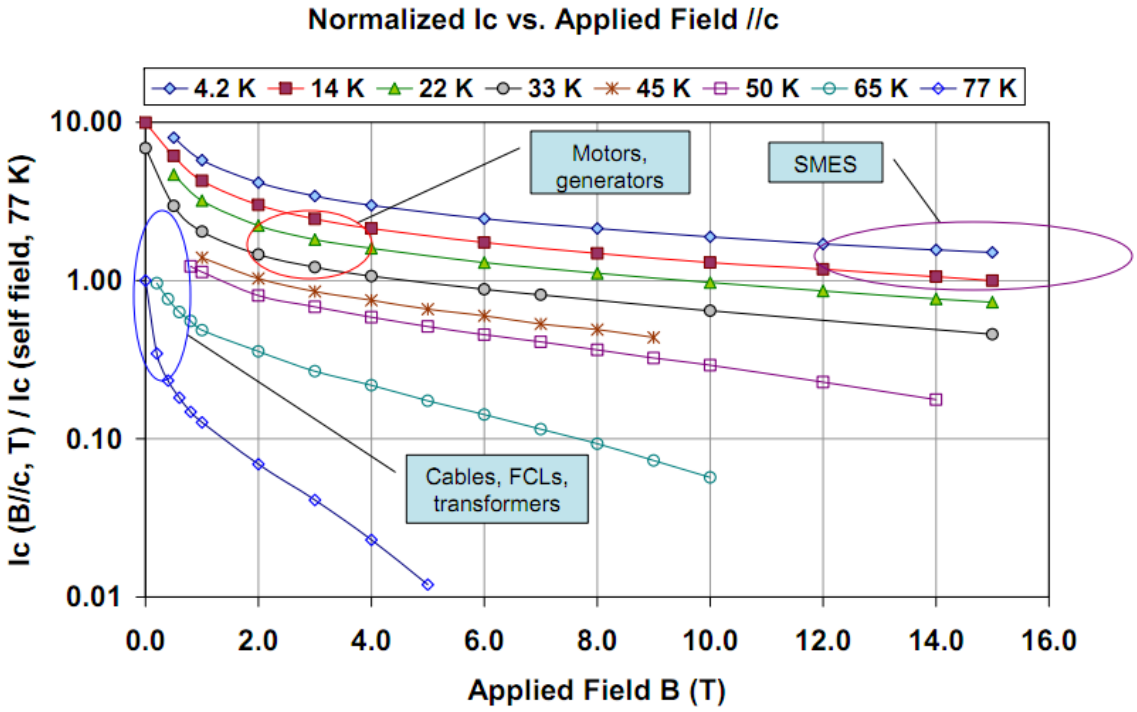

(b)

Fig. 2-10. Specifications of YBCO superconducting wire whose *Jc* is 310 A/w-cm (77 K, 0T) [20]. (a) and (b) show a diagram of the wire and I_c–B characteristics, respectively.

2-3-2. Armature Windings

2-3-2-1. Coil Conductor with Cu

The three types of wind turbine generator, PMSG, S-SCG, and NS-SCG, have copper armature windings, and their packing factor, λ, is 0.5. The current density of copper, J_{Cu}, is assumed to be 3 A/mm^2. The conductor size is defined using equations such as

$$S_{Cu} = \frac{I}{J_{Cu}} \tag{2.3}$$

$$w_c = d_c = S_{Cu} \div \sqrt{\lambda} \tag{2.4}$$

where I [A], S_{Cu} [mm^2], w_c [mm], and d_c [mm] are line current (1750 A), copper cross section, conductor width, and length, respectively.

2-3-2-2. Coil Conductor with MgB_2 Superconducting Wires

As explained in section 2-2-4, multifilament MgB_2 wire is suitable for the FSCG structure because of the AC loss reduction. The armature windings for the FSCG are made of MgB_2 superconducting wires, which were introduced by NIMS in 2010 [21]. This wire has 19 MgB_2 filaments, and they are surrounded by Cu and Cu–Ni (Fig. 2-11). This wire is fabricated by an internal Mg diffusion (IMD) process. Table 2-2 shows the geometrical specifications of the MgB_2 wire. The diameter D of this wire is almost 1.3 mm. The shape of the MgB_2 superconductor filaments is a hollow cylinder, with inner and outer radii (R_i and R_o) of 25 μm and 37.5 μm, respectively. Fig. 2-12 shows the Jc–B characteristics of the MgB_2 windings. Even under conditions of 20 K and 3.0 T, Jc exceeds 10^5 A/cm^2, which means that this wire has good performance in stronger magnetic fields.

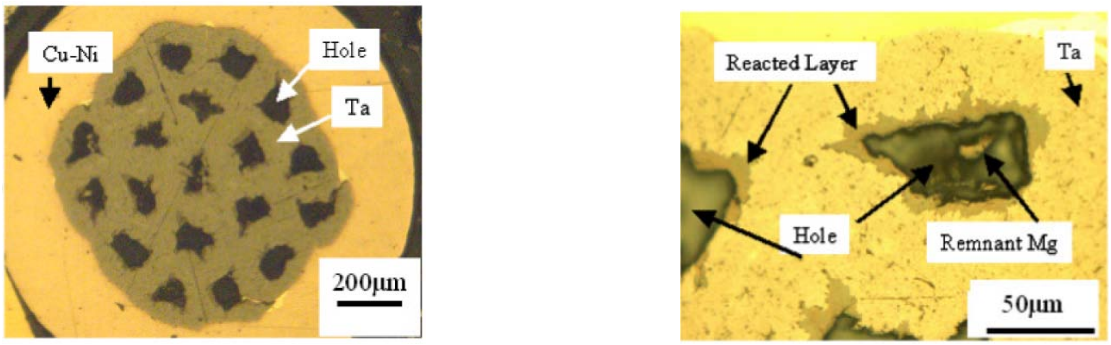

(a) (b)

Fig. 2-11. Cross section of MgB_2 superconducting wires with 19 filaments. (a) general view and (b) extended figure of an MgB_2 filament [21].

Table 2-2. Geometrical specifications of the MgB_2 wire

Diameter, D [mm]	1.3
Number of filaments	19
Outer filament radius, R_O [μm]	37.5
Inner filament radius, R_i [μm]	25

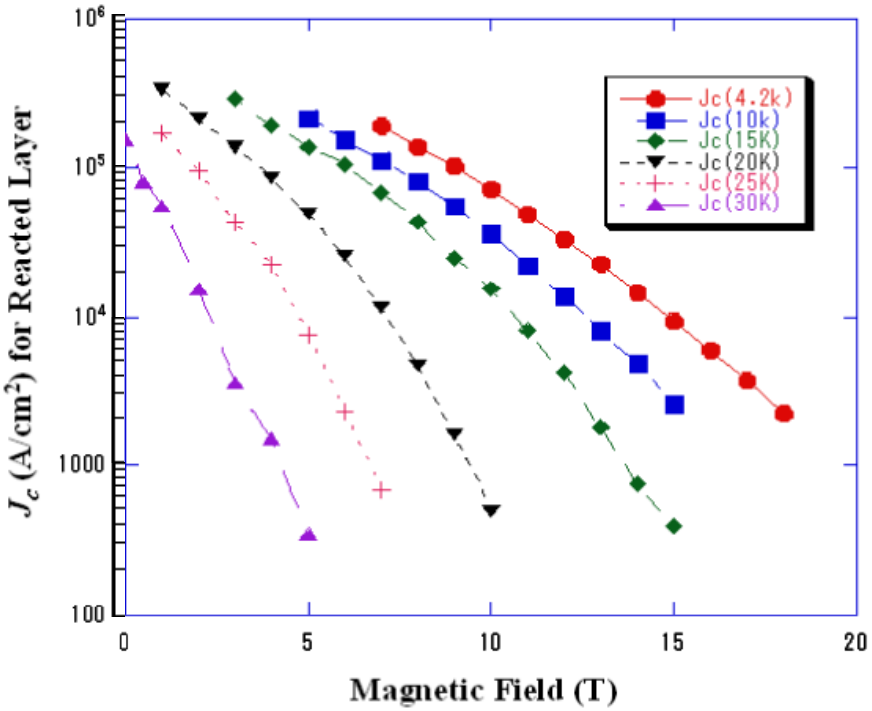

Fig. 2-12. Specifications of MgB_2 superconducting wire [21, modified].

When the armature windings are fabricated with the 19-filament MgB_2 wire, their conductor cross section, $S_{A\_MgB2,}$ is set with the following equations:

$$I_C = J_C \times 19 \times \pi \times \left(R_O{}^2 - R_i{}^2\right) \tag{2.5}$$

$$I = \alpha \ I_C \tag{2.6}$$

$$n = I_{\max} / I \tag{2.7}$$

$$S_{A\_MgB2} = \pi \times \left(\frac{D}{2}\right)^2 \times \left(\frac{n}{\lambda}\right) \tag{2.8}$$

where I_c [A], α, n, I_{max} [A], and λ are critical current, load factor (0.8), conductor number, current amplitude (2475 = 1750*$\sqrt{2}$), and packing factor (0.5), respectively.

Using the values in Table 2-2 and equations (2.4)–(2.7), the armature conductor sizes with MgB_2 are obtained as in Table 2-3. Two types of conductors which depend on the external magnetic flux density (1.5 or 2.0 T) have been designed.

Table 2-3. Specifications of MgB_2 armature conductors under two different magnetic field conditions

B [T]	1.5	2.0
Jc [A/m^2]	2.7×10^9	2.0×10^9
Ic [A]	125.9	93.3
I [A]	100.7	74.6
n	25	34
S_{A_MgB2} [mm^2]	8.1 × 8.1	9.5 × 9.5

2-3-2-3. Coil End Structure

The shape of Cu armature windings is assumed to be like that in Fig. 2-13. This coil is considered to have a diamond structure (Fig. 2-13(a)), and it is important to understand how to deal with the coil-end structure. In this thesis, the copper armature coil resistance, including the coil end, is defined from geometrical equations as follows:

$$R_U = \rho_{Cu} \times \frac{1}{S_{Cu}} \left(2L_{eff} + 4l_{end}\right) \times q \times P \times N \tag{2.9}$$

$$l_{end} = \frac{\left(a/2\right)}{\cos\vartheta} \tag{2.10}$$

where R_U [Ω], ρ_{Cu} [Ωm], L_{eff} [m], l_{end} [m], q, P, and N are coil resistance per phase, copper resistivity, effective length, coil end length, slot number, pole number, and number of copper conductors, respectively. The optimized value, θ = 50°, was chosen in this thesis. On the other hand, the MgB_2 armature windings are such concentrated winding structures that these equations are not required. This means that the armature winding is racetrack-type, as is the case with the superconducting field coils.

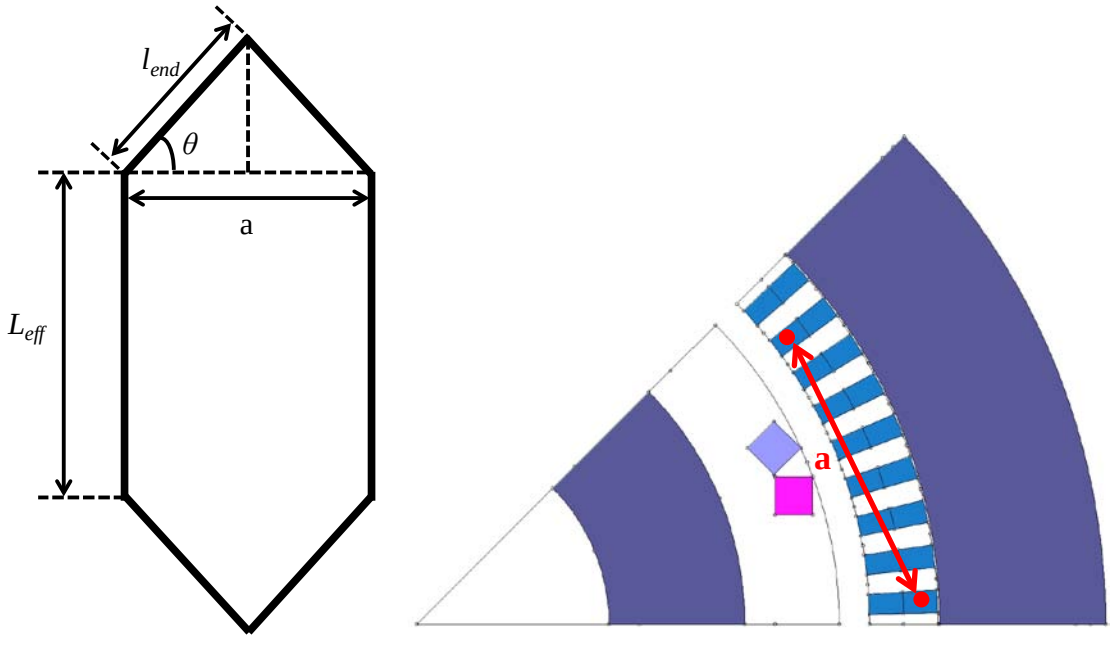

(a) (b)

Fig. 2-13. Diagram of copper armature windings

2-3-3. Back and Rotor Iron

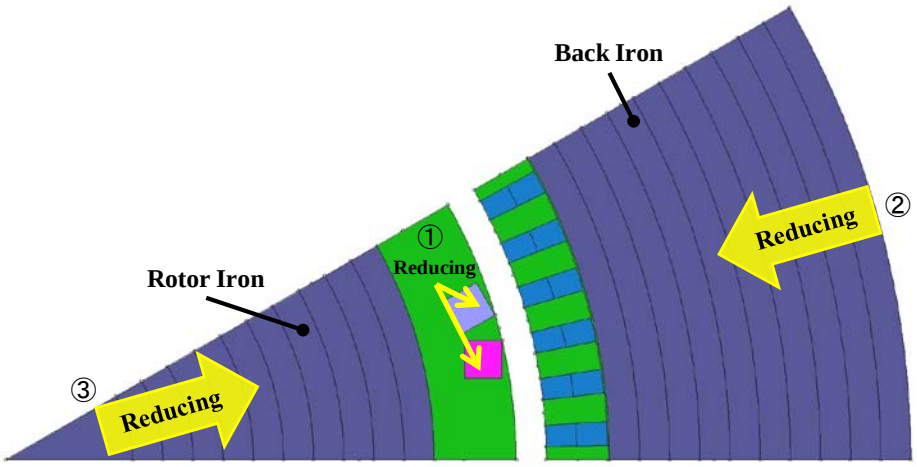

Fig. 2-14. Diagram of back and rotor iron design

Back and rotor irons have been designed for magnetic shielding. First, the iron is filled in the rotor and stator part, as in Fig. 2-14. After obtaining an output power of over 10 MW using the numerical calculations, the iron is reduced as follows.

1. Reduce the cross section of superconducting field coils until the output power reaches 10 MW.
2. Reduce the back iron from the outer diameter side, while maintaining an output power of 10 MW. The back iron thickness should therefore be maintained for an output of over 10 MW. If the output falls to 9.9 MW, the back iron thickness will be increased until the power again increases to 10 MW.
3. Reduce the rotor iron using the same method as with the back iron.

In the case of the FSCG structure, the maximum magnetic flux density at the MgB_2 armature windings should be considered because of the *Jc–B* characteristics at the operating temperature.

2-4. Summary of Chapter 2

This chapter explained the design conditions of four 10 MW class wind turbine generators, namely PMSG, S-SCG, NS-SCG, and FSCG. We first showed uniform design conditions and a direct-drive system. Next, we presented illustrations of four generators. The third section showed the design conditions for generator components such as superconducting field coils, armature windings, and back/rotor irons. Finally, we introduced the cooling systems for the generators.

Electromagnetic characteristics of these 10 MW class wind turbine generators obtained by performing FEM analysis will be investigated in the next chapter.

Chapter 3

Electromagnetic Design of

Permanent Magnet type Synchronous Generators

3-1. Steady State Analysis

3-1-1. Analysis Models and Conditions

This chapter deals with the electromagnetic design and characteristics of permanent magnetic synchronous generators (PMSG) using two-dimensional FEM analyses. Fig. 3-1 shows the FEM analysis model of PMSG. As mentioned in chapter 2, this structure is suitable for multipole structures. Hence, a pole number of 60 was chosen considering the converter frequency of 5 Hz. The outer diameter is defined around 10 m on the basis of a study by a Chinese and Dutch group [22]. The air gap was set as 15 mm on the basis of the value in low-speed and multipole synchronous machines, such as water turbine generators [23, 24]. As shown in chapter 2, the thickness of the back iron is infinitely large in radial direction. Also, the rotor is filled with iron. The two irons are reduced in the calculation process.

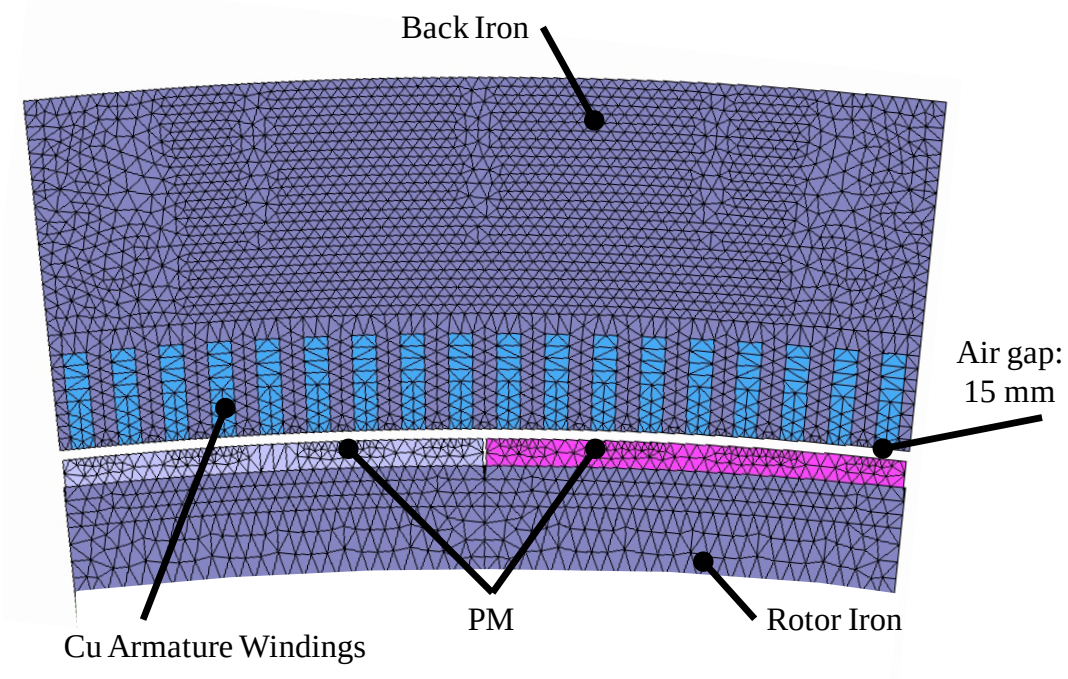

Fig. 3-1 FEM analysis model of the PMSG (1/30 periodic model).

3-1-2. Analysis Results

3-1-2-1. Generator Dimensions and Outputs

Table 3-1 explains the generator dimensions and output characteristics of PMSG. Finally, the stator diameter and effective length reached 13.1 m and 1.12 m, respectively. Also, the thicknesses of the back/rotor irons are 380 mm and 160 mm, respectively. The generator size is almost the same as a 7.5 MW class electrical excited synchronous machine made by Enercon.

Fig. 3-2 shows the magnetic flux density distributions for the PMSG. The maximum magnetic flux density B_{max} is 1.8 T. This value appears to be higher than that of conventional PM-type generators because of the widespread use of PM. In particular, the magnetic flux is concentrated on the part with the generator teeth. Figs. 3-3–3-5 show the output waveforms of the torque, line current, and phase voltage in steady state, respectively. All of them included harmonics, and many spikes were observed in the torque. To estimate the generator output, the amplitude of the fundamental wave was estimated using the Fourier transform. Finally, using the fundamental factors of current and voltage, we obtained an output power of 10.0 MW. The results show that this PMSG satisfies the initial design conditions in chapter 2.

Table 3-1. Generator dimensions and output characteristics of the PMSG.

Stator diameter [m]	13.1
Rotor diameter [m]	6.0
Effective length [m]	1.12
Air gap [mm]	15
Pole number	60
Armature conductor dimension [mm^2]	33.9 × 35.4
Slot number/phase, pole	3
Slot size [mm^2]	35 × 141
Thickness of back iron [mm]	380
Thickness of rotor iron [mm]	160
B_{max} [T]	1.8
Output power [MW]	10.0
Load line-to-line voltage [kV_{rms}]	3.34
Line current [kA_{rms}]	1.77

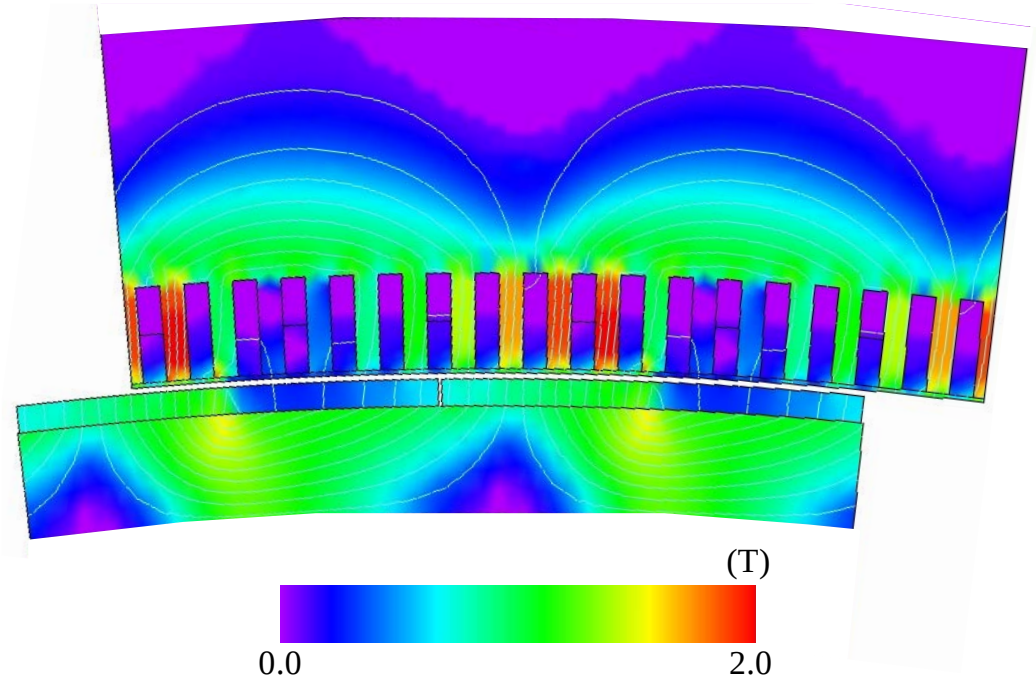

Fig. 3-2. Magnetic flux density distribution of the PMSG in steady state

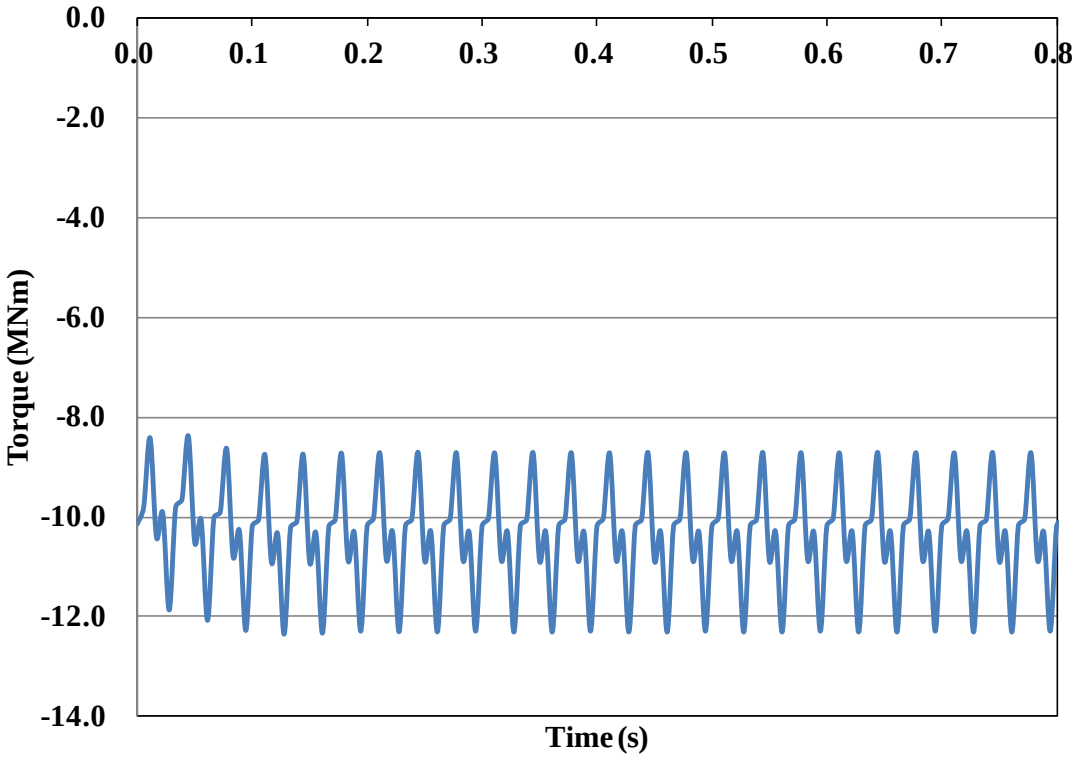

Fig. 3-3. Output torque of the PMSG.

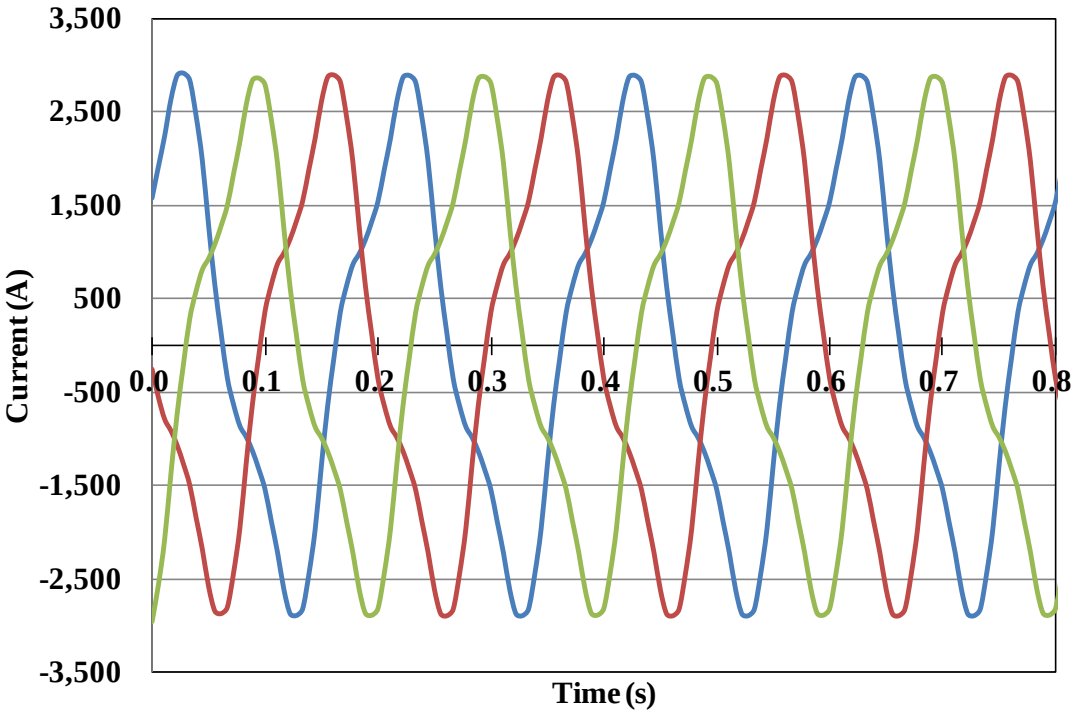

Fig. 3-4. Output current of the PMSG.

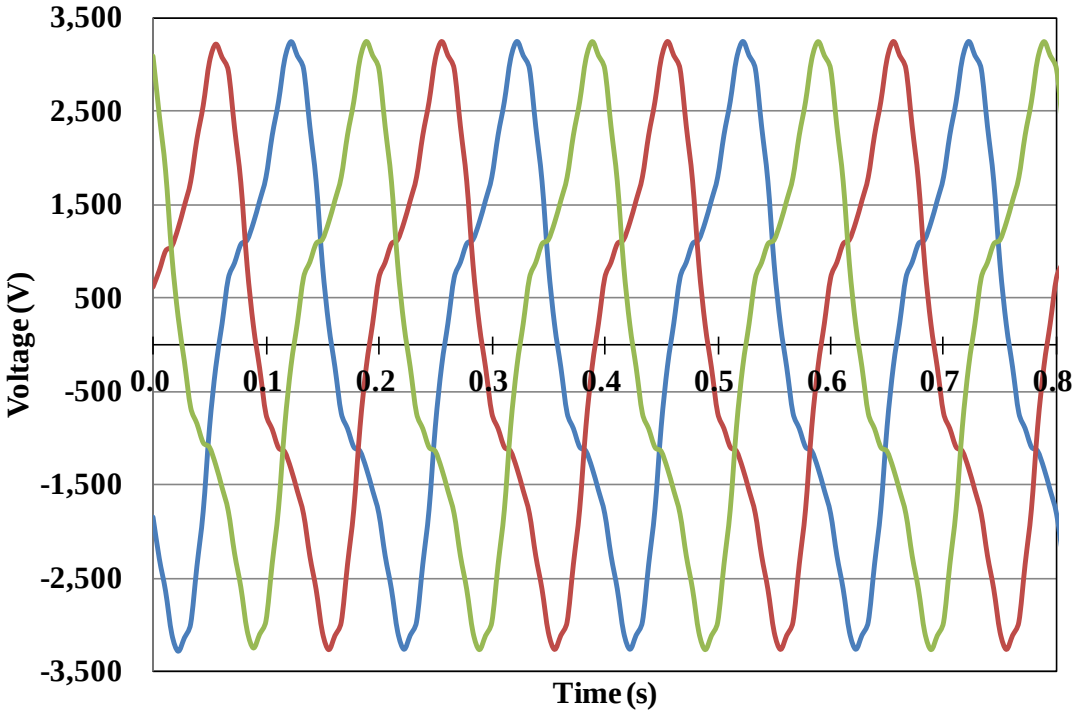

Fig. 3-5. Output phase voltage of the PMSG

3-1-2-2. Synchronous reactance

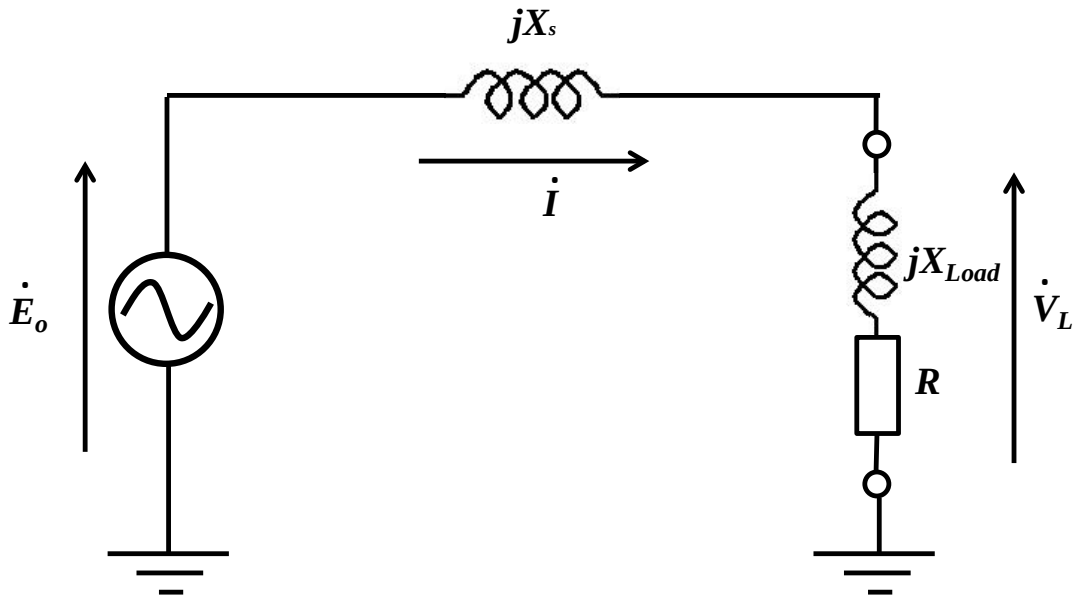

Fig. 3-6. Equivalent circuit for a non-salient pole type synchronous machine

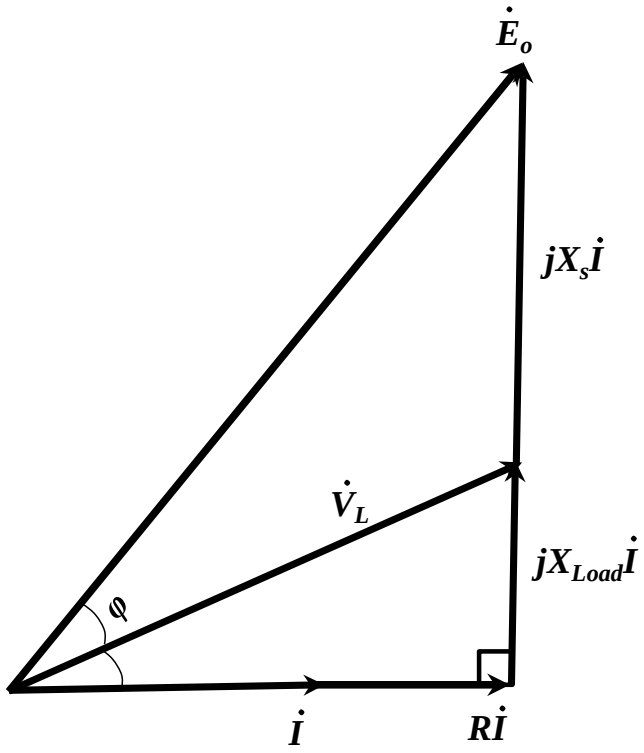

Fig. 3-7. Phasor diagram for a non-salient pole type synchronous machine

Synchronous reactance is calculated using the previous data and the circuit and phasor diagrams shown in Figs. 3-6 and 3-7, respectively. In particular, it is assumed that the synchronous reactance, X_s [Ω], of the armature winding is larger than the armature resistance.

First, using Kirchhoff's law, the circuit equation in Fig. 3-6 is expressed as follows:

$$\dot{E}_o - j X_s \dot{I} = \dot{V}_L \tag{2.1}$$

$$\dot{V}_L = \left(R + jX_{Load}\right)\dot{I} \tag{2.2}$$

where E_o [V_{rms}], I [A_{rms}], V_L [V_{rms}], R [Ω], and X_{Load} [Ω] are open phase voltage, line current, loaded phase voltage, load resistance, and reactance, respectively. In addition, j is an imaginary number.

Substituting (2.2) into (2.1), the upper equations are summarized as follows:

$$\dot{E}_o - j X_s \dot{I} = \left(R + jX_{Load}\right)\dot{I}. \tag{2.3}$$

Hence, the equation is

$$\dot{E}_o = \left\{R + j\left(X_s + X_{Load}\right)\right\}\dot{I}. \tag{2.4}$$

Now, $\dot{E}_o$ and $\dot{I}$ are respectively expressed as follows:

$$\dot{E}_o = \sqrt{2}\, E_o \exp\left\{j\left(\varphi + \delta\right)\right\} \tag{2.5}$$

$$\dot{I} = \sqrt{2}\, I \tag{2.6}$$

where φ is the phase between E_O and V_L. On the other hand, δ is the load angle with R and X_{Load}.

Substituting (2.5) and (2.6) into (2.4), the equation can be written as follows:

$$\sqrt{2}\, E_o \exp\left\{j\left(\varphi + \delta\right)\right\} = \sqrt{2}\, I \left\{R + j\left(V_s + X_{Load}\right)\right\}. \tag{2.7}$$

Using Euler's law, the upper equation is summarized by

$$\left(\frac{E_o}{I}\right)\left(\cos(\varphi + \delta) + j\sin(\varphi + \delta)\right) = R + j\left(X_s + X_{Load}\right). \tag{2.8}$$

Now, this equation can be divided into real and imaginary parts as follows:

$$\left(\frac{E_o}{I}\right)\cos\left(\varphi + \delta\right) = R\ , \tag{2.9}$$

$$\left(\frac{E_o}{I}\right)\sin\left(\varphi + \delta\right) = \left(X_s + X_{Load}\right). \tag{2.10}$$

By taking summation after squaring them, the following equation is obtained.

$$\left(\frac{E_o}{I}\right)^2 = R^2 + (X_S + X_{Load})^2 \tag{2.11}$$

Finally, X_s can be obtained using the following equation:

$$X_S = \sqrt{\left(\frac{E_o}{I}\right)^2 - R^2} - X_{Load}\,. \tag{2.12}$$

When X_S [Ω] is expressed with a per-unit system, the synchronous reactance, x_S [p.u.], is obtained using the following equation.

$$x_S = \frac{X_S}{\left(V_L \diagup I\right)}\,. \tag{2.13}$$

Table 3-2 shows the calculated synchronous reactance and its parameters. The value appears to be a little higher than the value for real, conventional, and low-speed synchronous machines such as hydro turbine generators (0.97) because of the widespread usage of back/rotor irons [25]. This value is defined as a standard value for this thesis, and will be compared with more recently developed superconducting synchronous machines.

Table 3-2. Synchronous reactance and calculated parameters.

Calculated Parameters	
Open phase voltage: E_o [V_{rms}]	3376
Load phase voltage: V_L [V_{rms}]	1928
Line current: I [A_{rms}]	1772
Load resistance: R [Ω]	1.07
Load reactance: X_{Load} [Ω]	0.126
Synchronous Reactance	
X_S [Ω]	1.45
x_S [p.u.]	1.33

3-1-2-3. Copper and Iron Losses

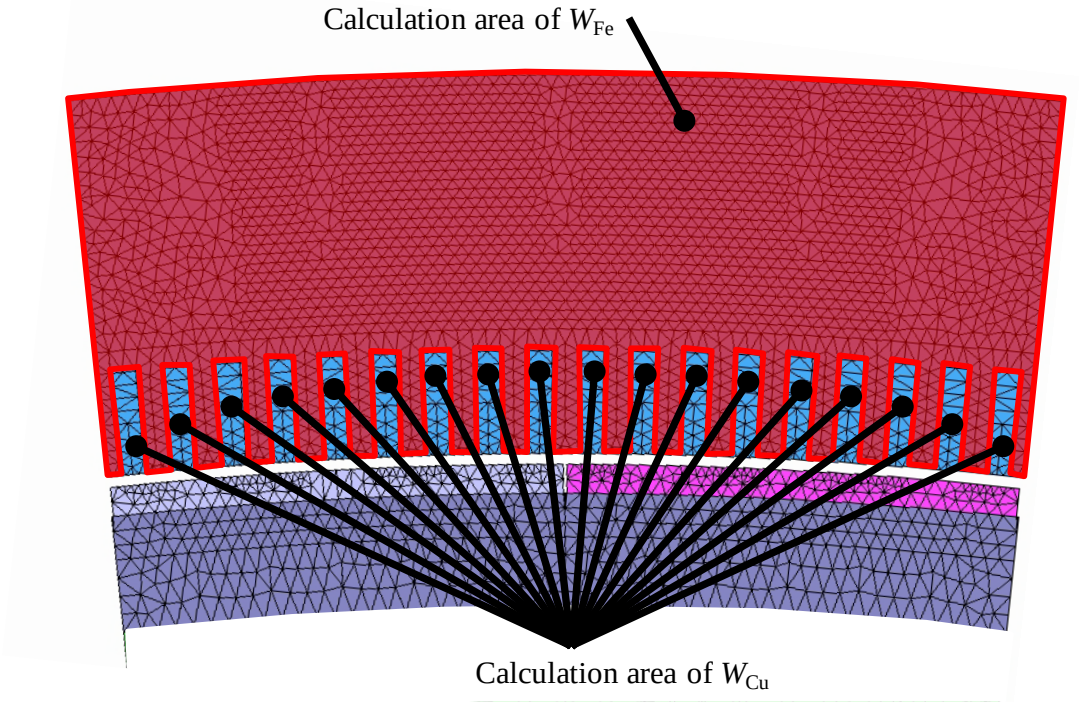

Fig. 3-8. Calculation areas of generator losses for the PMSG (1/30 periodic model).

This section focuses on the generator losses. Two types of losses were investigated, namely the three phase copper loss, W_{Cu}, and the iron loss, W_{Fe}. Fig. 3-8 shows the calculation areas of the generator losses for the PMSG. W_{Cu} is calculated using I [A_{rms}] and the armature resistance per phase, R_U, as follows:

$$W_{Cu} = 3 \times R_U \times I^2 . \qquad (2.14).$$

As shown in Fig. 3-8, the calculation area of W_{Fe} indicates the back iron part and the loss indicates hysteresis losses. W_{Fe} is estimated using the hysteresis curve shown in Fig. 3-9. The portion of the plot above 2.0 T was estimated using the *B–H* curve of 50JN1300, which is manufactured by JFE steel [26].

Table 3-3 shows the estimation results for the two losses. Compared to the losses, the ratio of W_{Cu} was somewhat higher than that of W_{Fe}, and this was because of the very low rotation speed and frequency. However, the sum of these values was over 400 kW, meaning that the maximum generator efficiency of the PMSG is almost 96%. If other losses, such as mechanical or rotor iron losses, are added, the efficiency may decrease to around 90%. This value was somewhat lower than that of other conventional multi-MW class wind turbine generators.

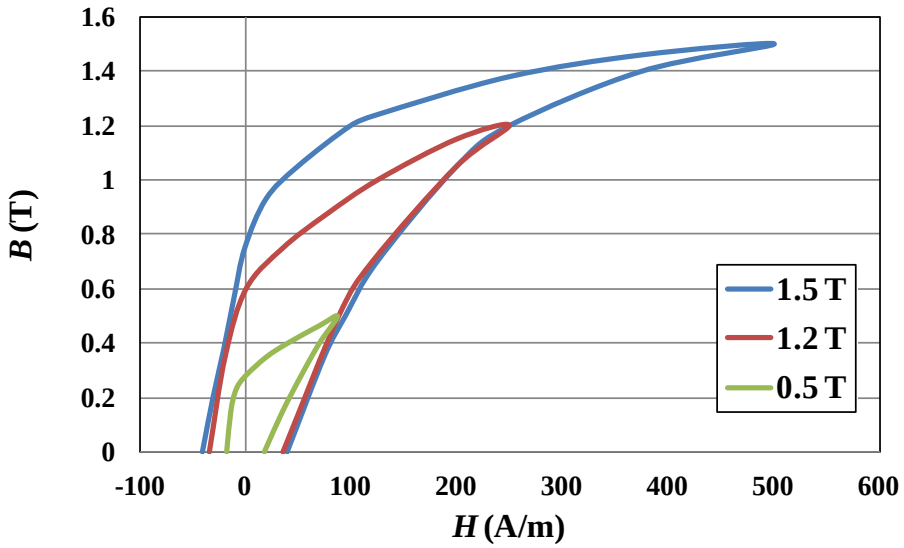

(a)

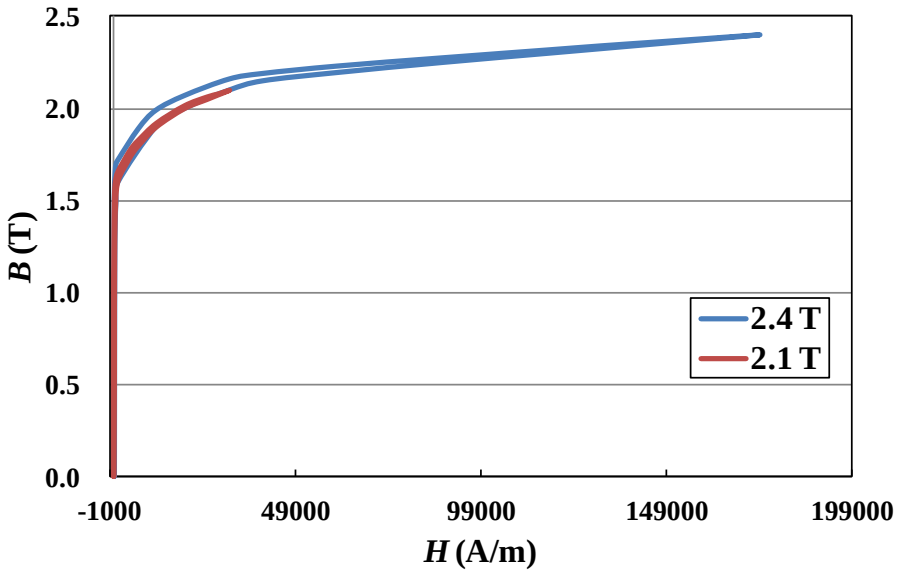

(b)

Fig. 3-9. Hysteresis curve of back iron. (a) shows the curve up to 1.5 T, and (b) shows the curve up to 2.4 T.

Table 3-3. Calculation results of copper and iron losses

Armature resistance per phase: R_U [Ω]	0.041
Line current: I [A_{rms}]	1772
Three phase Copper loss: W_{Cu} [kW]	386
Iron loss of the back iron: W_{Fe} [kW]	17.1

3-2. Discussions of the Generator Performances

The electromagnetic characteristics are summarized in Table 3-4. The results show that the development of a 10 MW class wind turbine generator with PM presents many challenging issues on account of its efficiency, weight, and cost. As shown in the previous section, the efficiency may be approximately 90%. With respect to the generator weight, the total weight of the PMSG is 231.7 tons. However, if we consider the materials that make up the mechanical supporting structures, the weight will exceed 250 tons. On the basis of this result, the weight of nacelle is estimated to be over three times higher, i.e., 750 tons. In the case of E-126 by Enercon, the nacelle weight is estimated to be around 712 tons. To date, it has been difficult to develop this generator because of the weight. In addition, the current market price of rare earth materials for PM is not stable.

Table 3-4. Electromagnetic characteristics of the 10 MW class PMSG.

Generator	PMSG
Stator Diameter [m]	13.1
Effective length [m]	1.12
Output [MW]	10.0
Line current [A_{rms}]	1.77
Line-to-line voltage [V_{rms}]	3.34
Pole number	60
Air gap [mm]	15
Operating temperature [K]	300
Rotor Field	PM
Armature conductor	Cu
Coil current density [A/m^2]	3×10^6
Packing factor	0.5
Wire length [km]	3.7
B_{max} [T]	1.8
Synchronous reactance [pu]	1.33
Copper loss [kW]	386
Iron loss [kW]	17.1
Weight	
Irons [tons]	198.7
Copper [tons]	19.9
Permanent magnet [tons]	13.1
Total weight [tons]	231.7

3-3. Transient Analysis for Three-phase Short-Circuit Problems

3-3-1. Analysis Models and Conditions

One of the challenging issues affecting the design of large-scale wind turbine generators is realizing a machine design that counters excessive torque caused by short-circuit problems. This problem occurs in cases involving lightning strikes on wind turbines. The electromagnetic force generated by a short-circuit current would lead to electromagnetic and mechanical problems such as torque transmission between the machine rotor and rotor blade. In particular, the maximum transient torque of large-scale direct-drive wind turbine generators may be very high because of its low-speed and higher-torque design. Therefore, current-limiting control would be important for the mechanical design of the generators. This section deals with the most serious case of sudden three-phase short-circuit problems.

Fig. 3-10 shows the equivalent circuit of sudden three-phase short-circuit problems for synchronous generators using copper armature windings. Initially, the generators are operated in the steady state. After several cycles of the generator frequency, which depends on the generator poles, the two switches are closed and a sudden three-phase short circuit occurs.

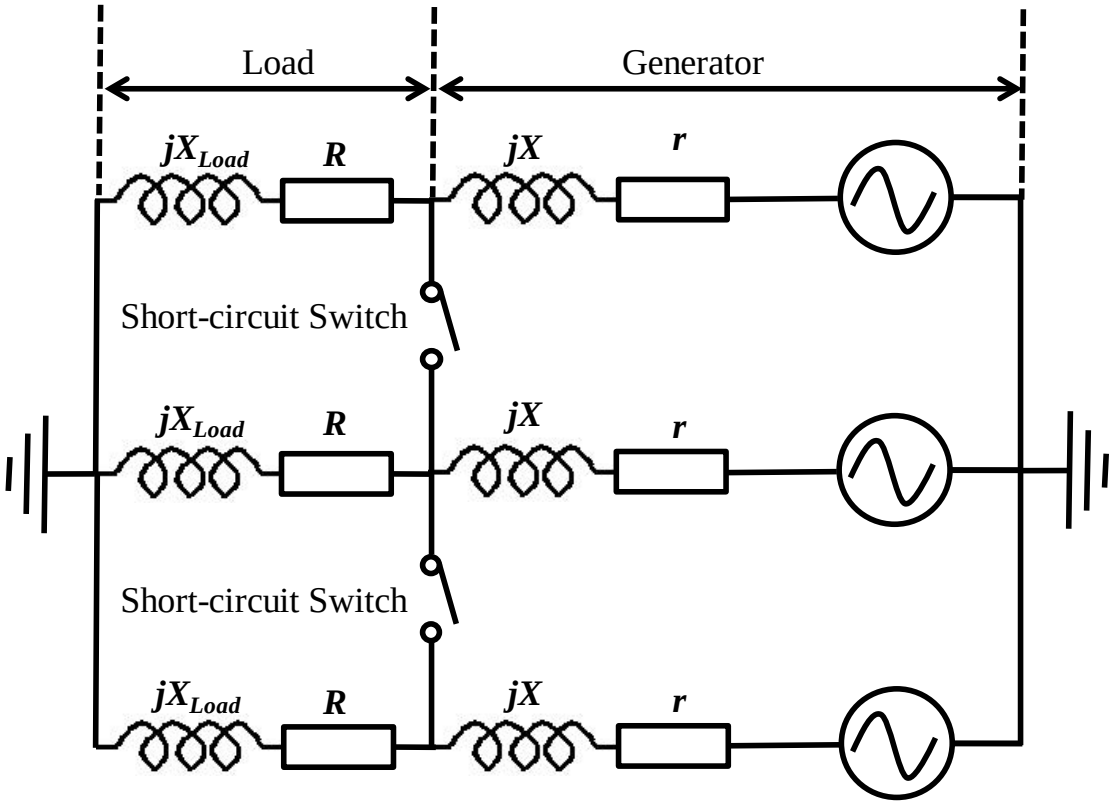

Fig. 3-10. Equivalent circuit of sudden three-phase short-circuit problems for synchronous generator using copper armature windings.

3-3-2. Analysis Results

Fig. 3-11 shows the magnetic flux density distribution of the PMSG. When compared with Fig. 3-2, the difference is clear. The magnetic field on the stator side is random and its strength is very low. This is because the magnetic fields of PM and short-circuit currents are compensated.

Figs. 3-12 to 3-14 show the waveform of transient torque, line current, and phase voltage at armature windings, respectively. Each value eventually converges from the transient state. The maximal transient torque is almost 17.0 MNm. The value is 70% higher than that of the rated value of 10.0 MNm. Also, the torque converges until it is less than 50% of the rated value. With respect to the transient current, the maximum value increases at 5770 A_{max}, which is over 130% of the maximum rated value of 2494 A_{max} (= 1750 A_{rms}). After the transient state, the current converges at around 4000 A_{max}.

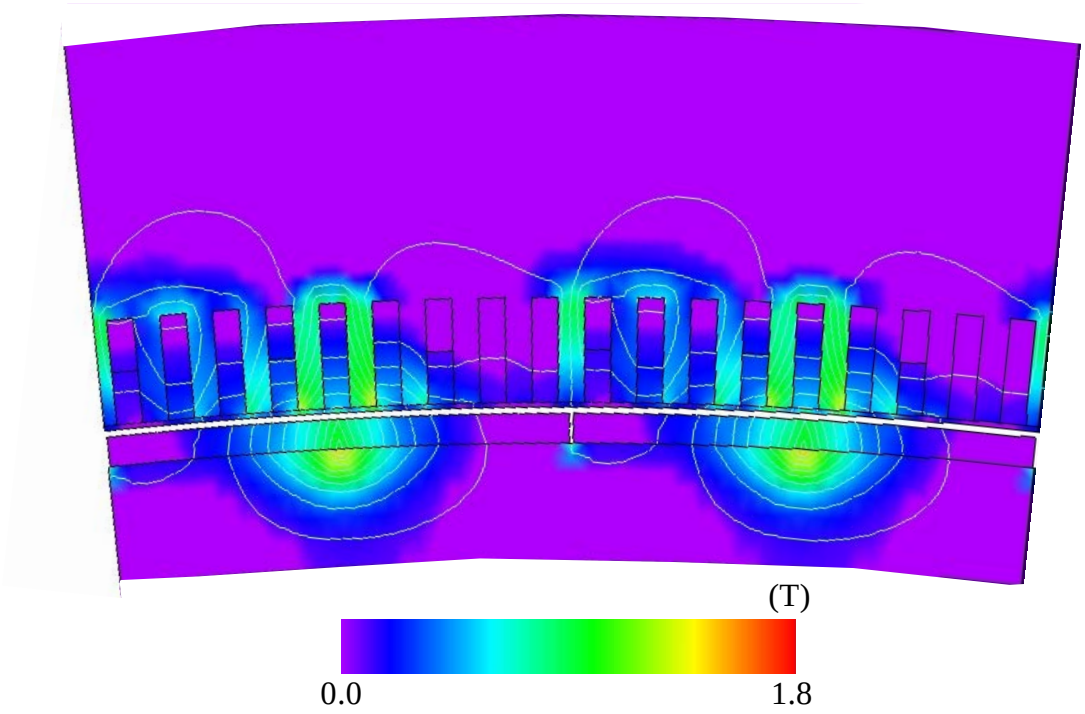

Fig. 3-11. Magnetic flux distribution of the PMSG in short-circuit state

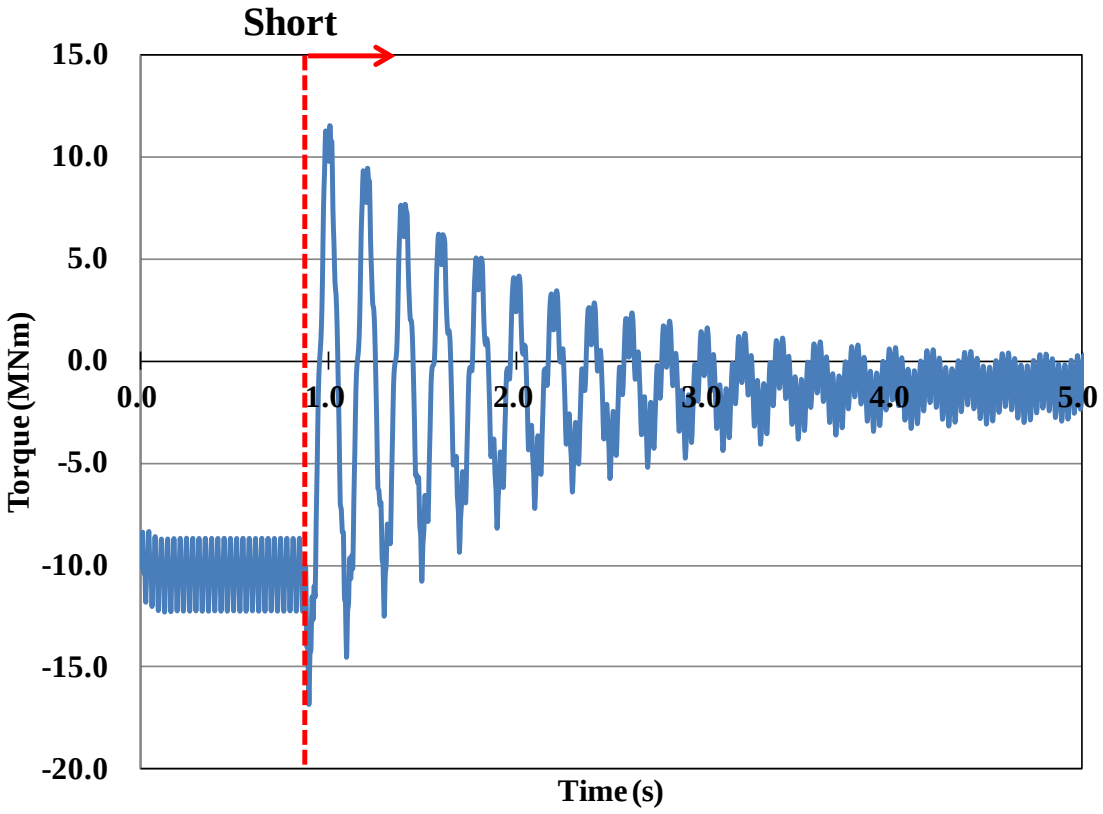

Fig. 3-12. Short-circuit torque of the PMSG.

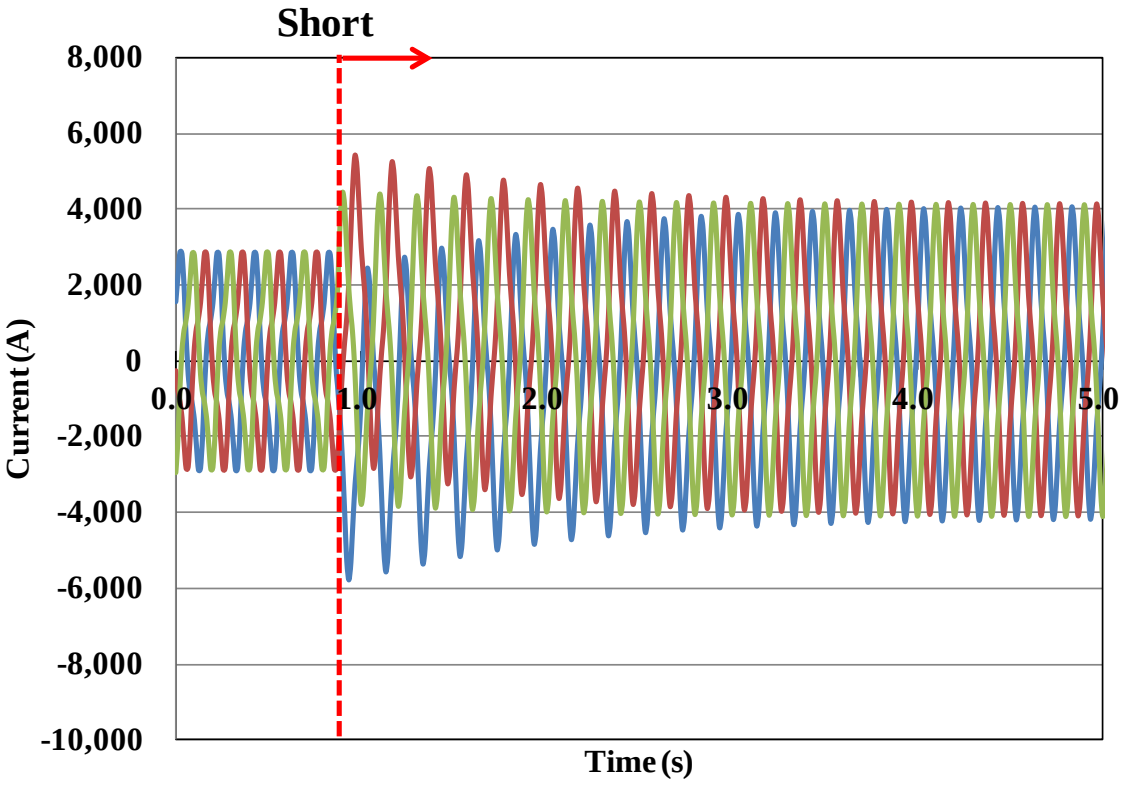

Fig. 3-13. Short-circuit current of the PMSG.

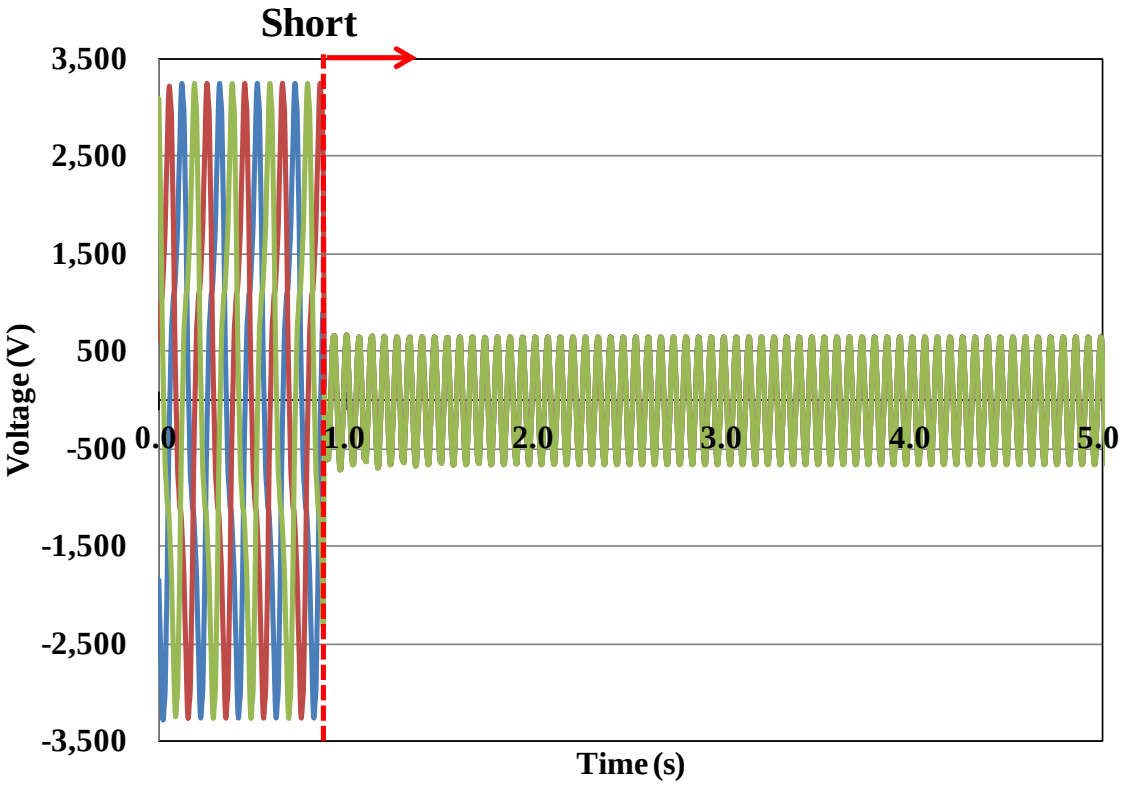

Fig. 3-14. Short-circuit phase voltage of the PMSG.

3-4. Summary of Chapter 3

This chapter showed the electromagnetic design of a 10 MW class PMSG with 2D FEM analysis. First, the steady state of the generator performance has been investigated. The results show that the PMSG has many challenging problems from the efficiency viewpoint, weight, and cost. The generator losses, including copper and iron losses, totaled almost 400 kW, which means that the generator efficiency decreases with only two losses, and would result in an efficiency of around 90% when all of the losses are included. Also, the generator and nacelle weight would exceed 250 and 750 tons, respectively. It is difficult to reduce the cost of the tower using conventional technologies. Also, the weight of the permanent magnet would be over 13 tons. The cost of PMs is currently unstable, and at times can be very high.

Second, we investigated the transient analysis for the sudden three-phase short-circuit problems. The results show that the transient torque and current are 70% and 130% higher than the rated values, respectively.

On the basis of the data presented in this chapter, the electromagnetic characteristics of superconducting wind turbine generators will be investigated in subsequent chapters.

Chapter 4

Electromagnetic Design of

Salient Pole type Superconducting Generators

4-1. Steady State Analysis

4-1-1. Analysis Models and Conditions

This chapter focuses on the electromagnetic design of salient pole-type superconducting generators (S-SCG). We investigated the two-dimensional FEM analysis using J-MAG. Fig. 4-1 shows the 2D FEM analysis model for the S-SCG.

As shown in chapter 2, this structure requires a large amount of iron, and should have a multipole structure. Two types of S-SCG are designed in this chapter. One is S-SCG-A, which has 36 poles and an air gap of 15 mm. The other is S-SCG-B, which has 60 poles and an air gap of 15 mm. The S-SCG-B is designed to have a diameter of around 8.0 m on the basis of values reported by other groups [15, 16]. On the other hand, the design concept of the S-SCG-A aims to realize a more compact structure, such as around 5.0 m. However, a smaller diameter results in a decrease in the pole number. The air gap values used for both generators were obtained from water turbine generators, such as the PMSG in chapter 3. The operating temperature is set as 33 K.

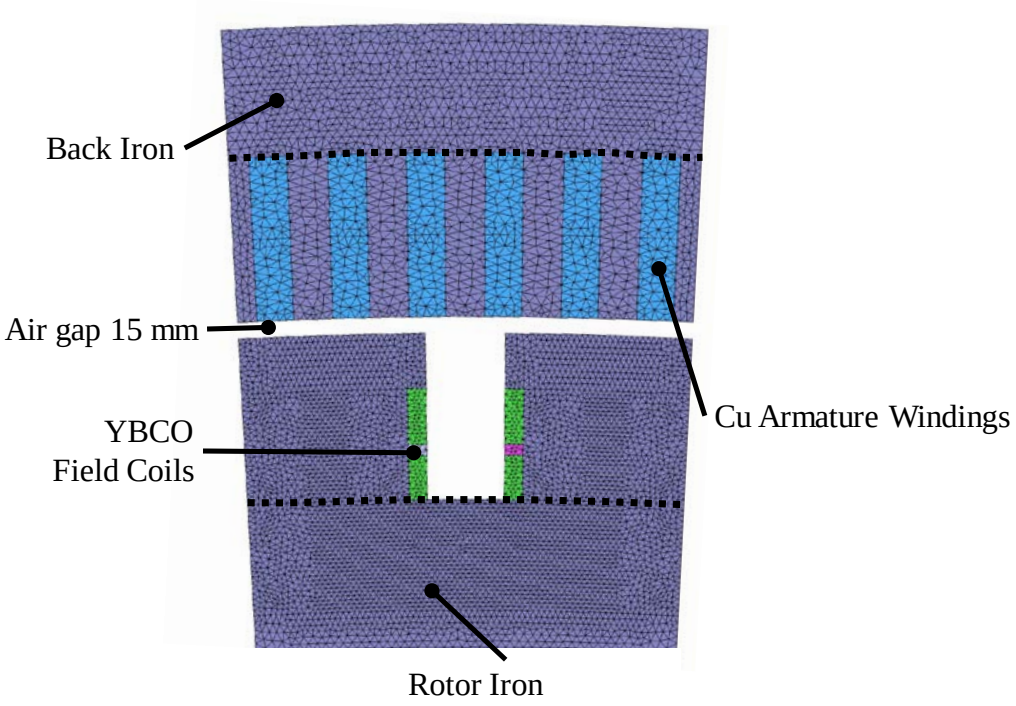

Fig. 4-1. FEM analysis model for the S-SCG (Periodic model).

4-1-2. Analysis Results

4-1-2-1. Generator Dimensions and Outputs

Table 4-1 shows the generator dimensions and output characteristics of the S-SCG. The diameter of the S-SCG-A and S-SCG-B are 5.45 m and 8.2 m, respectively. However, the effective length of the S-SCG-A exceeded twice that of S-SCG-B. Also, the back/rotor irons of S-SCG-A were thicker than those of S-SCG-B because the magnetic flux in the irons induces a large loop in the case of the low pole machines. Many irons are therefore needed to prevent magnetic flux leakage to the outer side. On the other side, both generators successfully obtained output power of 10.0 MW with diameters that were over 30% less than that of the PMSG structure in chapter 2. Fig. 4-2 shows magnetic flux density (*B*) distributions of FSCG-A. A part of the rotor iron was saturated because of the higher magnetic field generated by YBCO field coils, which was the same as that in case of S-SCG-B. Figs. 4-3 to 4-5 shows output waveforms of torque, current, and voltage of two S-SCG structures. Both wave included harmonics, but the waveform of S-SCG-B, which has 60 poles, contained fewer harmonics than that of S-SCG-A with 36 poles. In the case of the torque, as shown in Fig. 4-3, the amplitude of the torque ripple for S-SCG-B was reduced when compared with that of S-SCG-A. Also, the voltage and current waveform of S-SCG-B were close to that of a sinusoidal wave. It was therefore possible to realize an improvement of the output waveform.

Table 4-1. Generator dimensions and output characteristics of the S-SCG

Generator	S-SCG-A	S-SCG-B
Stator diameter [m]	5.45	8.2
Rotor diameter [m]	4.82	7.66
Effective length [m]	2.83	1.21
Air gap [mm]	15	15
Pole number	36	60
Field coil dimension	10 × 20.7	10 × 16.5
Armature conductor dimension [mm^2]	33.9 × 35.4	33.9 × 35.4
Slot number/phase, pole	2	2
Slot size [mm^2]	35 × 147	33 × 148
Thickness of back iron [mm]	150	116
Thickness of rotor iron [mm]	200	150
B_{max} [T]	2.6	2.4
Output [MW]	10.0	10.1
Line-to-line voltage [kV_{rms}]	3.29	3.31
Line current [kA_{rms}]	1.77	1.77

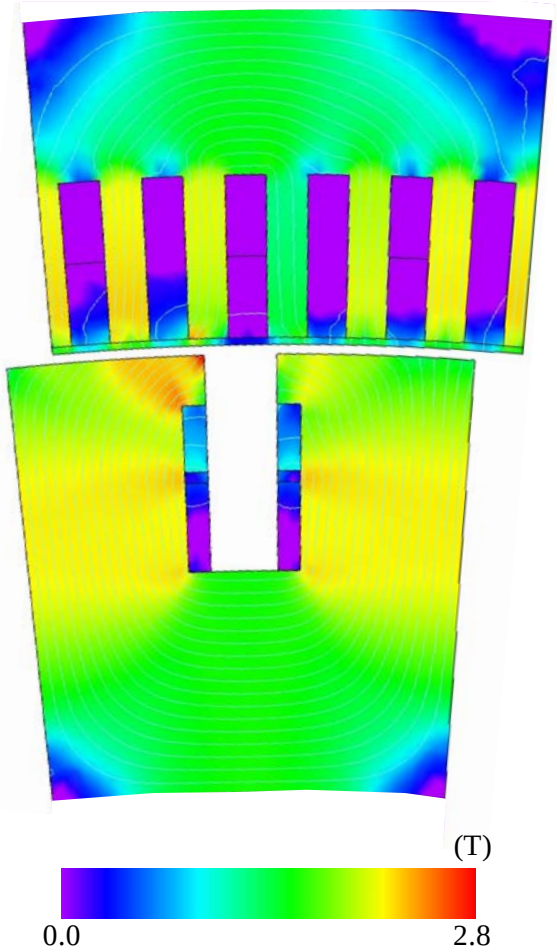

Fig. 4-2. Magnetic flux density distribution of the S-SCG in steady state. This figure is for the case of S-SCG-A.

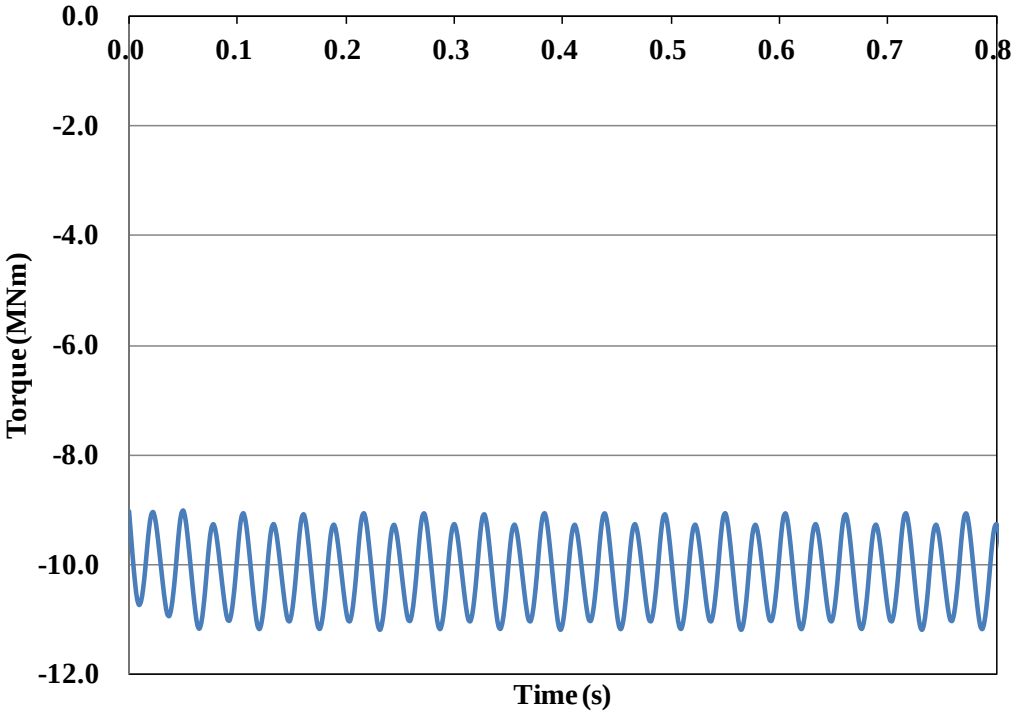

(a) S-SCG-A

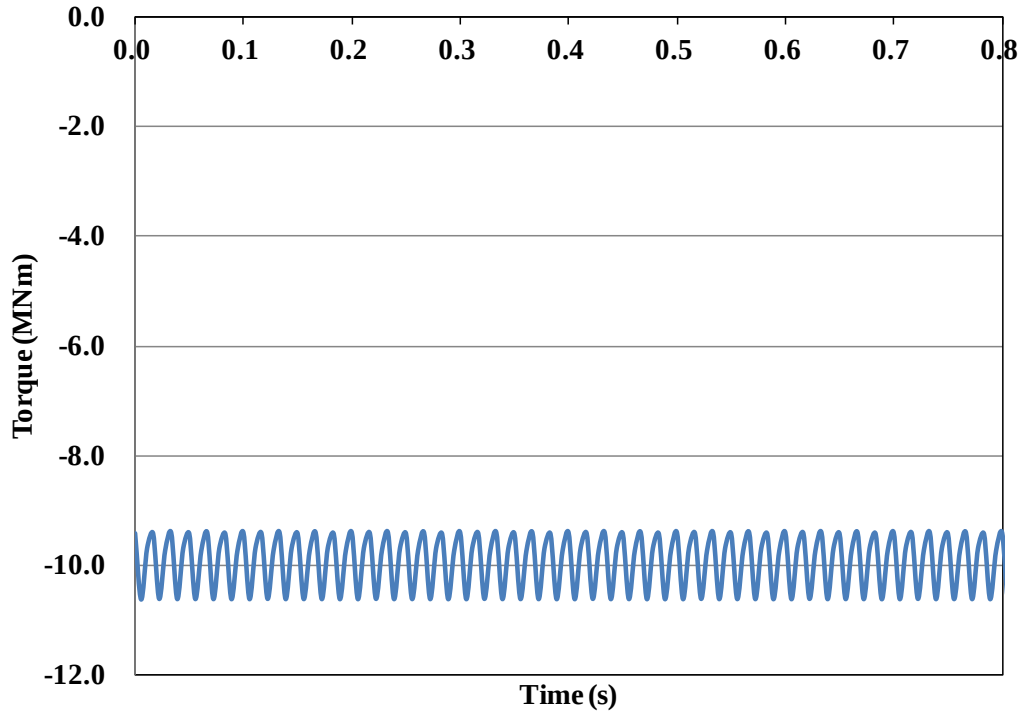

(b) S-SCG-B

Fig. 4-3. Output torque of both S-SCGs. (a) and (b) are the output characteristics of S-SCG-A and S-SCG-B, respectively.

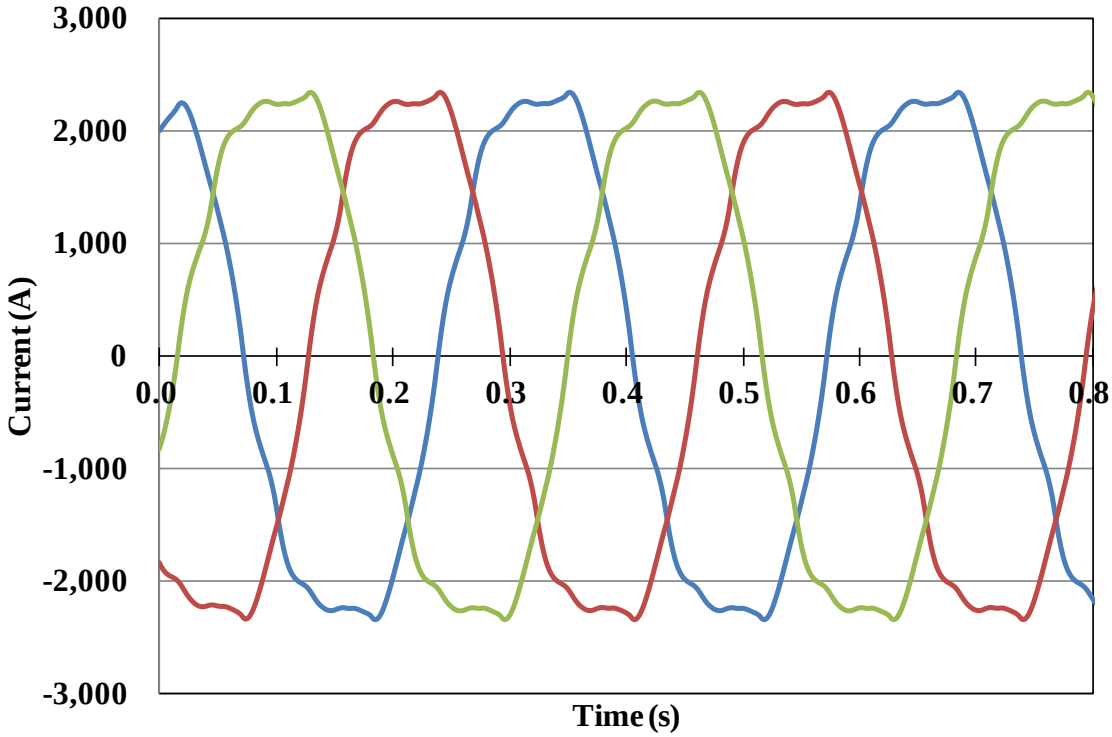

(a) S-SCG-A

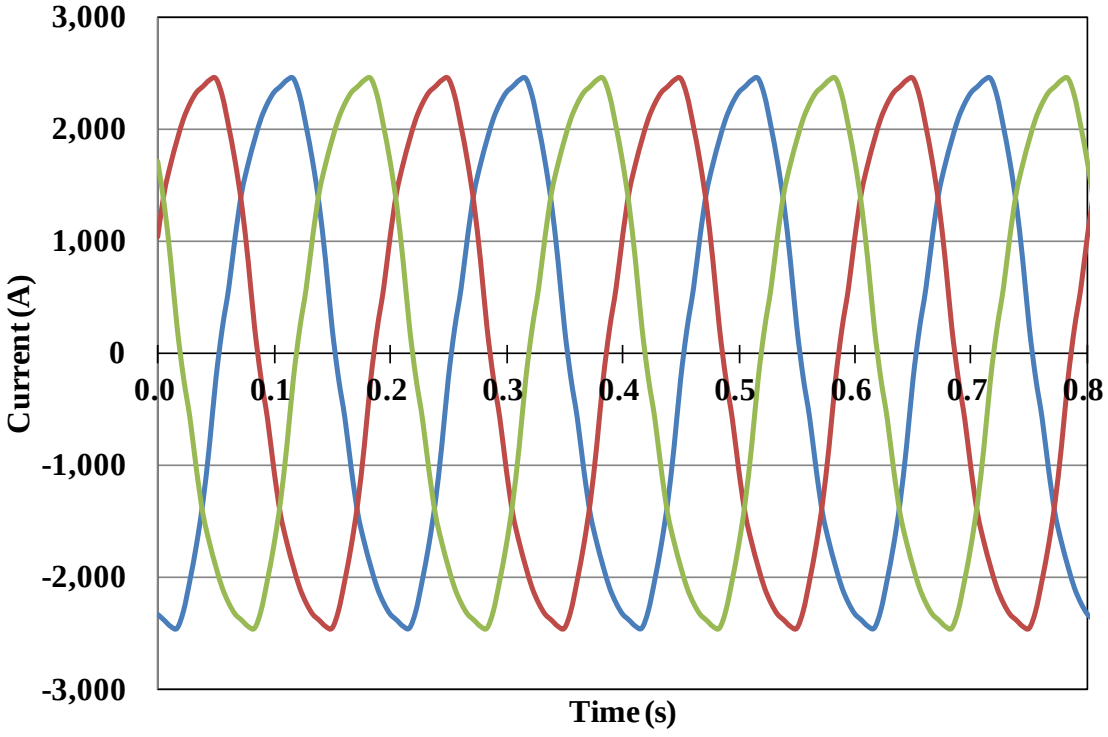

(b) S-SCG-B

Fig. 4-4. Output currents of both S-SCGs. (a) and (b) are the output characteristics of S-SCG-A and S-SCG-B, respectively.

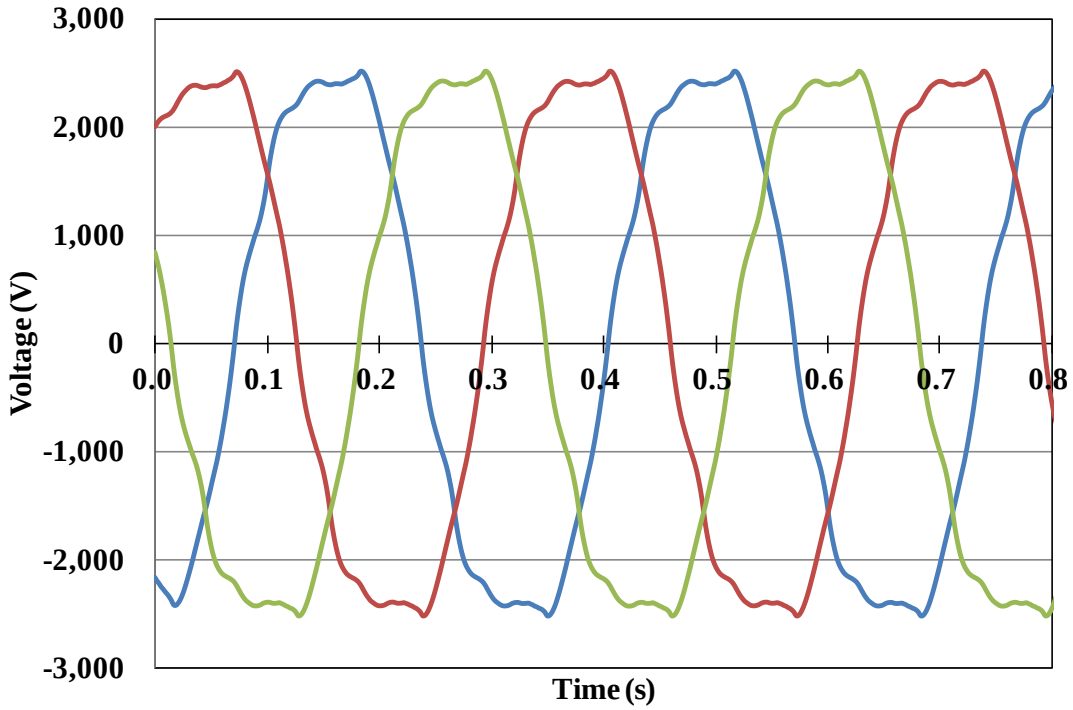

(a) S-SCG-A

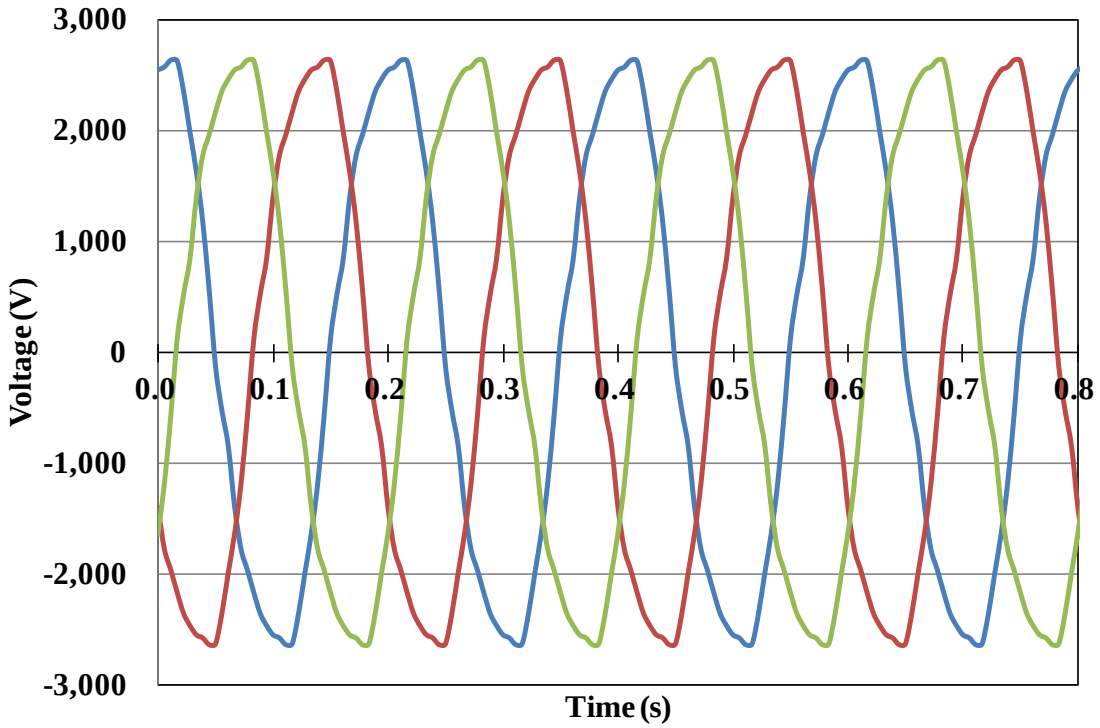

(b) S-SCG-B

Fig. 4-5. Output phase voltages of both S-SCGs. (a) and (b) are the output characteristics of S-SCG-A and S-SCG-B, respectively.

4-1-2-2. Synchronous reactance

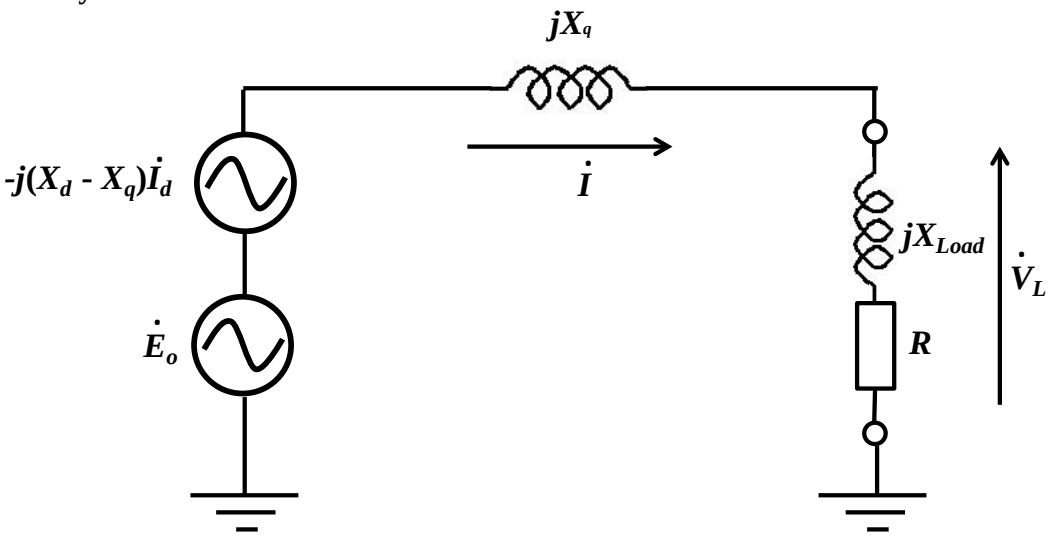

Fig. 4-6. Equivalent circuit for a salient pole type synchronous machine.

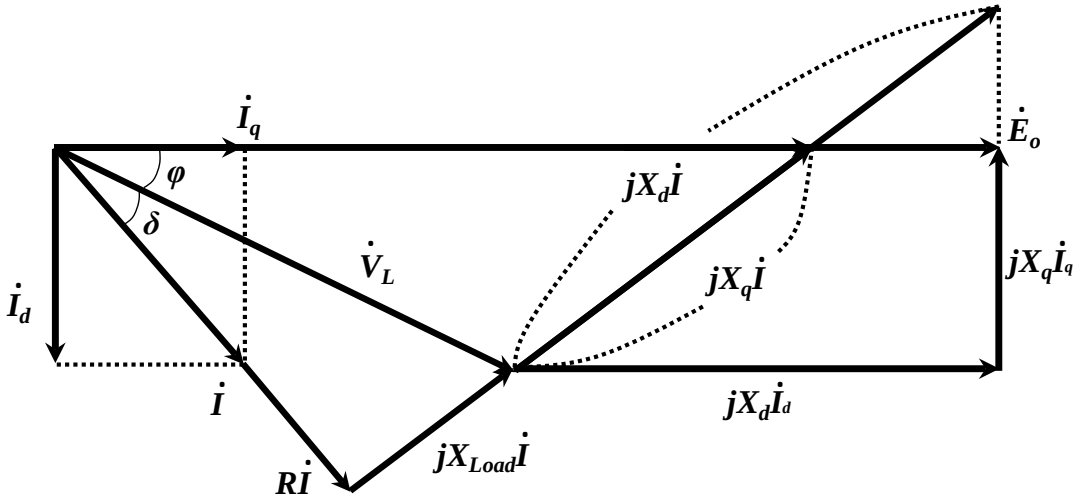

Fig. 4-7. Phasor diagram for a salient pole type synchronous machine.

In this section, we analyze the synchronous reactance of the two S-SCG structures. In general, the equivalent circuit and phasor diagram for salient pole-type synchronous machines are different from those of the nonsalient pole-type shown in chapter 3. Figs. 4-6 and 4-7 show the equivalent circuit and phasor diagram for salient pole-type machines. The generator characteristics should be considered using d and q axis as in the figures.

First, using Kirchhoff's law, the circuit equation in Fig. 3-4 is expressed as follows:

$$\dot{E}_o - j\left(X_d - X_q\right)\dot{I}_d = jX_q\dot{I} + \dot{V}_L \qquad (4.1).$$

$$\dot{V}_L = \left(R + jX_{Load}\right)\dot{I} \tag{4.2}$$

where E_O [V_{rms}], I [A_{rms}], V_L [V_{rms}], R [Ω], and X_{Load} [Ω] are open-phase voltage, line current, loaded-phase voltage, load resistance, and reactance, respectively. Also, j is an imaginary number.

Substituting (2.2) into (2.1), the upper equations are summarized as follows:

$$\dot{E}_o - j\left(X_d - X_q\right)\dot{I}_d = jX_q\dot{I} + \left(R + jX_{Load}\right)\dot{I}. \tag{4.3}$$

So, the equation is

$$\dot{E}_o - j\left(X_d - X_q\right)\dot{I}_d = \left\{R + j\left(X_q + X_{Load}\right)\right\}\dot{I}. \tag{4.4}$$

Now, $\dot{E}_o$, $\dot{I}$, and $\dot{I}_d$ are respectively expressed as follows:

$$\dot{E}_o = \sqrt{2}\,E_o \tag{4.5}$$

$$\dot{I} = \sqrt{2}\,I\ \exp\left\{-j\left(\varphi + \delta\right)\right\} \tag{4.6}$$

$$\dot{I}_d = \sqrt{2}\,I\ \sin\left(\varphi + \delta\right)\exp\left\{-j\frac{\pi}{2}\right\} \tag{4.7}$$

where φ is the phase between E_O and V_L. On the other hand, δ is the load angle with R and X_{Load}.

Substituting (4.5), (4.6), and (4.7) into (4.4), the equation can be expressed as follows:

$$E_o - \left(X_d - X_q\right)I\ \sin\left(\varphi + \delta\right) = \left\{R + j\left(X_s + X_{Load}\right)\right\}I\ \exp\left\{-j\left(\varphi + \delta\right)\right\}. \tag{4}$$

Using Euler's law, the right side of (4.8) is summarized as follows:

$$\begin{aligned}(Right) = {} & \left\{RI\ \cos(\varphi + \delta) + \left(X_q + X_{Load}\right)I\ \sin(\varphi + \delta)\right\} \\ & + j\left\{\left(X_q + X_{Load}\right)I\ \cos(\varphi + \delta) - RI\ \sin(\varphi + \delta)\right\}.\end{aligned} \tag{4.9}$$

By comparing the real and imaginary parts of (4.8) with those of (4.9), the following two equations are obtained.

$$E_o - (X_d - X_q) I \sin(\varphi + \delta) = RI \cos(\varphi + \delta) + (X_q + X_{Load}) I \sin(\varphi + \delta) \quad (4.10).$$

$$0 = (X_q + X_{Load}) I \cos(\varphi + \delta) - RI \sin(\varphi + \delta) \quad (4.11).$$

Using (4.10) and (4.11), X_d and X_q can be obtained as follows:

$$X_d = \frac{E_o}{I \sin(\varphi + \delta)} - \frac{R}{\tan(\varphi + \delta)} - X_{Load}, \quad (4.12).$$

$$X_q = R \tan(\varphi + \delta) - X_{Load}. \quad (4.13).$$

When X_d [Ω] and X_q [Ω] are expressed for the per-unit system, the two synchronous reactances x_d [p.u.] and x_q [p.u.] are obtained using the following equation.

$$x_d = \frac{X_d}{\left(V_L / I\right)} \quad (4.14).$$

$$x_q = \frac{X_q}{\left(V_L / I\right)} \quad (4.15).$$

Table 4-1 shows the calculated synchronous reactance and its parameters. The results show that x_d is lower than that of the PMSG because of the reduced generator size and quantity of materials. Also, S-SCG-B has a value that is 1.3 times higher than that of S-SCG-A, which is owing to their different load reactances. This value is related to the generator frequency. The frequency is estimated from the generator pole number and rotation speed, and results in 3.0 Hz for S-SCG-A and 5.0 Hz for S-SCG-B, respectively. Because S-SCG-A has a frequency lower than that of S-SCG-B, the values of x_d and x_q are low.

Table 4-2. Synchronous reactance and calculated parameters.

Generator	S-SCG-A	S-SCG-B
Open phase voltage: E_o [V_{rms}]	2047	2226
Load phase voltage: V_L [V_{rms}]	1899	1910
Line current: I [A_{rms}]	1772	1774
Load resistance: R [Ω]	1.07	1.07
Load reactance: X_{Load} [Ω]	0.0283	0.11
Phase between E_o and V_L : φ [deg]	14.58	18.9
Load angle: δ [deg]	1.51	5.87
Synchronous Reactance		
X_d [Ω]	0.43	0.57
x_d [p.u.]	0.4	0.52
X_q [Ω]	0.28	0.38
x_q [p.u.]	0.26	0.36

4-1-2-3. Copper and Iron Losses

In this section, we estimate the three phase copper loss, W_{Cu}, and the iron loss, W_{Fe}. The estimated areas of W_{Cu} and W_{Fe} are shown in Fig. 4-8. All the conditions of analysis are the same as those mentioned in chapter 3. In particular, W_{Fe} represents the hysteresis loss of the back iron, and eddy currents are not considered.

Table 4-3 shows the analysis results for two losses. The value of W_{Cu} is higher than that of W_{Fe} in both generator structures. With respect to W_{Cu}, the value for S-SCG-A is higher than that of S-SCG-B because of the length of copper armature windings. As shown in the previous section, the effective length of S-SCG-A is over twice that of S-SCG-B. This results in the different resistance value of 0.031 [Ω] and 0.025 [Ω] for the losses of 292 [kW] and 236 [kW], respectively. For S-SCG-A, W_{Cu} is almost 3.0% of the total output. If W_{Fe} is added to W_{Cu}, the total loss will increase to over 3.6%. Also, with the addition of other losses, it may exceed 4.0%, and this machine will not be considered to be as efficient. On the other hand, the losses of S-SCG-B are almost 280 kW, which is 2.8% of the total output. Finally, this loss may be around 3.0% after adding the other losses. While this value is not so low, it is better than that of S-SCA. From the viewpoint of generator efficiency, S-SCG-B is better than S-SCG-A and PMSG.

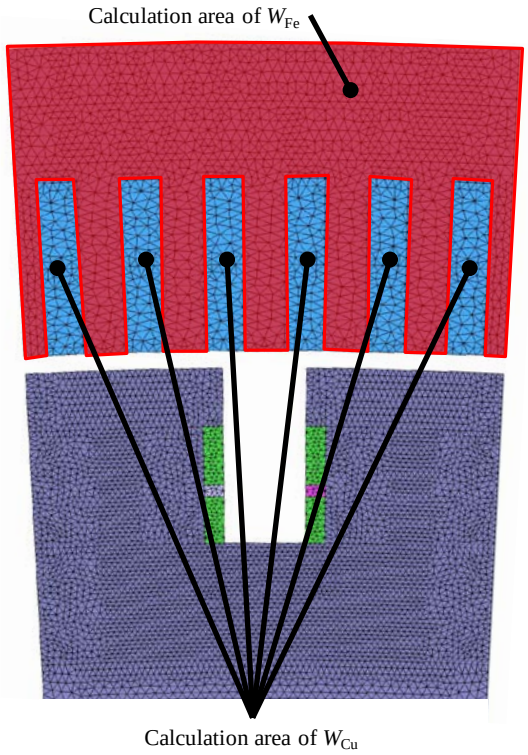

Fig. 4-8. Calculation areas of generator losses for S-SCG (Periodic model).

Table 4-3. Calculation results of copper and iron losses

Generator	S-SCG-A	S-SCG-B
Armature resistance per phase: R_U [Ω]	0.031	0.025
Line current: I [A_{rms}]	1772	1774
Three phase Copper loss: W_{Cu} [kW]	292	236
Iron loss of the back iron: W_{Fe} [kW]	68.5	42.5

4-2. Discussions of the Generator Performances

The electromagnetic characteristics of two S-SCG structures in steady state are summarized in Table 4-4. With respect to the YBCO superconducting wire length, both structures require lengths that are less than several tens of kilometers. In general, superconducting generators that are studied worldwide require several hundreds of kilometers of HTS wires for field coils, as shown in chapter 1. By comparing them with S-SCG, we can significantly reduce the generator cost because of the considerable use of iron. By focusing on individual generators, the YBCO length of S-SCG-B is almost 60% of that of S-SCG-A in spite of a higher pole structure. On the other hand, the generator weight is almost the same. The difference between them is almost 6.0 tons. With respect to the generator size, efficiency, and cost, S-SCG is suitable for higher pole number and larger pole structure.

Table 4-4. Electromagnetic characteristics of the 10 MW class S-SCG.

Generator	S-SCG-A	S-SCG-B
Stator Diameter [m]	5.45	8.2
Effective length [m]	2.83	1.21
Output [MW]	10.0	10.1
Line current [A_{rms}]	1.77	1.77
Line-to-line voltage [kV_{rms}]	3.29	3.31
Pole number	36	60
Operating temperature [K]	33	33
Rotor		
Field	YBCO	YBCO
Coil current density [A/m^2]	1.8×10^8	1.8×10^8
B_{max} [T]	2.6	2.4
Wire length [km]	62.0	36.9
Stator		
Conductor	Cu	Cu
Wire length [km]	2.8	2.3
Synchronous reactance [pu]	0.4	0.52
Copper loss [kW]	292	236
Iron loss [kW]	68.5	42.5
Weight		
Irons [tons]	124.3	121.4
Copper [tons]	14.8	12.1
YBCO [tons]	0.54	0.32
Total weight [tons]	139.6	133.8

4-3. Transient Analysis for Three-phase Short-Circuit Problems

4-3-1. Analysis Models and Conditions

This section deals with the sudden three-phase short-circuit problem, which is the most serious kind of accident in short-circuit problems. The equivalent circuit for this analysis is the same as that of the PMSG mentioned in chapter 3.

4-3-2. Analysis Results

Fig. 4-9 shows the magnetic flux density distribution of S-SCG-A in the short-circuit state. Compared with Fig. 4-2, the difference was clear. The magnetic flux did not flow in a circular direction in the back iron. Also, the strength of the magnetic flux density decreased because the magnetic flux generated by the short-circuit current influenced the rotor side magnetic field

owing to YBCO field coils. With respect to the transient torque shown in Fig. 4-10, the maximum transient value for S-SCG-B (17.3 MNm) was less than that of S-SCG-A (21.1 MNm) because of the higher synchronous reactance. However, the convergence value was almost the same. Figs. 4-11 and 4-12 show the short-circuit current and voltage, respectively. The maximum transient current of S-SCG-B (7.62 kA_{max}) was also lower than that of S-SCG-A (9.44 kA_{max}). However, compared with the results for the PMSG, the transient torque and current of S-SCG structures were higher because of its lower synchronous reactance relative to that of the PMSG structure.

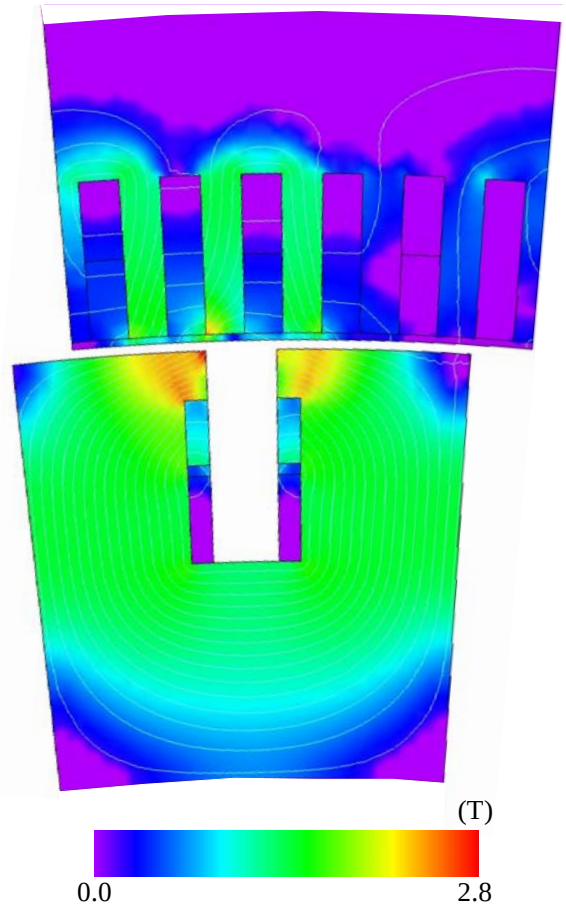

Fig. 4-9. Magnetic flux distribution of the S-SCG in the short-circuit state. This figure is for the case of S-SCG-A.

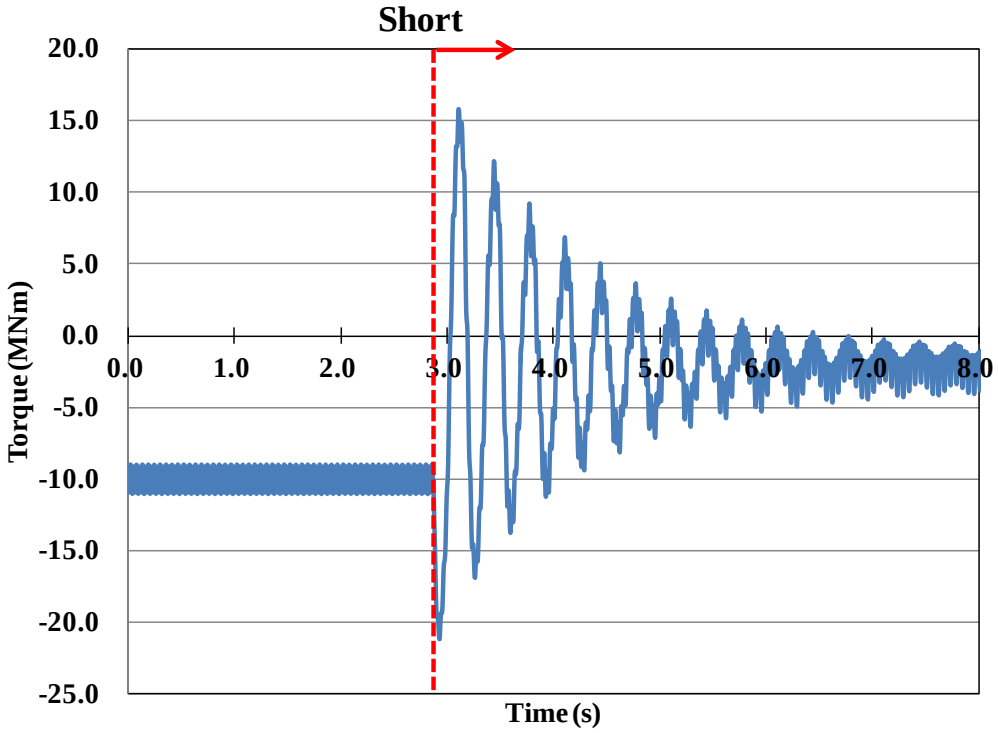

(a) S-SCG-A

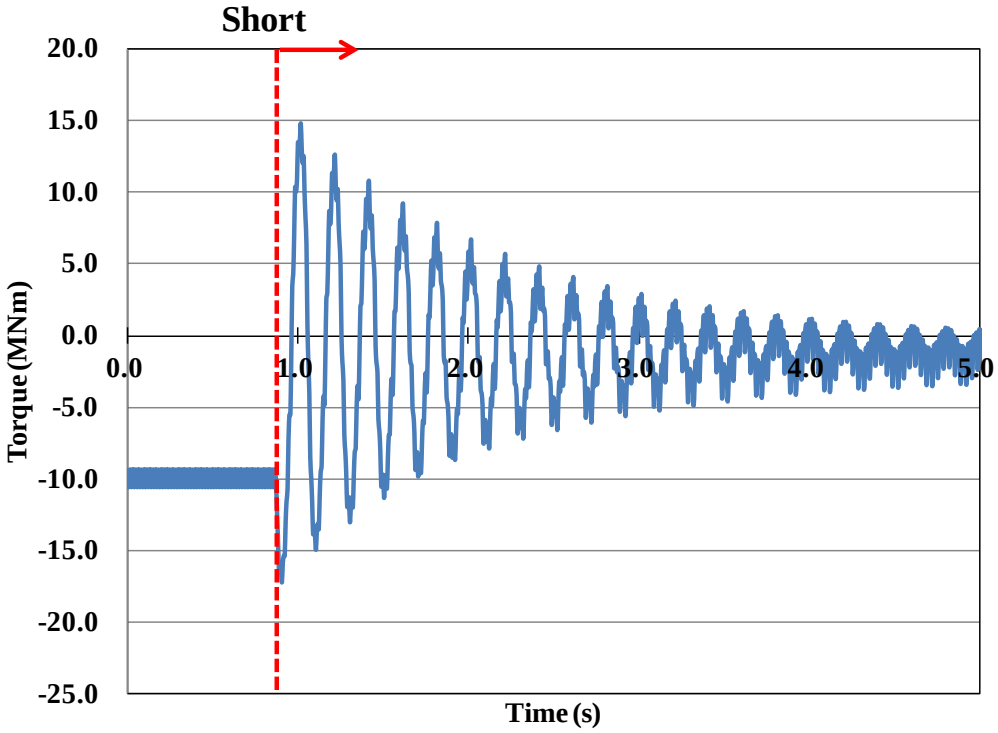

(b) S-SCG-B

Fig. 4-10. Short-circuit torque of both S-SCGs. (a) and (b) are the output characteristics of S-SCG-A and S-SCG-B, respectively.

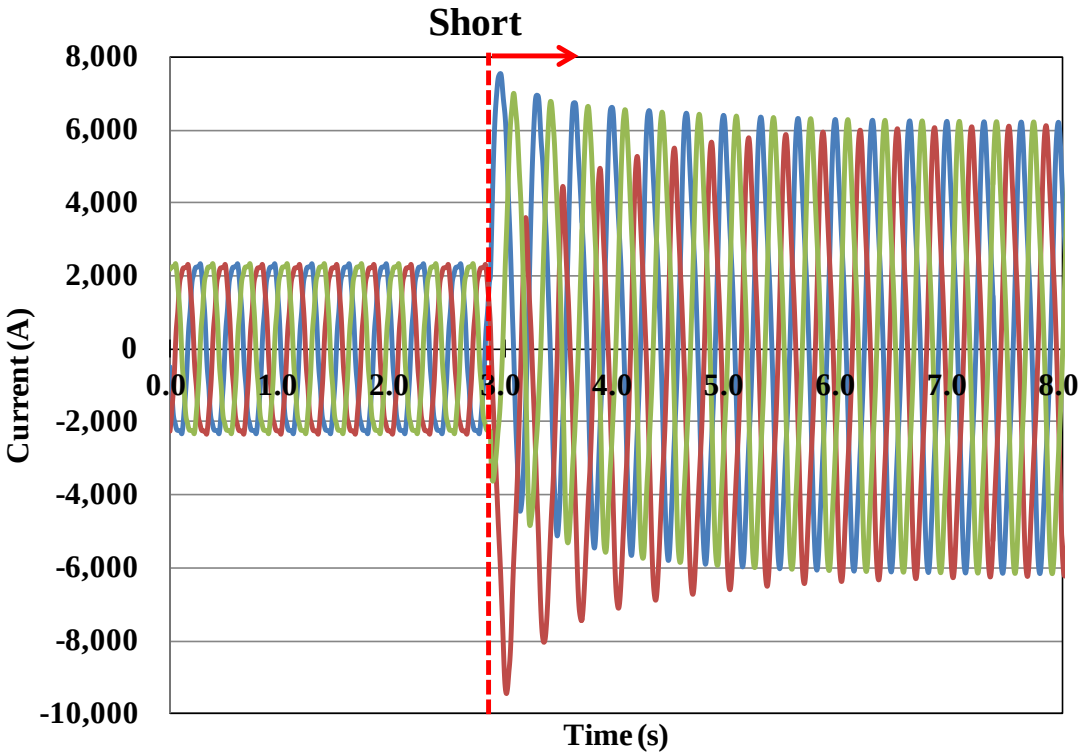

(a) S-SCG-A

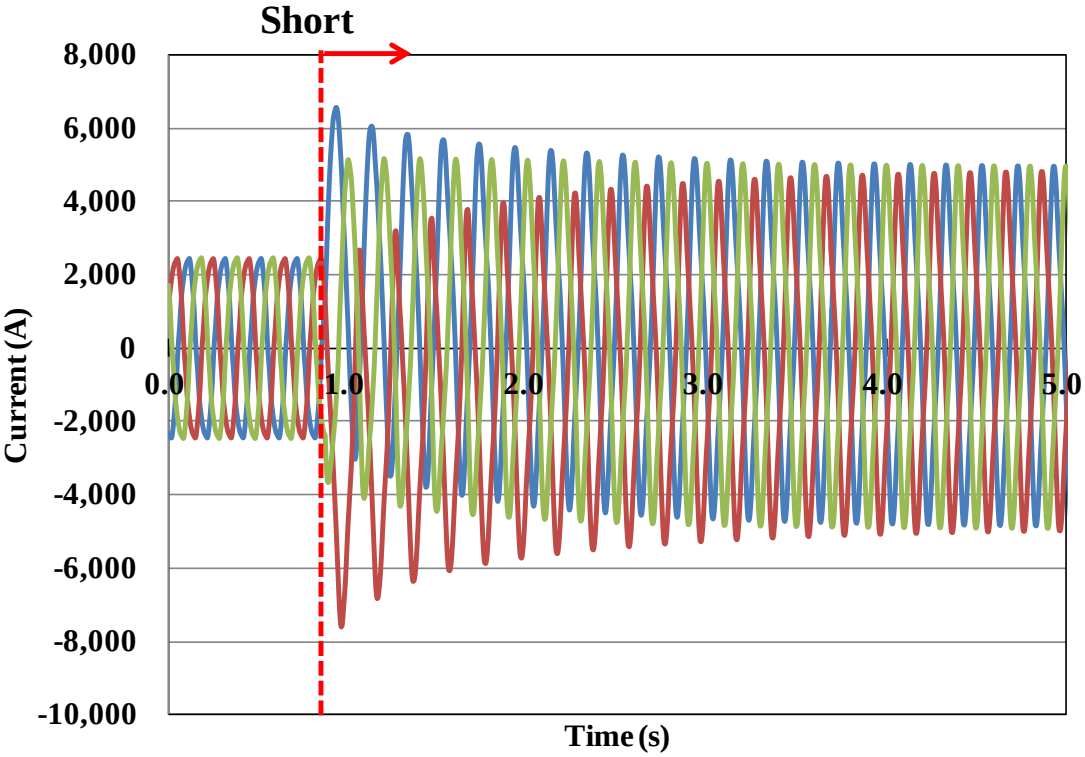

(b) S-SCG-B

Fig. 4-11. Short-circuit currents of both S-SCGs. (a) and (b) are the output characteristics of S-SCG-A and S-SCG-B, respectively.

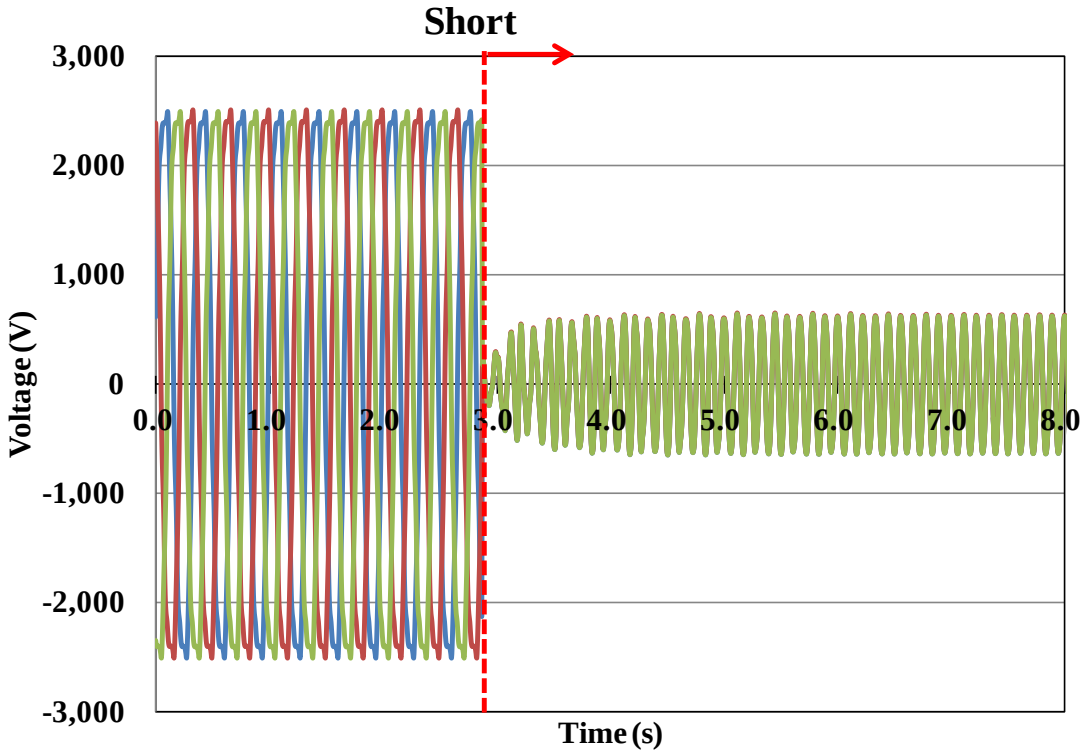

(a) S-SCG-A

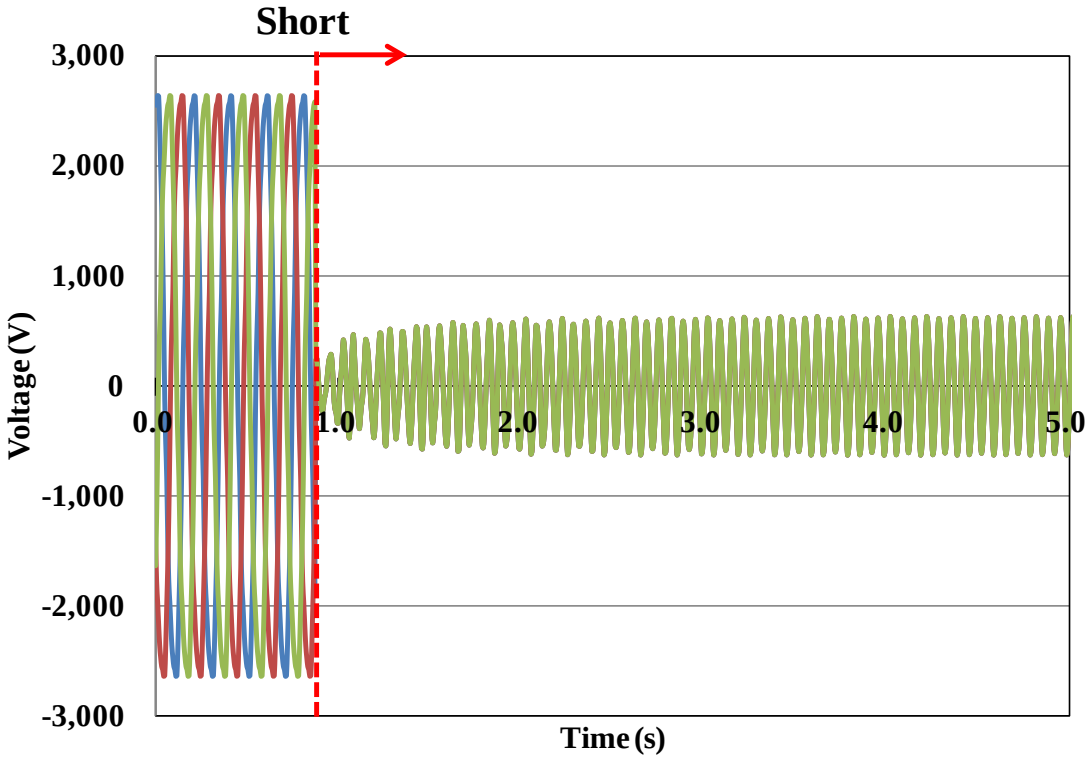

(b) S-SCG-B

Fig. 4-12. Short-circuit phase voltages of both S-SCGs. (a) and (b) are the output characteristics of S-SCG-A and S-SCG-B, respectively.

4-4. Summary of Chapter 4

This chapter discussed the electromagnetic design of salient pole-type superconducting generators (S-SCG) using 2D FEM. Two types of generators with different pole numbers and outer diameters were designed and investigated. The results showed that S-SCG can lead to a reduction in the generator diameter of over 30 percent when compared to PMSG. Also, the required length of YBCO superconducting wire was several tens of kilometers because of the use of a large amount of iron. This may contribute to the volume and cost reduction.

Focusing on the individual generators, S-SCG-B, which has a larger diameter and higher pole number, had better performances. It may be concluded that S-SCG is suitable for the design of multiple and larger diameter structures. Also, in the case of transient analysis, the transient torque was almost the same as that of PMSG. However, the transient current value was a little higher than that of PMSG because of its lower synchronous reactance.

Chapter 5

Electromagnetic Design of

Non-salient Pole type Superconducting Generators

5-1. Steady State Analysis

5-1-1. Analysis Models and Conditions

This chapter deals with the electromagnetic design of non-salient pole type superconducting generators (NS-SCG). This is an air-cored structure, and is expected to be lighter than S-SCG structures. Fig. 5-1 shows the FEM analysis model for the NS-SCG structure. Two types of generators with diameters of around 4.0 and 8.0 m were designed, and are referred to as NS-SCG-A and NS-SCG-B, respectively. From the perspective of the cost reduction of the YBCO field coils, a 12-pole generator was chosen. The air gap was set to be 100 mm, including the vacuum thermal insulation layer and cryostat wall layer. On the other side, 100 mm of the mechanical space between the field coils and rotor iron was set for the thermal insulation layer. The operating temperature was set to 22 K.

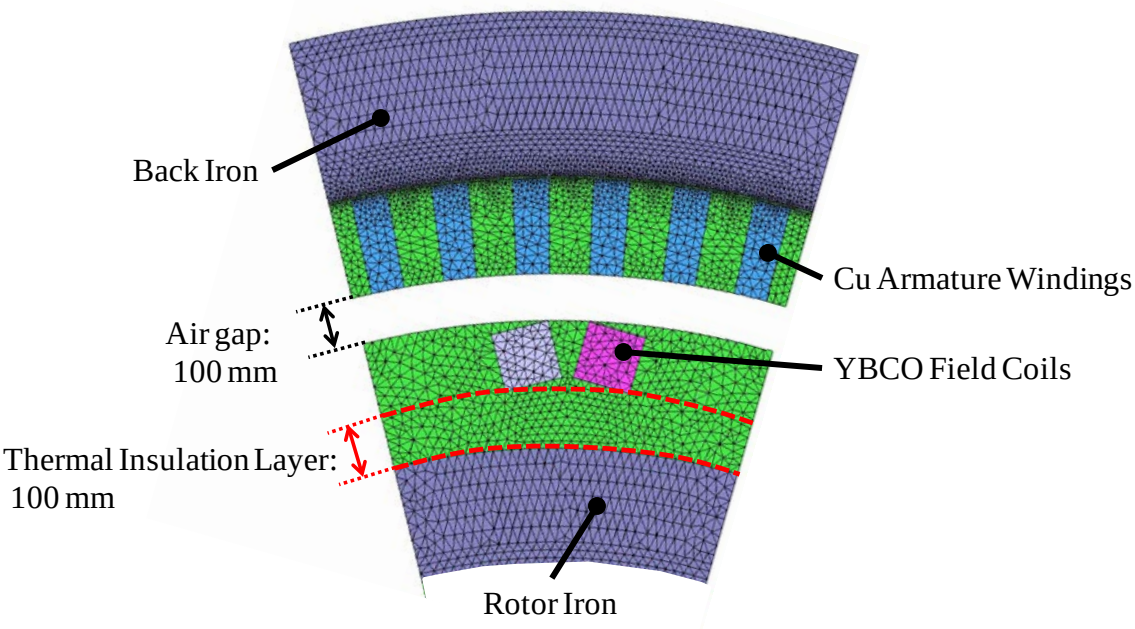

Fig. 5-1. FEM analysis model for the NS-SCG (1/12 periodic model).

5-1-2. Analysis Results

5-1-2-1. Generator Dimensions and Outputs

Table 5-1 represents the generator dimensions and output characteristics of the two NS-SCG structures. Both structures were able to successfully realize an output power of 10.0 MW. The diameter of NS-SCG-B was almost 1.8 times higher than that of NS-SCG-A. However, the effective length of NS-SCG-B was only 0.5 m. On the other hand, the increase in the diameter influenced the thickness of the rotor iron. The rotor iron thickness of NS-SCG-B is 600 mm, and 2.4 times thicker than that of NS-SCG-A (250 mm). This is because the magnetic flux of NS-SCG-B induced a larger loop, and required the addition of a large amount of iron to prevent magnetic flux leakage. Fig. 5-2 shows the magnetic flux distribution of NS-SCG-A. The back and rotor iron area are saturated because of the high magnetic field at the field coils. By focusing on the maximum magnetic flux density of the two generators, they both generated almost the same value of around 8.3 T, which implies that the design of a supporting structure for YBCO superconductor field coils is technically challenging. Compared with the S-SCG structures, these values are somewhat high. Figs. 5-3 to 5-5 represent the waveforms of torque, current, and voltage, respectively. The results indicate that the waveforms of NS-SCG-B possessed many harmonics because of the expansion of the coil pitch due to a larger diameter. On the other hand, NS-SCG-A possessed only a few harmonics, and the current and voltage waveform is a clear, sinusoidal wave because of its air-cored structure.

Table 5-1. Generator dimensions and output characteristics of the two NS-SCGs

Generator	NS-SCG-A	NS-SCG-B
Stator diameter [m]	4.7	8.4
Rotor diameter [m]	3.4	7.1
Effective length [m]	1.6	0.5
Air gap [mm]	100	100
Pole number	12	12
Field coil dimension [mm^2]	125 × 125	125 × 125
Cu conductor dimension [mm^2]	33.9 × 35.4	33.9 × 35.4
Slot number/phase, pole	2	5
Slot size [mm^2]	71 × 204	62.3 × 154
Thickness of back iron [mm]	350	400
Thickness of rotor iron [mm]	250	600
B_{max} [T]	8.4	8.2
Output [MW]	10.1	10.0
Line-to-line voltage [kV_{rms}]	3.33	3.31
Line current [kA_{rms}]	1.77	1.76

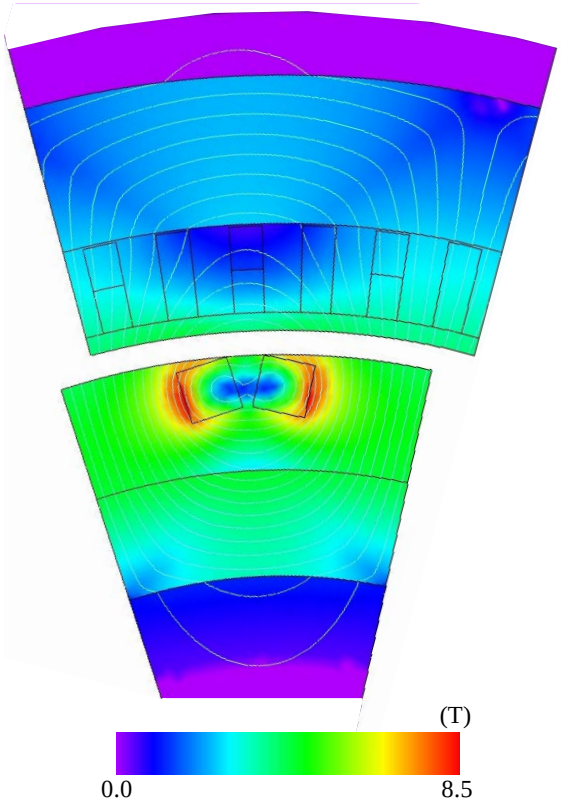

Fig. 5-2. Magnetic flux density distribution of NS-SCG in steady state. This figure is for the case of NS-SCG-A.

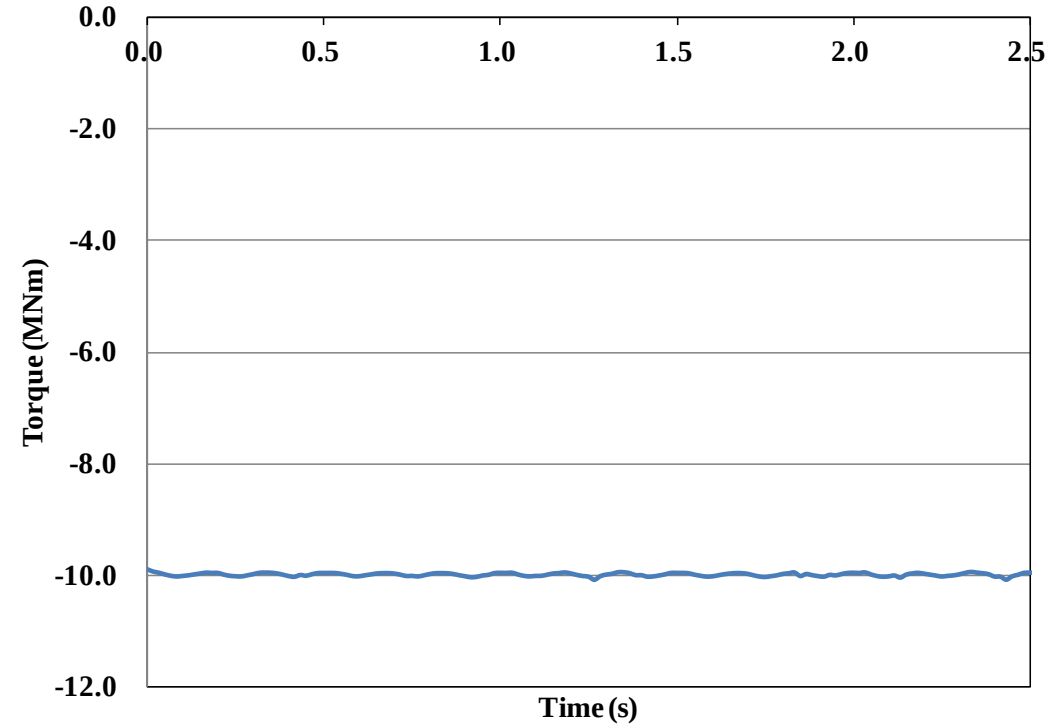

(a) NS-SCG-A

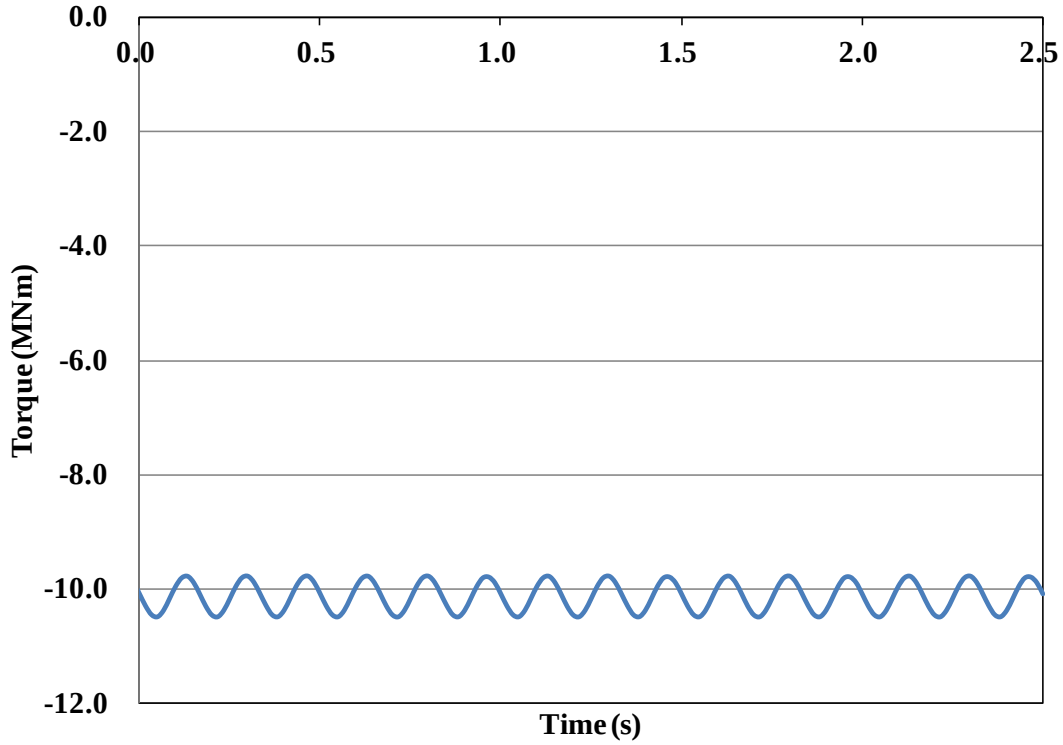

(b) NS-SCG-B

Fig. 5-3. Output torque of both NS-SCGs. (a) and (b) are the output characteristics of NS-SCG-A and NS-SCG-B, respectively.

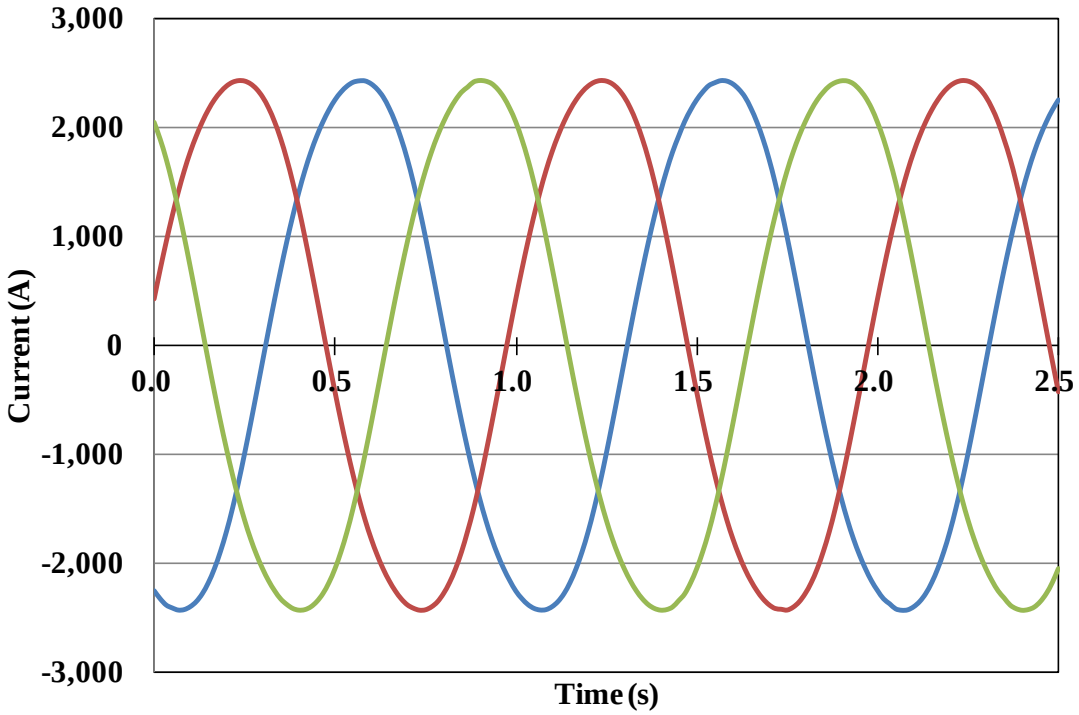

(a) NS-SCG-A

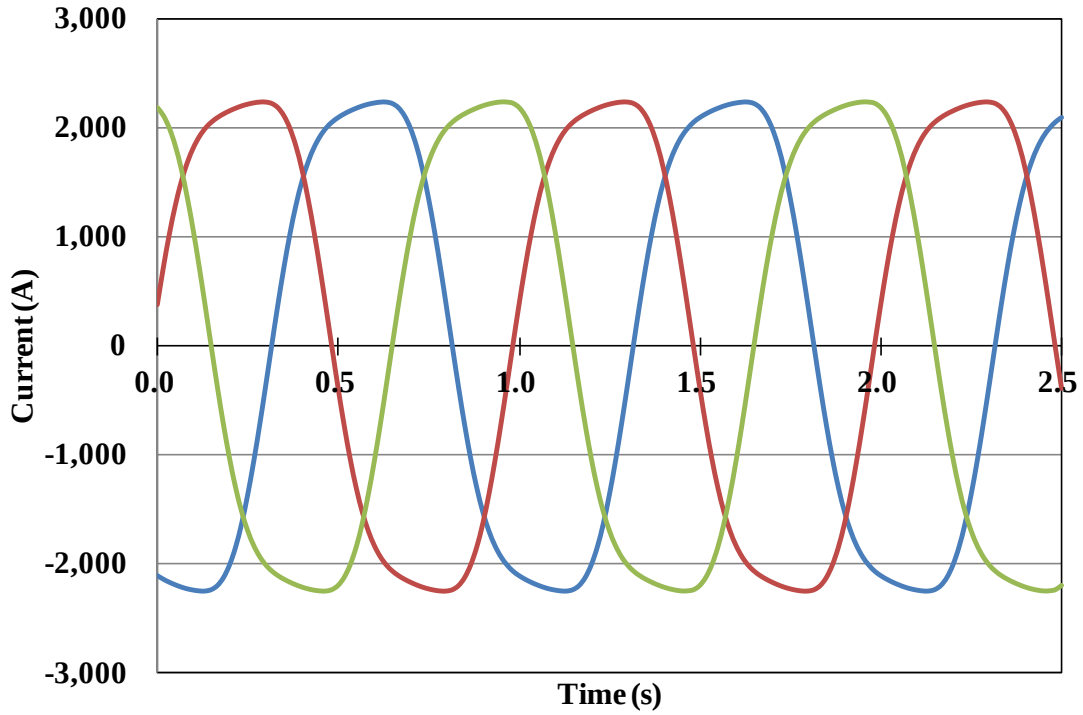

(b) NS-SCG-B

Fig. 5-4. Output current of both NS-SCGs. (a) and (b) are the output characteristics of NS-SCG-A and NS-SCG-B, respectively.

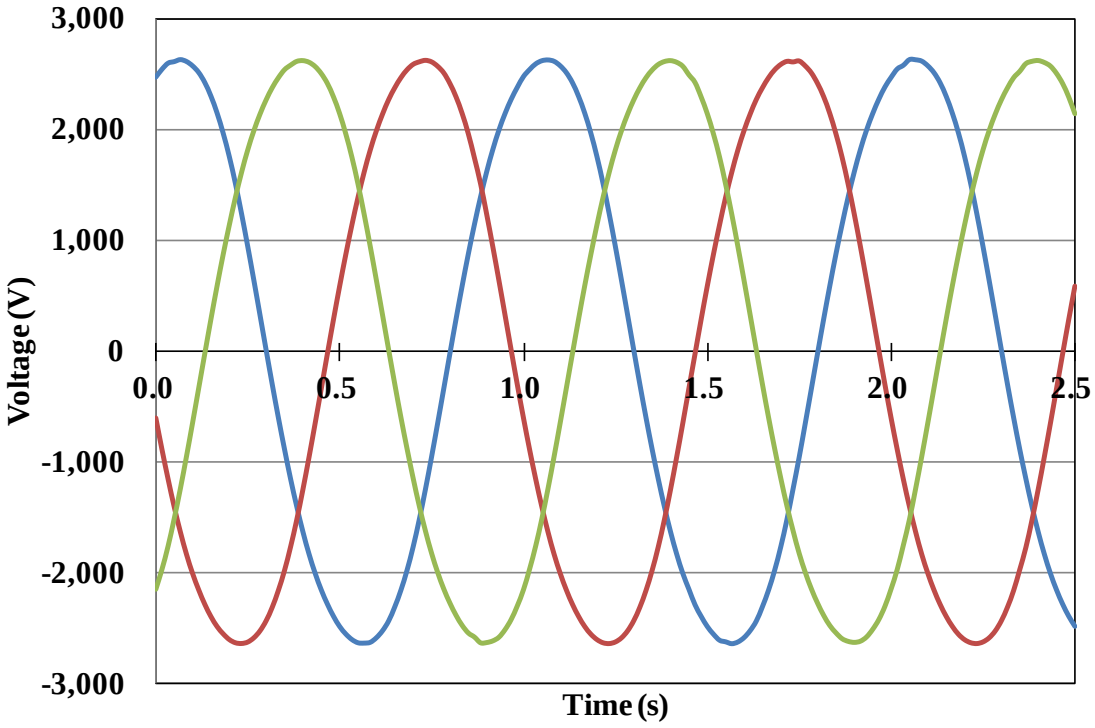

(a) NS-SCG-A

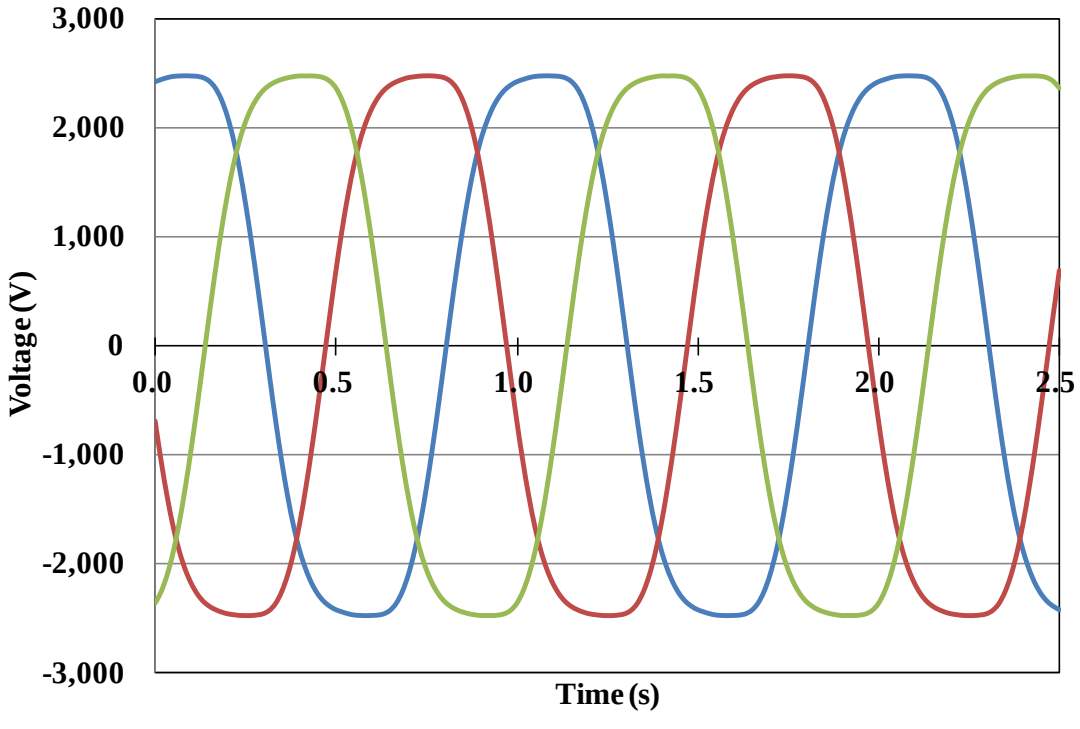

(b) NS-SCG-B

Fig. 5-5. Output phase voltage of both NS-SCGs. (a) and (b) are the output characteristics of NS-SCG-A and NS-SCG-B, respectively.

5-1-2-2. Synchronous reactance

In this section, we estimate the synchronous reactance of the NS-SCG structure. The equivalent circuit and phasor diagram are the same as those mentioned in chapter 3.

Table 5-2 shows the calculation results for both NS-SCG structures. Both values were almost the same, i.e., 0.2 and 0.25, respectively. Compared with the values in the previous chapters, these values are somewhat low because of the air-cored structures of NS-SCG.

Table 5-2. Synchronous reactance and calculated parameters of both NS-SCGs.

Generator	NS-SCG-A	NS-SCG-B
Open voltage: E_o [V_{rms}]	1971	1981
Load voltage: V_L [V_{rms}]	1921	1911
Line current: I [A_{rms}]	1772	1764
Load resistance: R [Ω]	1.08	1.08
Load reactance: X_{Load} [Ω]	0.05	0.04
Synchronous Reactance		
X_S [Ω]	0.22	0.27
x_S [p.u.]	0.2	0.25

5-1-2-3. Copper and Iron Losses

In this section, we estimated the three phase copper loss, W_{Cu}, and the iron loss, W_{Fe}. The estimated area of W_{Cu} and W_{Fe} are shown in Fig. 5-6. All of the conditions of analysis are the same as those mentioned in chapter 3. In particular, W_{Fe} refers to the hysteresis loss of the back iron, and eddy currents are not considered.

Table 5-3 represents the calculation results of W_{Cu} and W_{Fe}. Both losses are somewhat high for each generator. To date, even the highest value, W_{Fe}, was less than 0.7% of the output. However, in the case of the NS-SCG structure, both W_{Fe} were almost 1.0%. In particular, the W_{Fe} of NS-SCG-B was over 1.4% (142.1 kW) of the total output. This is because the higher magnetic field, which is over 2.0 T, was distributed in the back iron. In addition, the W_{Cu} for both structures was also 2.3–3.4 % of the total output. For NS-SCG-B, W_{Cu} was higher than that of NS-SCG-A because the expansion of the outer diameter results in an increase in the length of the copper armature windings. Also, the sum of the losses of NS-SCG-B was estimated to be almost 4.8%. If other losses such as mechanical and cooling are added to these losses, the total efficiency would be around 90%, which is not considered to be efficient for superconducting generators studied worldwide. From the viewpoint of the efficiency of generators, the NS-SCG structure had low performances compared with those of the PMSG and S-SCG structures.

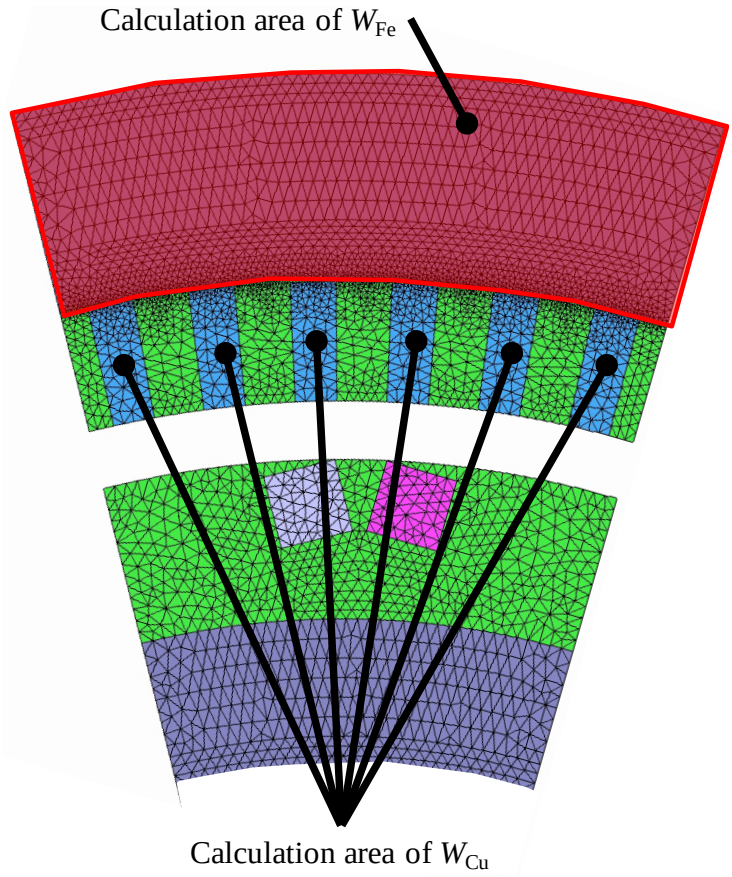

Fig. 5-6. Calculated areas of generator losses for NS-SCG (1/12 periodic model).

Table 5-3. Calculation results for copper and iron losses

Generator	NS-SCG-A	NS-SCG-B
Armature resistance per phase: R_U [Ω]	0.024	0.036
Line current: I [A_{rms}]	1772	1764
Three phase Copper loss: W_{Cu} [kW]	226	336
Iron loss of the back iron: W_{Fe} [kW]	92.8	142.1

5-2. Discussions of the Generator Performances

The electromagnetic characteristics of the two NS-SCG structures are summarized in Table 5-4. As shown in the previous sections, these structures generate an output power of 10 MW with high copper and iron losses. With respect to the number of YBCO field coils, NS-SCG-A and NS-SCG-B require YBCO wires with lengths of 1240 km and 876.6 km, respectively. Compared with the S-SCG structures, the YBCO length of NS-SCG is somewhat high because of its air-cored structure and large air gap (e.g., 100 mm). NS-SCG-A has a smaller diameter and is lighter than S-SCG. However, it requires a large magnetic motive force instead of a smaller quantity of iron. NS-SCG appears to have a few advantages for 10 MW class wind turbine generators.

Table 5-4. Electromagnetic characteristics of the 10 MW class NS-SCG.

Generator	NS-SCG-A	NS-SCG-B
Stator Diameter [m]	4.7	8.4
Effective length [m]	1.6	0.5
Output [MW]	10.1	10.0
Line current [kA_{rms}]	1.77	1.76
Line-to-line voltage [kV_{rms}]	3.33	3.31
Pole number	12	12
Operating temperature [K]	22	22
Rotor		
Field	YBCO	YBCO
Coil current density [A/m^2]	1.45×10^8	1.45×10^8
B_{max} [T]	8.4	8.2
Wire length [km]	1240	876.6
Stator		
Conductor	Cu	Cu
Wire length [km]	2.1	3.2
Synchronous reactance [pu]	0.2	0.25
Copper loss [kW]	226	336
Iron loss [kW]	92.8	142.1
Weight		
Irons [tons]	85.6	202
Copper [tons]	11.4	17.4
YBCO [tons]	10.8	7.63
Total weight [tons]	107.8	227

5-3. Transient Analysis for Three-phase Short-Circuit Problems

5-3-1. Analysis Models and Conditions

This section deals with the sudden three-phase short-circuit problem, which is the most serious accident case of all short-circuit problems. The equivalent circuit for this analysis is the same as that mentioned in chapter 3.

5-3-2. Analysis Results

Fig. 5-7 shows the magnetic flux distribution of NS-SCG-A. Because of the higher magnetic flux density due to YBCO field coils, a magnetic field of over 5.0 T was generated, even for the armature winding area. Figs. 5-8 to 5-10 show the waveforms of the torque, current, and voltage, respectively. In particular, the transient values of torque and current for the two machines were quite high. In the case of the transient torque, it was over 160 MNm for both generators. These values were over 16 times higher than the rated torque of 10 MNm. Also, the maximum transient current values were over 50,000 A_{max}, which was over 20 times higher than that of the rated current of 2,500 A_{max} (= 1770 A_{rms}). These were because of the low synchronous reactance value shown in the previous section. These results show that synchronous machines having very low synchronous reactances are risky in cases involving short-circuit trouble.

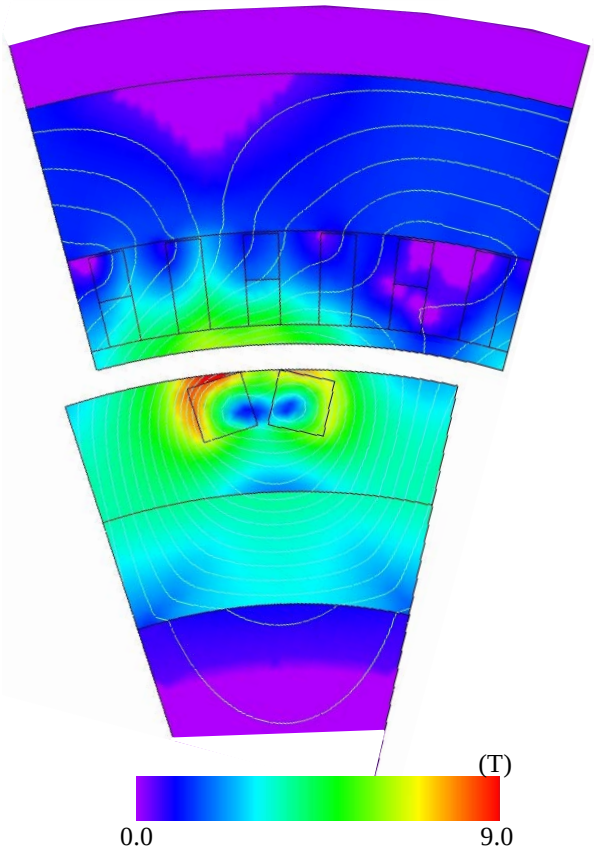

Fig. 5-7. Magnetic flux distribution of NS-SCG in short-circuit state. This figure is for the case of NS-SCG-A.

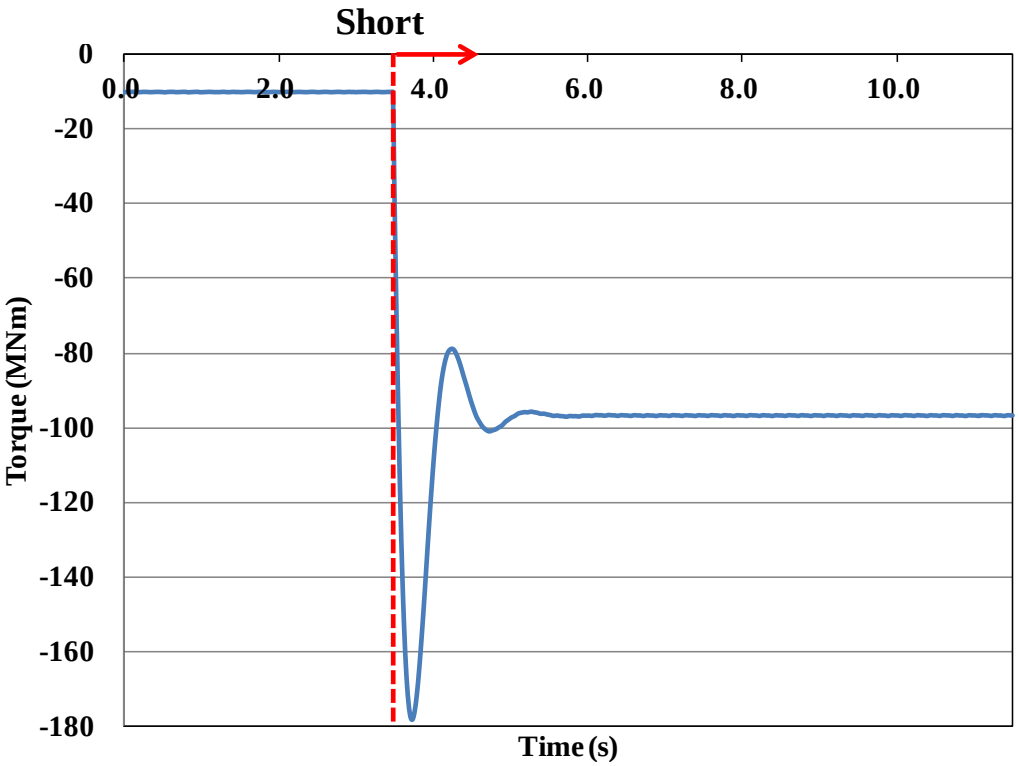

(a) NS-SCG-A

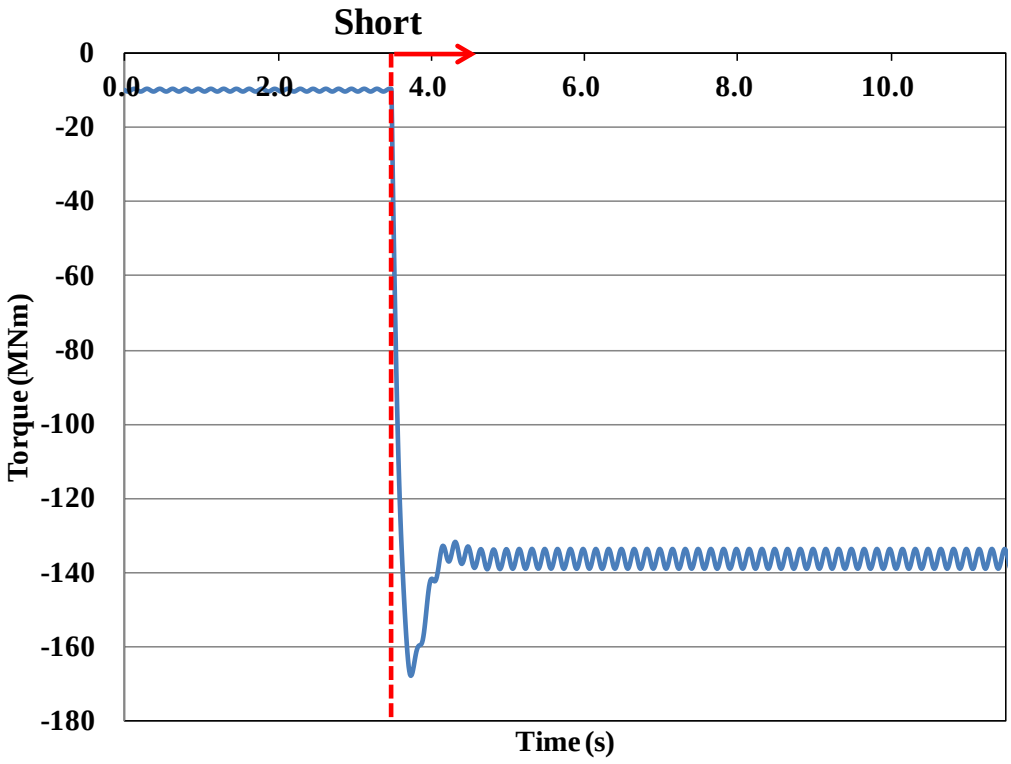

(b) NS-SCG-B

Fig. 5-8. Short-circuit torque of both NS-SCGs. (a) and (b) are the output characteristics of NS-SCG-A and NS-SCG-B, respectively.

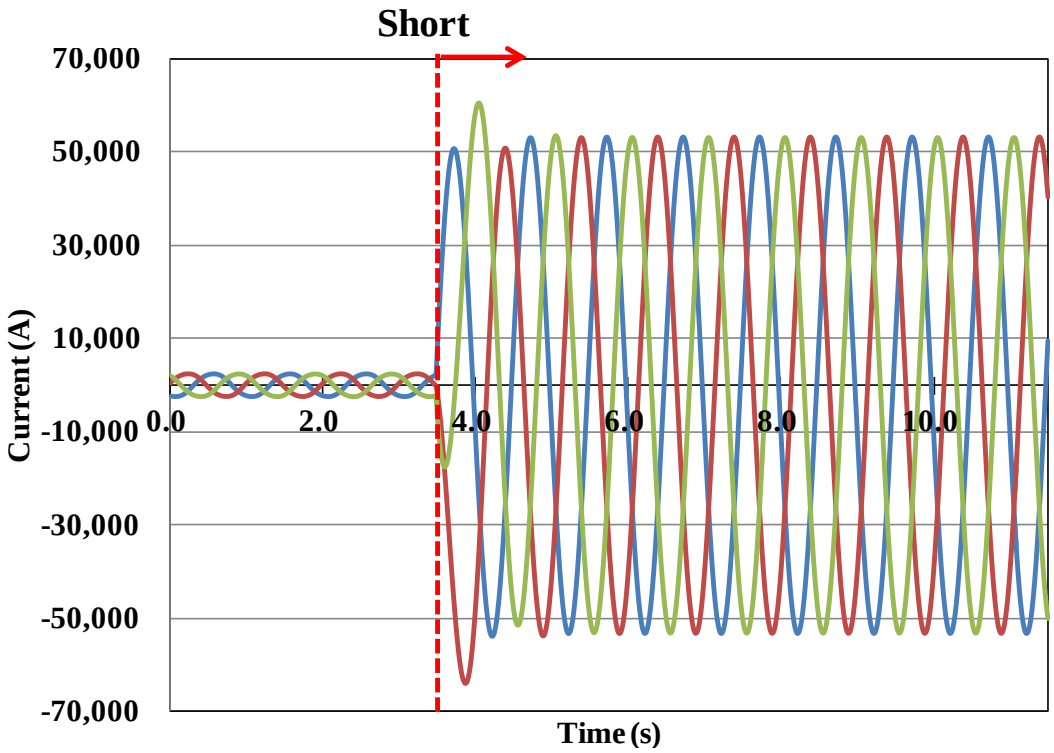

(a) NS-SCG-A

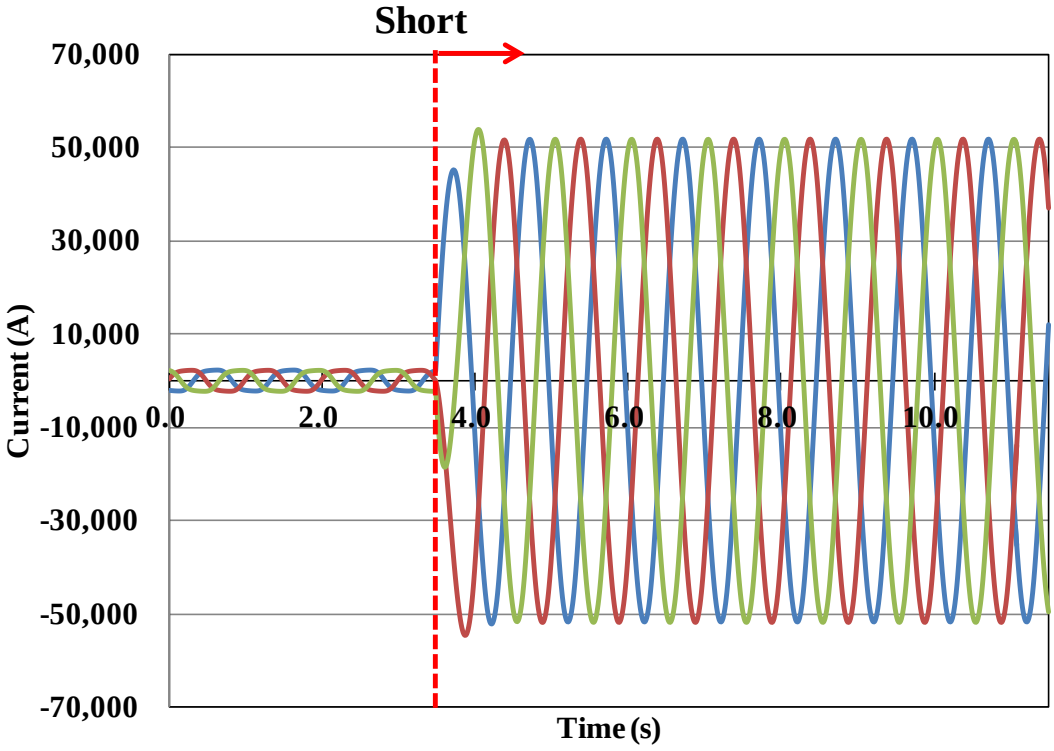

(b) NS-SCG-B

Fig. 5-9. Short-circuit currents of both NS-SCGs. (a) and (b) are the output characteristics of NS-SCG-A and NS-SCG-B, respectively.

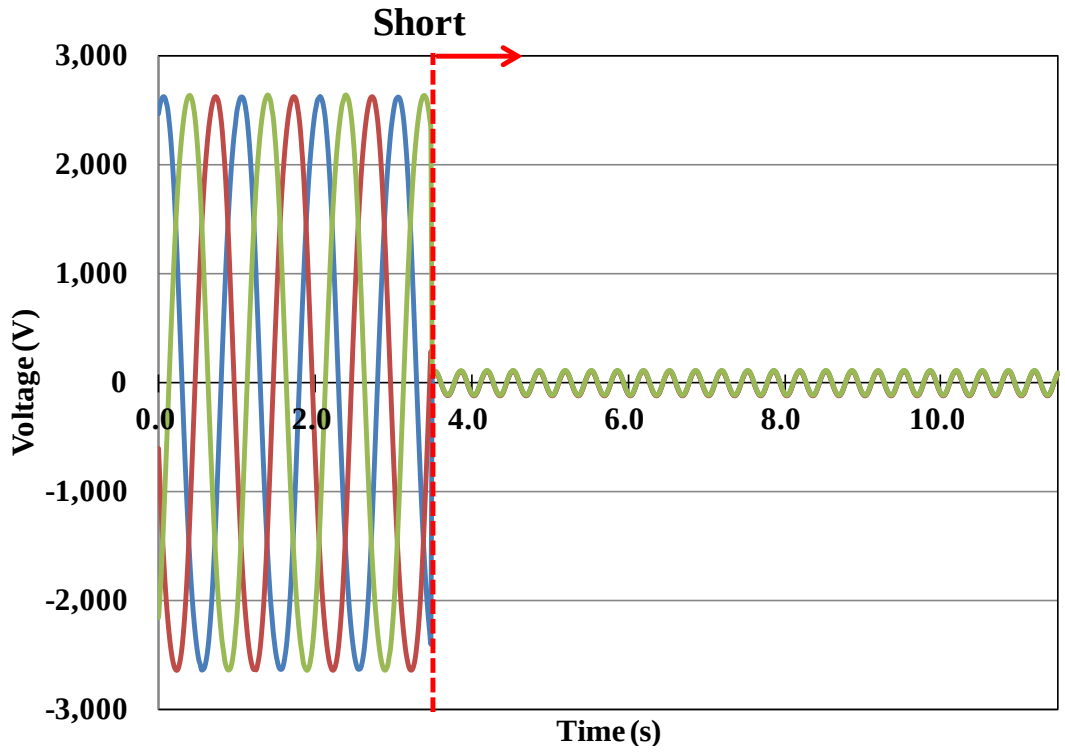

(a) NS-SCG-A

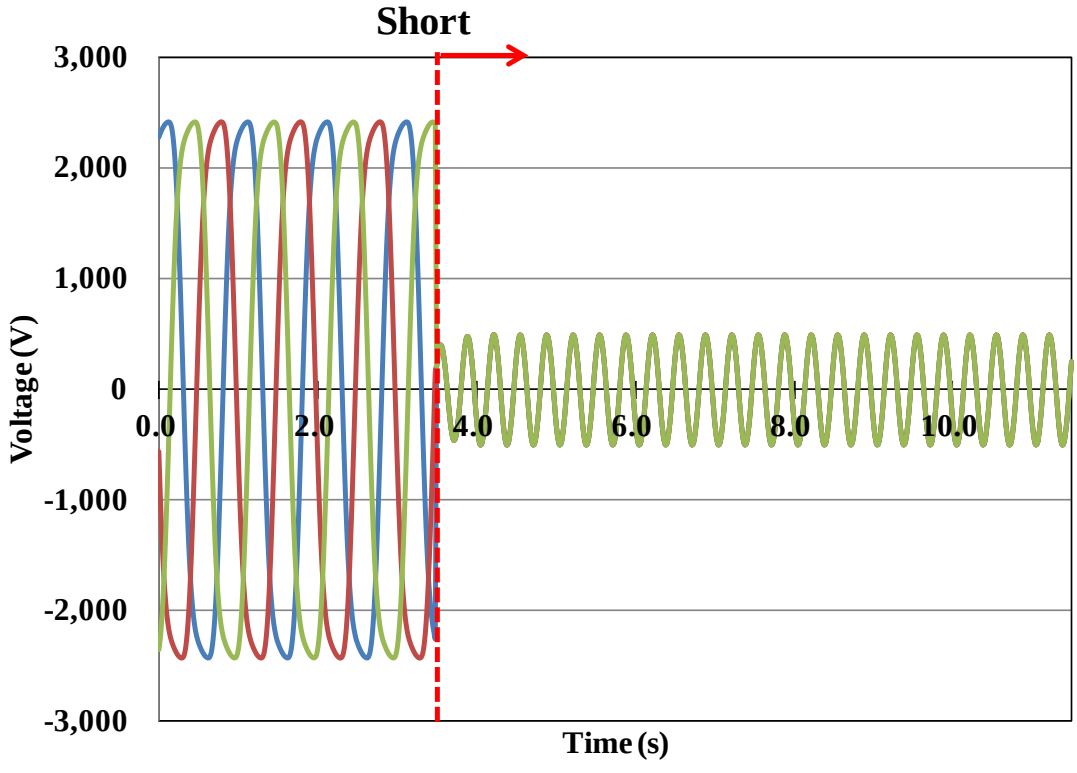

(b) NS-SCG-B

Fig. 5-10. Short-circuit phase voltage of both NS-SCGs. (a) and (b) are the output characteristics of NS-SCG-A and NS-SCG-B, respectively.

5-4. Summary of Chapter 5

This chapter explained the electromagnetic design of NS-SCG using 2D FEM. Two types of NS-SCG having diameters of 4.7 m and 8.4 m were designed. Their generator characteristics showed that both NS-SCG structures had many technical challenges. In particular, from the cost perspective, it was clear that the S-SCG structures have many advantages. In particular, the NS-SCG structure required around 1000 km of YBCO wires, and this value was not feasible. In addition, the low synchronous reactance of this structure may be risky for dealing with generator problems.

Chapter 6

Electromagnetic Design of

Fully Superconducting Generators

6-1. Steady State Analysis

6-1-1. Analysis Models and Conditions

This chapter introduces the electromagnetic design of fully superconducting wind turbine generators which have YBCO field coils and MgB_2 armature windings. This design is one of the original works in this thesis. In this chapter, two types of generators are designed. One is FSCG-A, for which the maximum magnetic flux density at the armature winding is 1.5 T. The other is FSCG-B, for which the maximum magnetic flux density at the armature winding is 2.0 T. These were obtained from the J_c–B characteristics of the MgB_2 wire shown in chapter 2. The diameters of both generators are fixed as 4.0 m, aiming to realize the most compact structure of all the 10 MW class wind turbine generators mentioned in this thesis. This value can be used to transport power not only offshore but also onshore without the need for dividing it. The pole number was set as 12 because the lower pole structure is suitable for this generator to reduce AC losses. Fig. 6-1 shows the FEM analysis model for the FSCG. The air gap is set to 80 mm, which is 20% lower than that of NS-SCG because the field and armature windings are put in the same cryostat. Also, there is a vacuum layer of 50 mm between the armature coils and back iron. In addition, at the rotor side, a vacuum layer of 100 mm is inserted between the field coils and rotor iron. The operation temperature is set as 22 K.

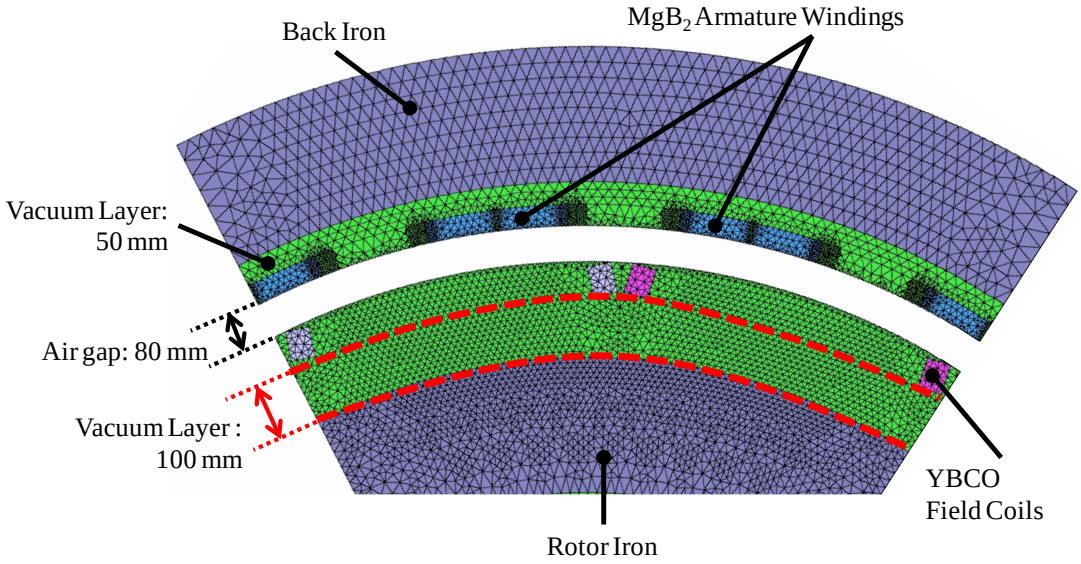

Fig. 6-1. FEM analysis model for FSCG (1/6 periodic model).

6-1-2. Analysis Results

6-1-2-1. Generator Dimensions and Outputs

Table 6-1 represents the generator dimensions and output characteristics of two FSCG structures. The generator outputs were estimated by applying the Fourier transform to the output waveforms. The geometrical structure and output characteristics of both FSCGs were almost the same. However, the maximum magnetic flux density, B_{max}, of FSCG-B (5.3 T) is a little higher than that of FSCG-A (5.0 T), as shown in Fig. 6-2. This is because FSCG-B requires a higher magnet motive force to generate 2.0 T of magnetic flux at its armature windings, whereas FSCG-A generates 1.5 T its the armature windings. On the other side, the effective length of the FSCG-A (1.54 m) is longer than that of FSCG-B (1.23 m) because FSCG-A requires a larger interlinkage area than FSCG-B to obtain a magnetic flux for 3.3 kV_{rms}. Figs. 6-3 to 6-5 show the waveform of the output torque, current, and voltage, respectively. Both structures contained many harmonics, and one of the reasons for this was the concentrated armature winding structures. In general, this structure contains more harmonics than distributed winding structures. There was a tradeoff between having an easy cryostat structure and a reduction in the harmonics. However, according to the torque waveform, the waveforms of the FSCG-B structure contained fewer harmonics than FSCG-A because of the higher magnetic flux generated by its field coils.

Table 6-1. Generator dimensions and output characteristics of the FSCG

Generator	FSCG-A	FSCG-B
Stator diameter [m]	4.0	4.0
Rotor diameter [m]	3.16	3.04
Effective length [m]	1.54	1.23
Air gap [mm]	80	80
Pole number	12	12
MgB_2 conductor dimension [mm^2]	8.1 × 8.1	9.5 × 9.5
Thickness of back iron [mm]	250	300
Thickness of rotor iron [mm]	250	300
B_{max} [T]	5.0	5.3
Output [MW]	10.0	10.1
Line-to-line voltage [kV_{rms}]	3.32	3.32
Line current [kA_{rms}]	1.77	1.77

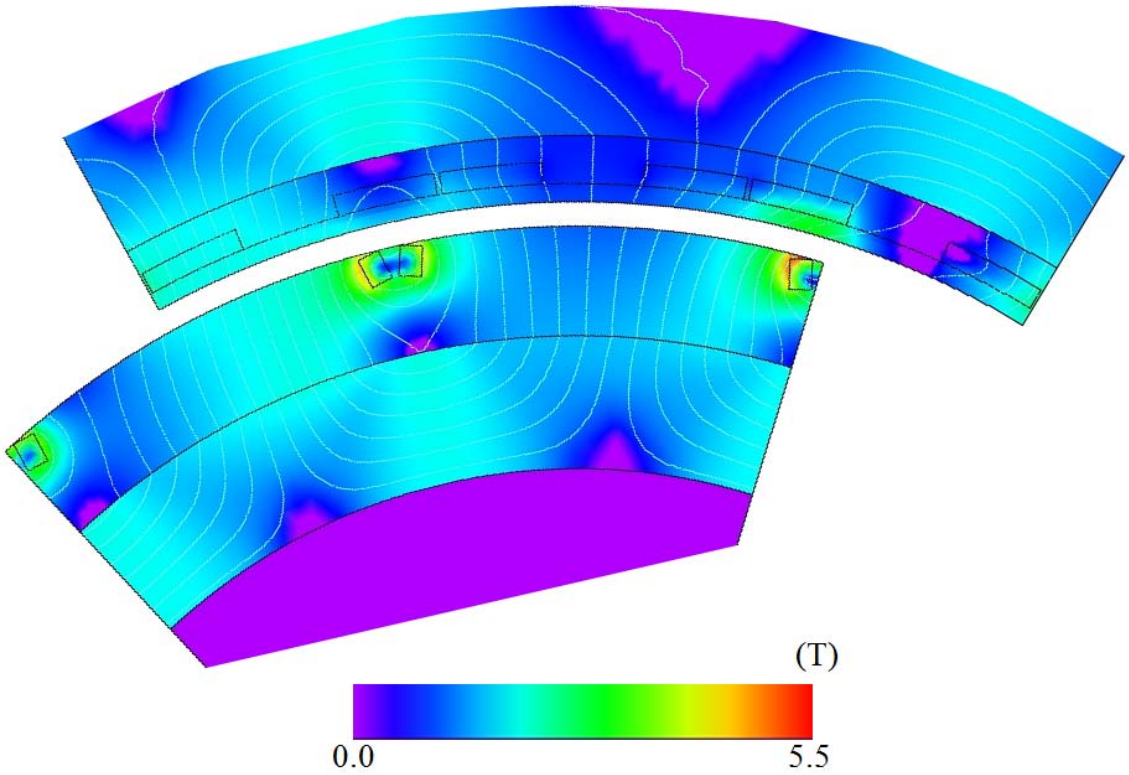

Fig. 6-2. Magnetic flux density distribution of the FSCG in steady state. This figure is for case of FSCG-A.

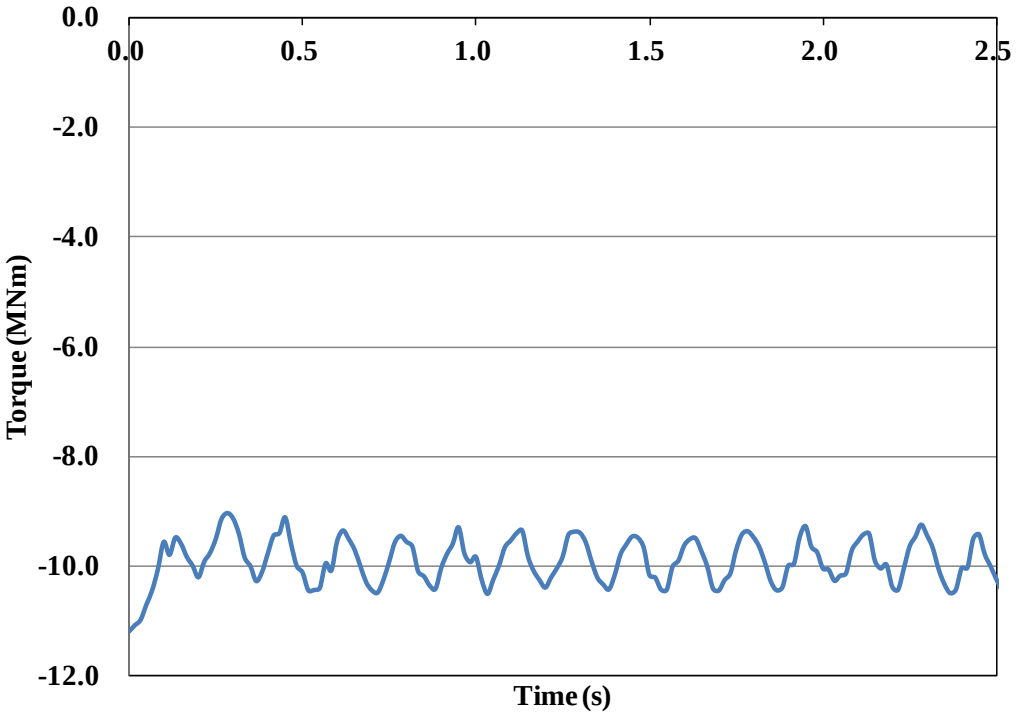

(a) FSCG-A

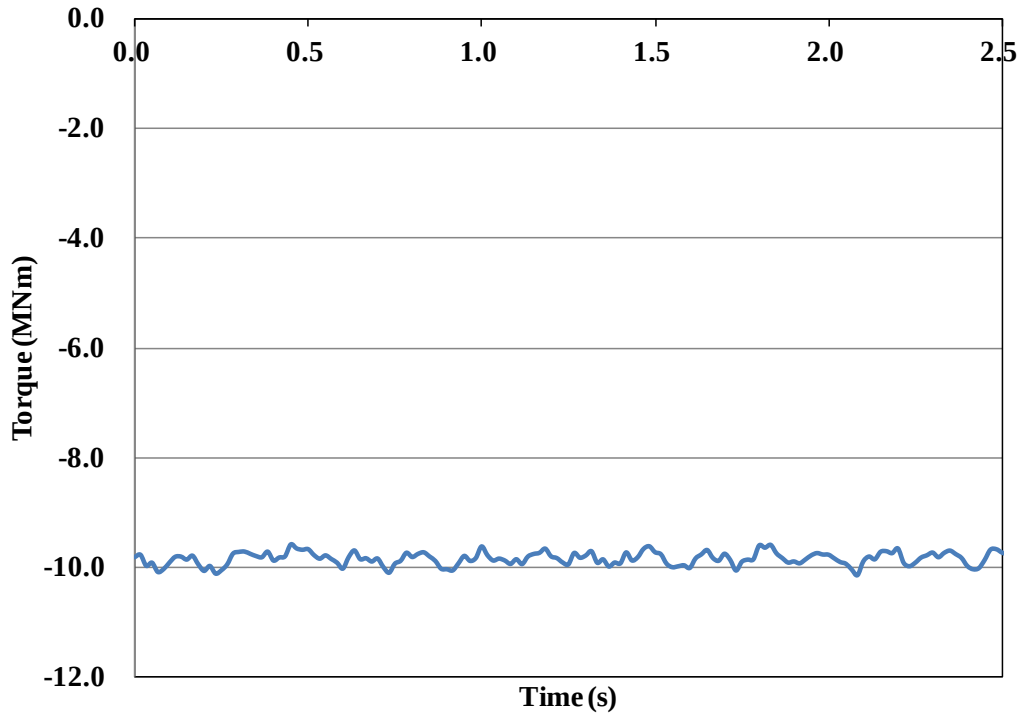

(b) FSCG-B

Fig. 6-3. Output torque of both FSCGs. (a) and (b) are the output characteristics of FSCG-A and FSCG-B, respectively.

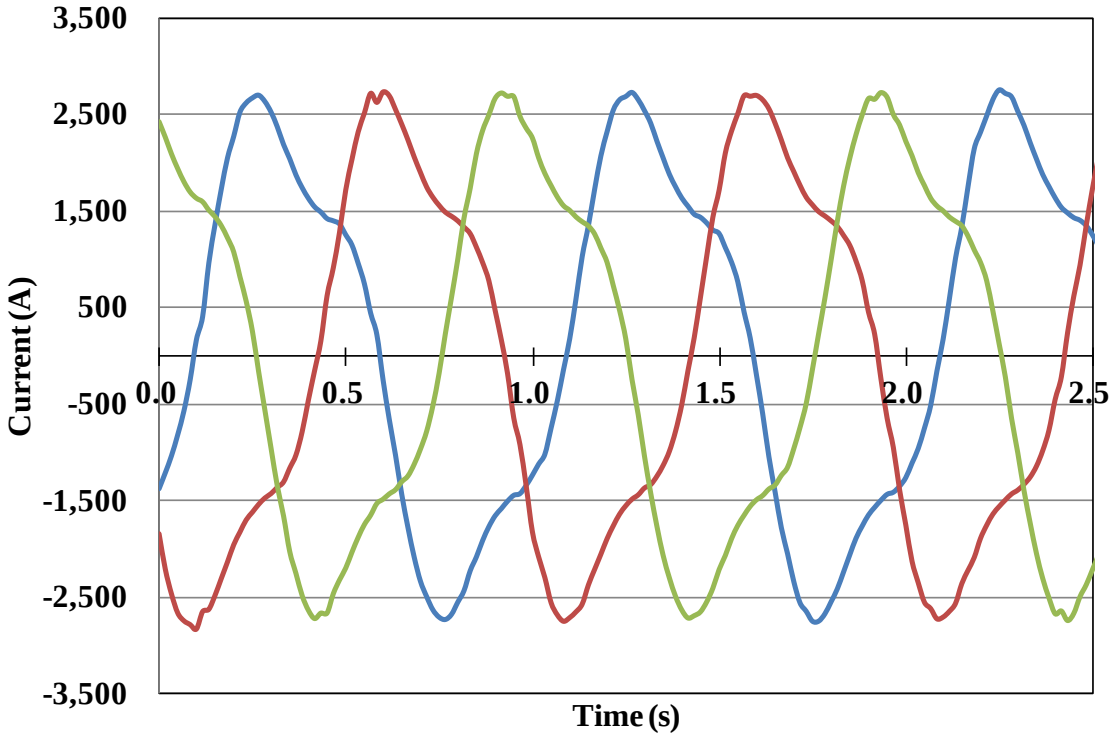

(a) FSCG-A

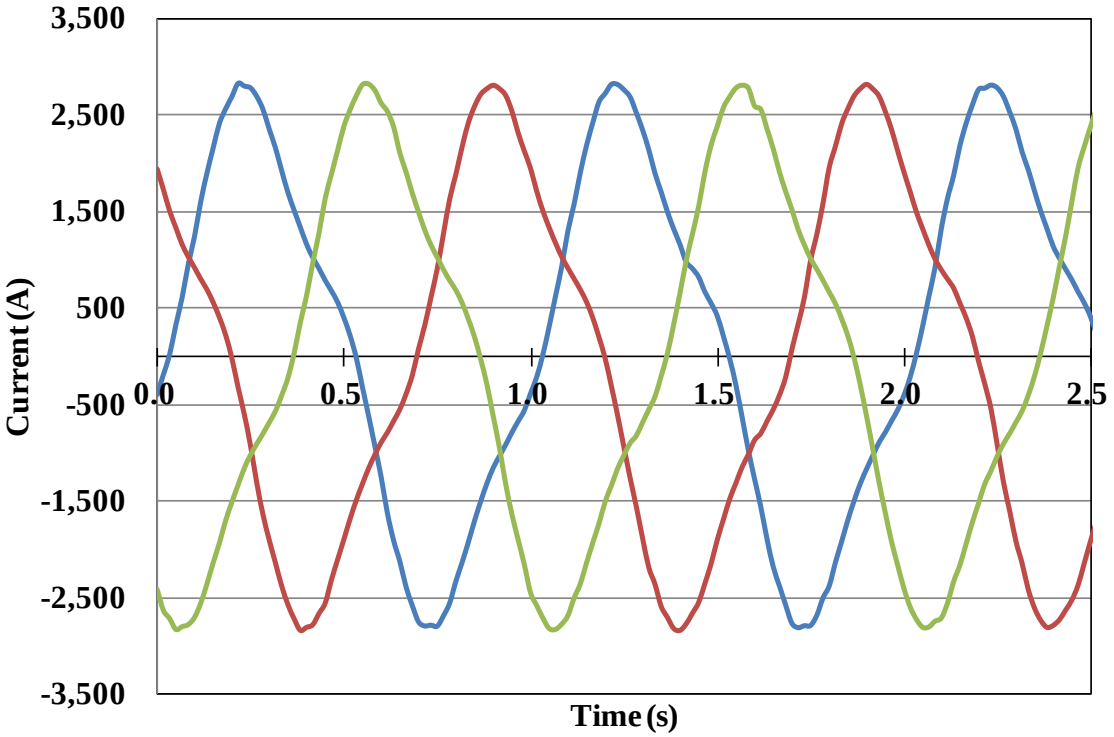

(b) FSCG-B

Fig. 6-4. Output current of both FSCGs. (a) and (b) are the output characteristics of FSCG-A and FSCG-B, respectively.

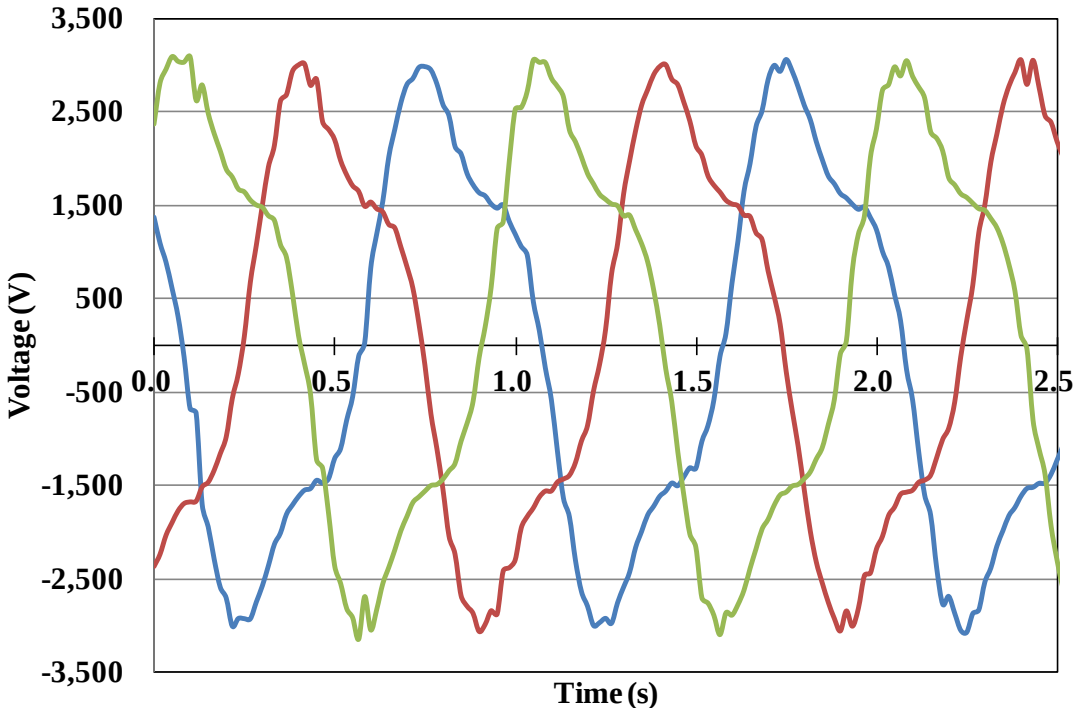

(a) FSCG-A

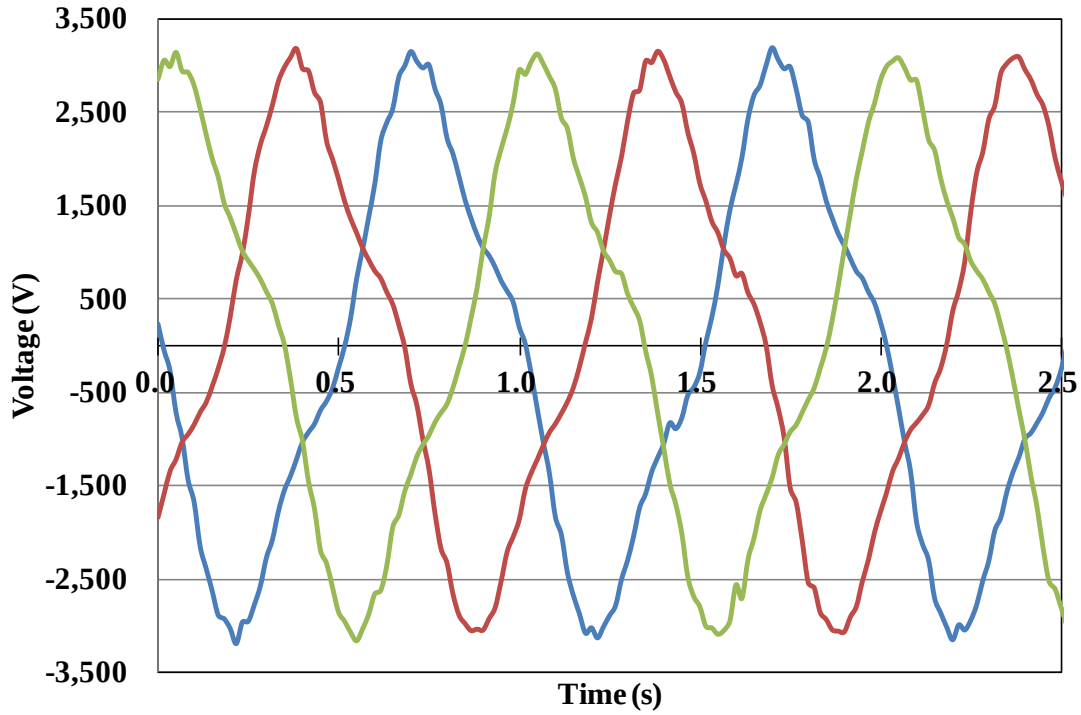

(b) FSCG-B

Fig. 6-5. Output phase voltage of both FSCGs. (a) and (b) are the output characteristics of FSCG-A and FSCG-B, respectively.

6-1-2-2. Synchronous reactance

In this section, we estimate the synchronous reactance of the NS-SCG structure. The equivalent circuit and phasor diagram are the same as those mentioned in chapter 3.

Table 6-2 shows the calculation results for both FSCG structures. For FSCG-A, x_S was 1.18 [p.u.], which was more than twice that of FSCG-B, which was 0.47 [p.u.]. This was because of the difference in the number of armature conductor turns between FSCG-A and FSCG-B, which were 120 and 80 [turns/phase], respectively. Compared with NS-SCG structures, these values are very high, even though they have the same air-cored structures.

Table 6-2. Synchronous reactance and calculated parameters.

Generator	FSCG-A	FSCG-B
Open phase voltage: E_o [V_{rms}]	3129	2201
Load phase voltage: V_L [V_{rms}]	1914	1916
Line current: I [A_{rms}]	1766	1768
Load resistance: R [Ω]	1.07	1.07
Load reactance: X_{Load} [Ω]	0.126	0.126
Synchronous Reactance		
X_S [Ω]	1.29	0.51
x_S [p.u.]	1.18	0.47

6-1-2-3. AC and Iron Losses

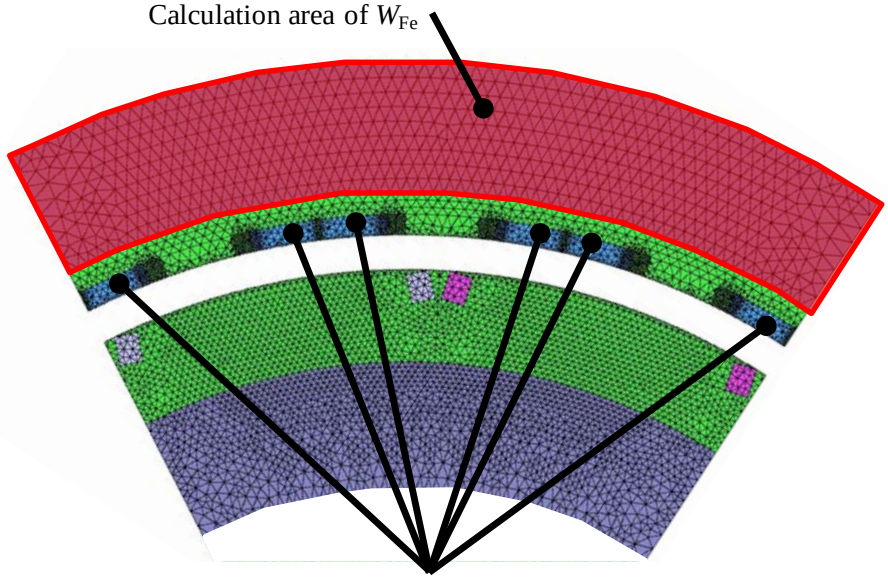

Fig. 6-6. Calculated areas of generator losses for the FSCG (1/6 periodic model).

This section deals with two different generator losses. The iron loss, W_{Fe}, is estimated in the same manner as that mentioned in chapters 3–5. However, unlike the case in chapters 3–5, FSCG has an AC loss, W_{AC}, as opposed to a copper loss because it has MgB_2 "superconducting" armature windings. Fig. 6-6 represents the calculated areas for W_{Fe} and W_{AC}. In particular, W_{AC} in this section refers to the "no load" condition and the hysteresis loss of the MgB_2 superconductor part.

First, W_{AC} is assumed as that in (6.1).

$$W_{AC} = f \times L \times Q \tag{2.1}$$

where f [Hz] is the frequency of the rotational magnetic field, which depends on the rated speed and the pole number of generators. L [km] is the total length of the MgB_2 armature windings. Also, Q [J/m/cycle] represents the AC loss per wire length and per cycle.

L is calculated as follows:

$$L = m \times \left(\frac{P}{2}\right) \times l \times n \times N \tag{2.2}$$

where m (= 3), P, l [m], n, and N are the phase number, pole number, average length of the armature windings shown in Fig. 6-7, number of parallel conductors and the number of armature winding turns, respectively.

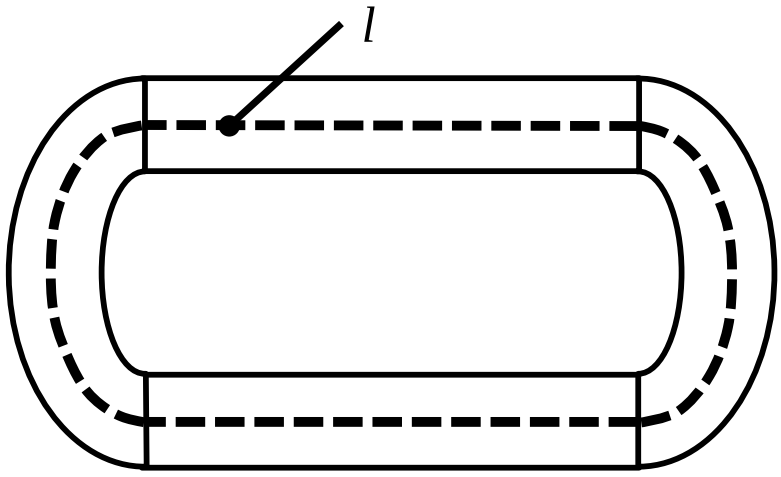

Fig. 6-7. Diagram showing the average length of the MgB_2 armature windings

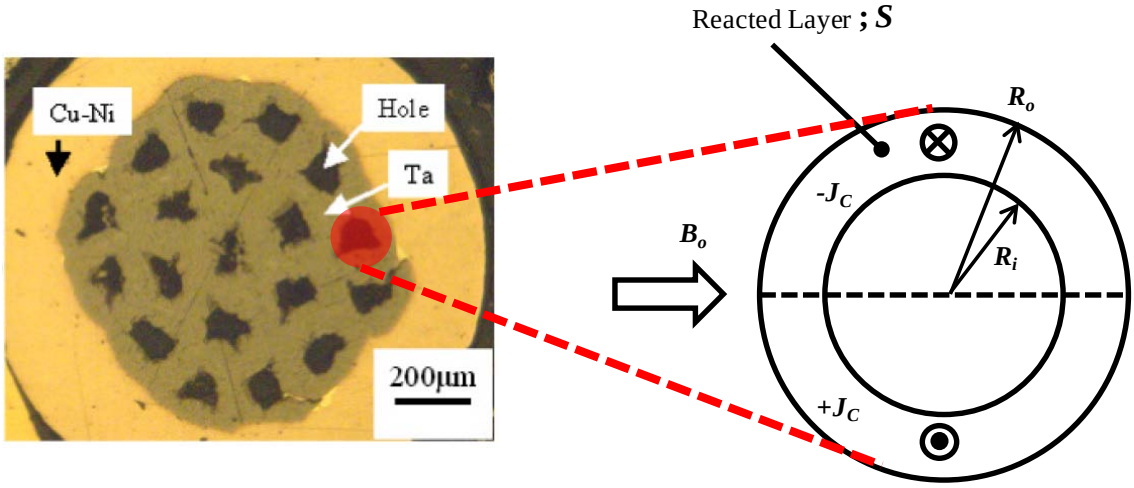

Fig. 6-8. Cross section of an MgB_2 filament that is fully penetrated by the applied magnetic field, B_o.

Fig. 6-8 shows an MgB_2 superconductor filament cross section in the applied magnetic field, B_o. This model is based on the Bean's model [27]. The AC loss density of a hollow cylinder, q [J/m^3/cycle], is expressed as that in (6.3) [28], and is proportional to the outer diameter R_O, B_o, and J_c. Finally, Q is calculated using the reacted layer, $S = \pi \times (R_o^2 – R_i^2)$, filament number, 19, and q, as shown in (6.4).

$$q = \frac{16}{3\pi} B_o R_O \left\{ J_c \left[1 - \left(\frac{R_i}{R_O} \right)^3 \right] \right\} \tag{2.3}$$

$$Q = 19 \times \pi \left(R_O^2 - R_i^2 \right) \times q \tag{2.4}$$

Table 6-3 shows the AC loss estimation results. These losses were calculated using the values from Table 2-2 in chapter 2. The AC losses for FSCG-A and FSCG-B were 1.9 and 1.5 kW, respectively. If the COP of the cooling system and thermal intrusion were assumed to be 0.01 and 100 kW, respectively, the total AC losses were estimated to be 250–290 kW. These values would be almost 3.0% of the total output, and are not considered to be low for entire systems. However, if the armature windings are made with a twisted structure, there is a possibility of realizing AC loss reduction. In other words, AC losses can be further reduced by optimizing the design of the armature windings.

On the other hand, the values of W_{Fe} of the two generators are 3.0 and 5.9 kW, respectively. The ratio of these losses to the total output is only 0.03–0.059%, which is quite low compared to those of other generators owing to low frequency such as 1.0 Hz.

Table 6-3. Calculation results of AC and iron losses

Generator	FSCG-A	FSCG-B
Frequency: f [Hz]	1.0	1.0
Pole number: P	12	12
l [m]	4.3	3.7
Parallel conductor number: n	25	34
Number of armature winding turns: N [turns/phase/pole pair]	120	80
MgB_2 armature wire length: L [m]	231×10^3	181×10^3
B_o [T]	1.56	2.00
J_c [A/m^2]	2.7×10^9	2.0×10^9
Outer filament radius; R_O [μm]	37.5	37.5
Inner filament radius; R_i [μm]	25	25
AC loss density of a hollow cylinder q [J/m^3/cycle]	1.83×10^5	1.80×10^5
AC loss / wire length, per cycle: Q [J/m/cycle]	0.0084	0.0084
AC loss: W_{AC} [kW]	1.9	1.5
Iron loss of the back iron: W_{Fe} [kW]	3.0	5.9

6-2. Discussions Regarding Generator Performances

The electromagnetic characteristics of both FSCG structures are shown in Table 6-4. The output of 10 MW was obtained with fewer lengths of YBCO wires, and they were more lightweight compared with NS/S-SCG structures. In particular, FSCG-A required 196 km of YBCO wires, which is only 15.8% that of NS-SCG-A. This is because of the air gap reduction from 100 mm to 80 mm, and implies that the magnetic flux generated by the field windings was effectively used. Also, the reduction in the YBCO wire length also contributed to the decrease of B_{max} at the field coils to 5.0 T. As for the weight of the cooling system which can remove AC loss and other losses, it is estimated at less than 5 tons [29]. This value is only several percent of the total weight of FSCG.

Table 6-4. Electromagnetic characteristics of the 10 MW class FSCG.

Generator	FSCG-A	FSCG-B
Stator Diameter [m]	4.0	4.0
Effective length [m]	1.54	1.23
Output [MW]	10.0	10.1
Line current [A_{rms}]	1.77	1.77
Line-to-line voltage [V_{rms}]	3.32	3.32
Pole number	12	12
Operating temperature [K]	22	22
Rotor		
Field	YBCO	YBCO
Coil current density [A/m^2]	2.0×10^8	2.0×10^8
B_{max} [T]	5.0	5.3
Wire length [km]	196	260
Stator		
Conductor	MgB_2	MgB_2
Coil current density [A/m^2]	1.08×10^9	0.8×10^9
B_{max} [T]	1.56	2.0
Wire length [km]	231	181
Synchronous reactance [pu]	1.18	0.47
AC loss [kW]	1.9	1.5
Iron loss [kW]	3.0	5.9
Weight		
Irons [tons]	58.2	54.6
YBCO [tons]	1.7	2.3
MgB_2 [tons]	3.7	2.9
Total weight [tons]	63.6	59.8

6-3. Transient Analysis for Three-phase Short-Circuit Problems

6-3-1. Analysis Models and Conditions

This section deals with the sudden short-circuit characteristics for FSCG. The analysis concept is almost the same as that of the previous chapters. However, for a fully superconducting wind turbine generator, MgB_2 armature windings are expected to have a current-limiting control function based on its *I–V* characteristics and higher short-circuit currents. Fig. 6-9 shows the equivalent circuit of the sudden three-phase short-circuit problem for FSCG. Initially, the generators are operated in the steady state. After several cycles of the generator frequency, which depends on the generator poles, the two switches are closed and a sudden three-phase short circuit occurs. In particular, FSCG has MgB_2 superconducting armature windings with a critical current density J_c of 2.7×10^9–2.0×10^9 A/m^2 ($E_c = 10^{-4}$ V/m) at 22 K and 1.5–2.0 T. The MgB_2 wire was modelled using two resistances that were connected in parallel. One was MgB_2 (R_{MgB2}) and the other was the metals around the superconductors (R_{Metal}). In the analysis, we evaluated the peak value of the short-circuit torque and current. Temperature rise was ignored; the temperature of MgB_2 was constant during this calculation process. MgB_2 is represented by a nonlinear resistance using the *I–V* characteristics based on the n-value model (n = 25). The metal resistances, R_{Metal}, including Ta and Cu–Ni, remain constant at 22 K.

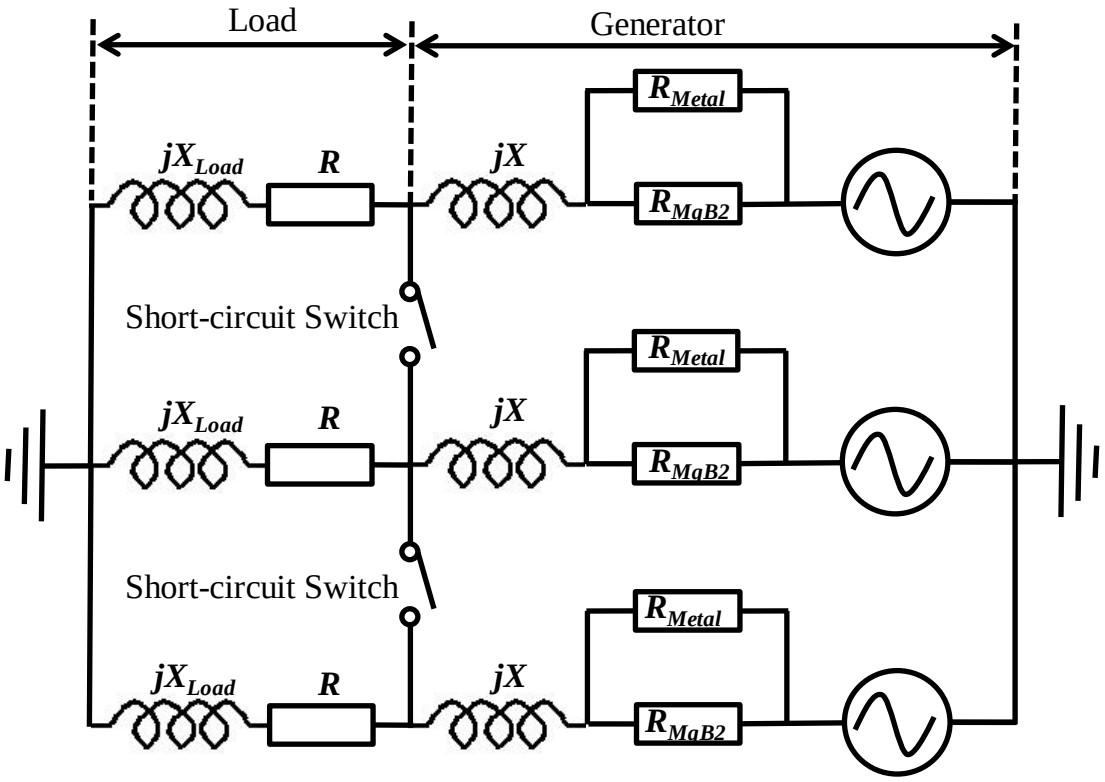

Fig. 6-9 Equivalent circuit of sudden three-phase short-circuit problem for the FSCG.

6-3-2. Analysis Results

Fig. 6-10 represents the magnetic flux distribution of FSCG-A in the short-circuit state.Compared with Fig. 6-2, the magnetic flux induced many loops in the stator side. The strength of the magnetic field was also weakened because of interactions with the field of the short-circuit armature current and field coils. Figs. 6-11 to 6-13 show the waveforms of torque, current, and voltage, respectively. The transient torque and current of FSCG structures were observed to be quite lower than those of NS-SCG structures. The nonlinear resistance obtained using the *I–V* characteristics of FSCG contributed to the higher short-circuit current area. In other words, when the problem occurred, the current-limiting control function based on the *I–V* characteristics of MgB_2 had worked at the armature windings. With respect to the individual generators, the current-limiting control of FSCG-A is better than that of FSCG-B. The transient torque of FSCG-A was 13.6 MNm, which was almost over 1.3 times higher than the rated torque of 10.0 MNm. Also, the transient current was 5260 A_{max}, which was approximately twice the value of the rated current of 2500 A_{max}. On the other hand, the transient torque and current of FSCG-B were 25.5 MNm and 11600 kA_{max}, respectively. The differences caused by the number of armature winding turns were same as those in the case of the previous AC losses. For FSCG-A, the length of the MgB_2 wires is longer than that of FSCG-B, as shown in Table 6-3. In general, the conductor resistance is proportional to the conductor length. In this analysis, the R_{Metal} of FCSG-A was higher than that of FSCG-B, and it influenced the difference between both generators' current-limiting control functions. It was concluded that FSCG had good characteristics from the perspective of ensuring generator protection from various accidents.

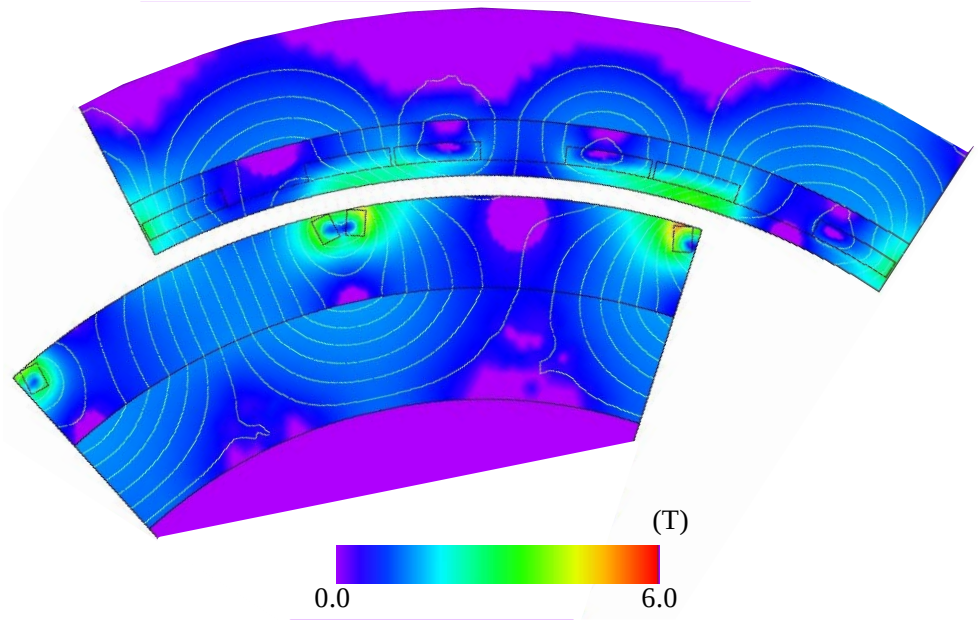

Fig. 6-10. Magnetic flux distribution of FSCG in the short-circuit state. This figure is for the case of FSCG-A.

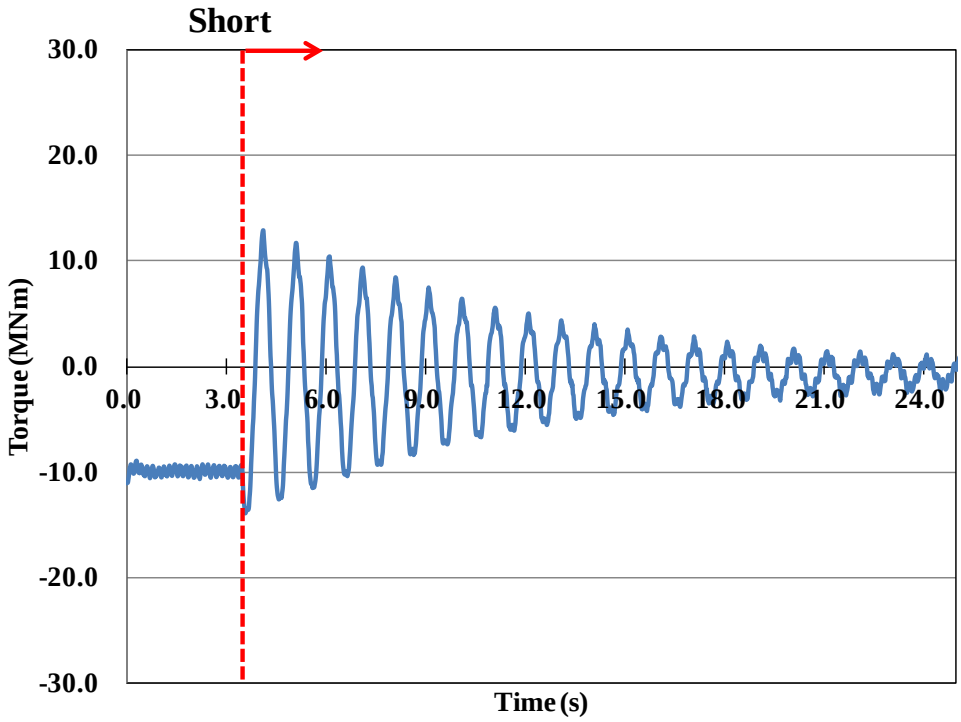

(a) FSCG-A

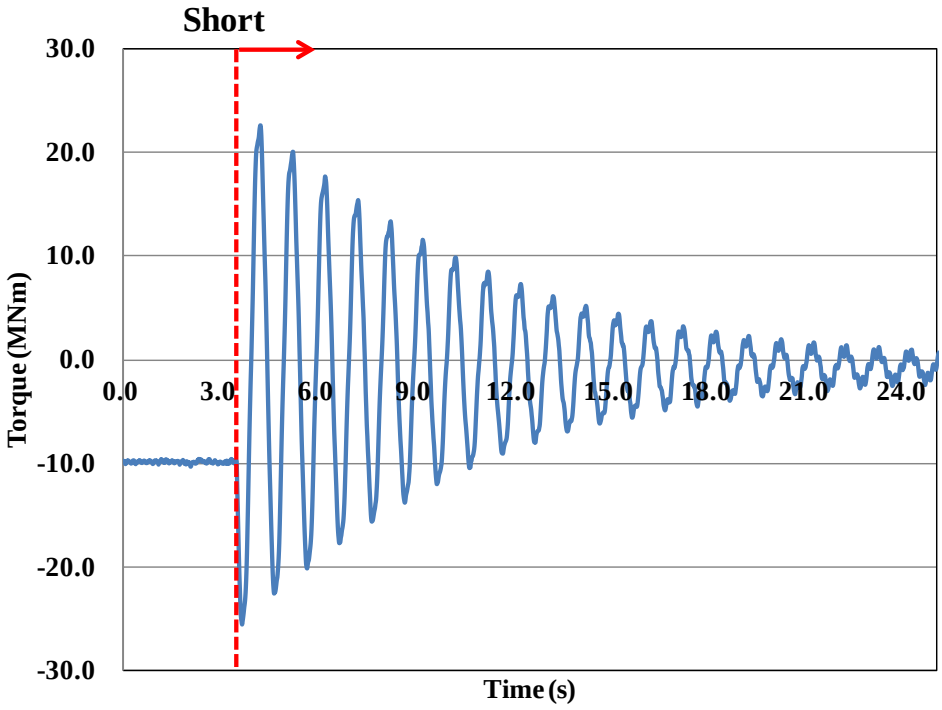

(b) FSCG-B

Fig. 6-11. Short-circuit torque for both FSCGs. (a) and (b) are the output characteristics of FSCG-A and FSCG-B, respectively.

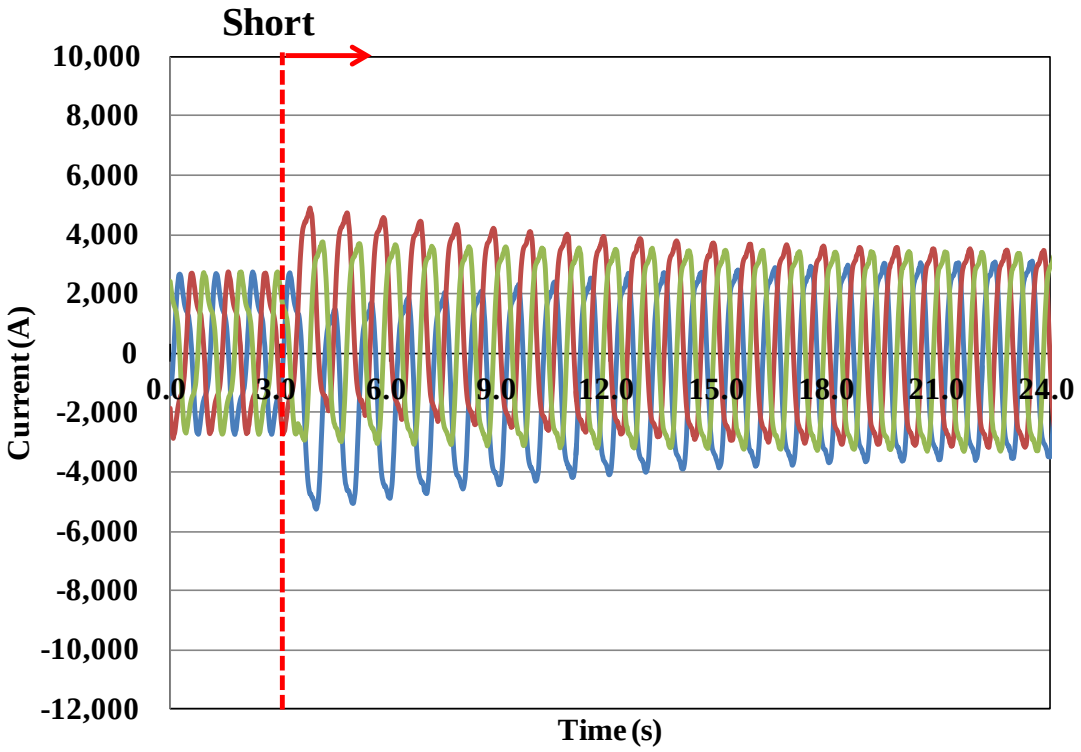

(a) FSCG-A

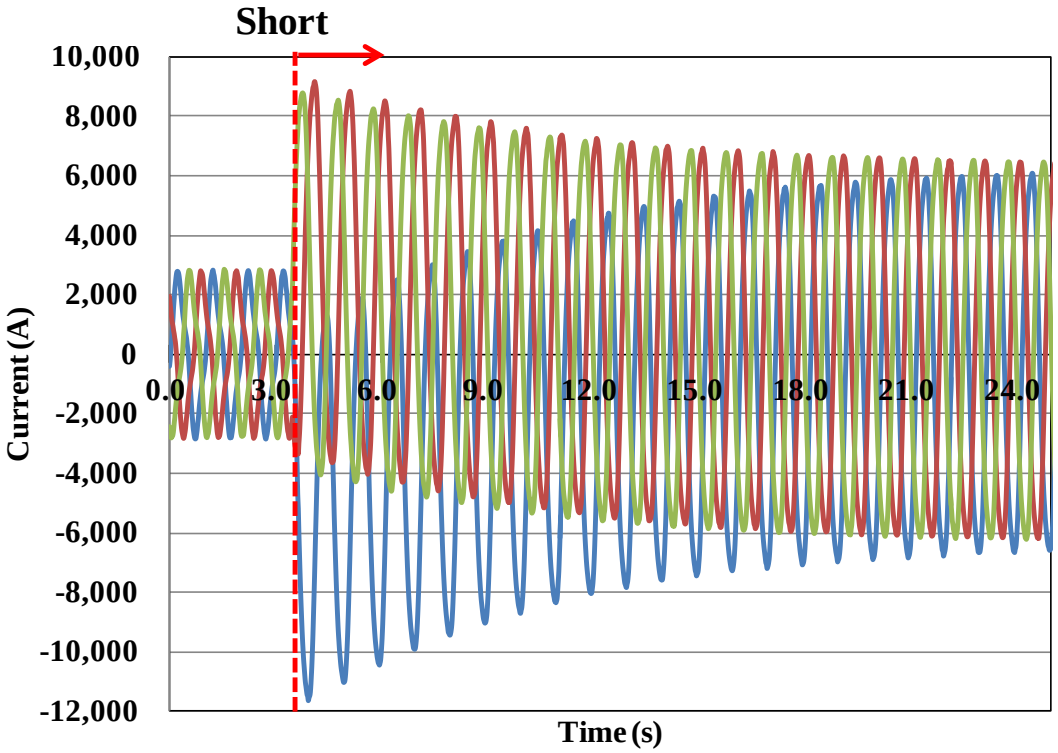

(b) FSCG-B

Fig. 6-12. Short-circuit current for both FSCGs. (a) and (b) are the output characteristics of FSCG-A and FSCG-B, respectively.

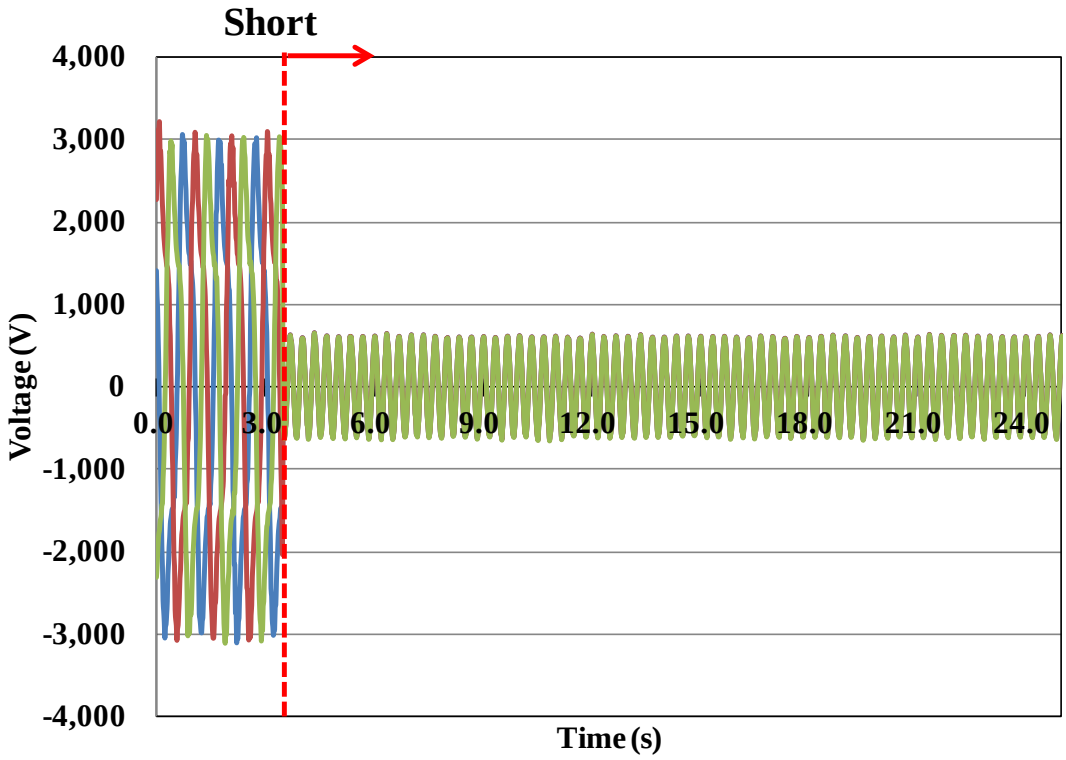

(a) FSCG-A

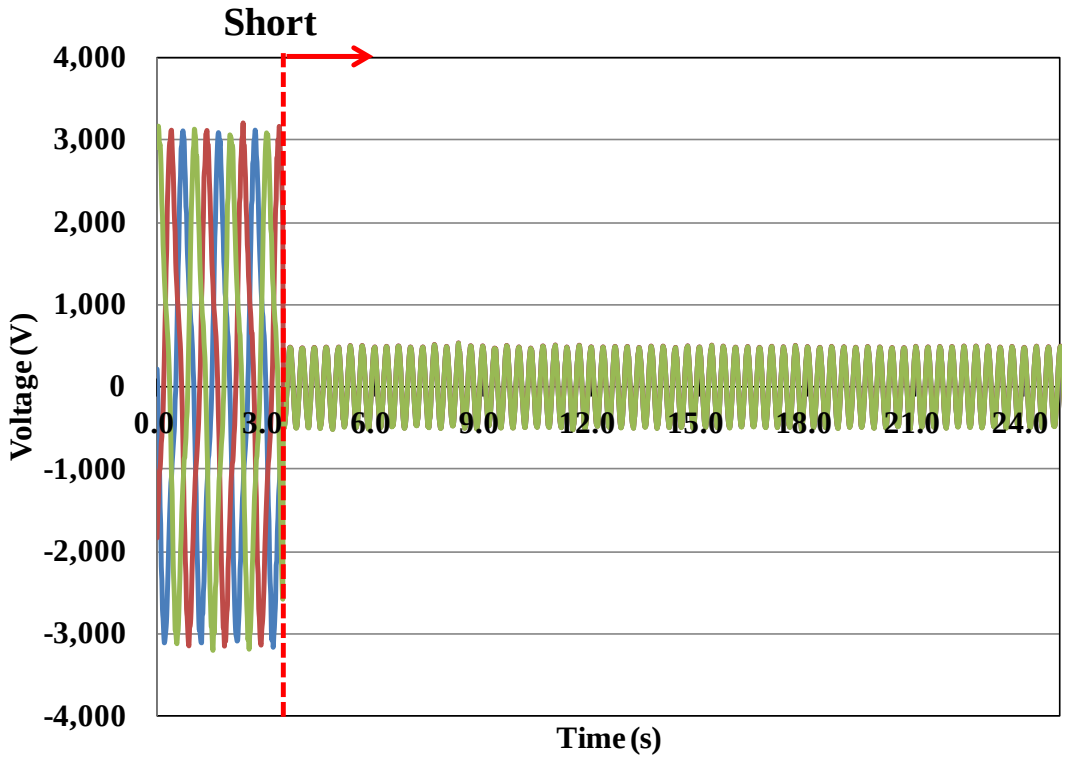

(b) FSCG-B

Fig. 6-13. Short-circuit phase voltage for both FSCGs. (a) and (b) are the output characteristics of FSCG-A and FSCG-B, respectively.

6-4. Summary of Chapter 6

This chapter presented the electromagnetic design for a fully superconducting wind turbine generator using two types of superconductor coils. Two types of generators were designed with different values of B_{max} at MgB_2 armature windings, such as 1.5 and 2.0 T. FEM analysis results showed that the 10 MW output is achievable with less than 200 km of HTS tapes and with the smallest generator diameter of 4.0 m. This result suggested that a fully superconducting generator is a good candidate for future large-scale wind turbine generators. However, no-load AC losses may be almost 2.0 kW. Considering the COP of the cooling system and other losses, the total loss would be almost 3.0% of the output, and lower losses are desirable. For short-circuit problems, the use of FSCGs could reduce the transient torque and current due to the *I*–*V* characteristics of MgB_2 armature windings. These results may be helpful from the perspective of protecting the generator from different accidents.

Chapter 7

Comparisons of 10 MW class Wind Turbine Generators with Different Structures

In this chapter, we compare the electromagnetic characteristics of four wind turbine generators, PMSG, S-SCG-B, NS-SCG-A, and FSCG-A. In our discussion, the symbols “A” and “B” are omitted.

7-1. Generator Size and Weight

Fig. 7-1 and Table 7-1 show the comparison of the four wind turbine generator sizes. With a size of 13.1 m, PMSG is the largest 10 MW class generator of those listed. The use of a 60-pole structure is one reason for the expansion of the generator size. The increase in the pole number also leads to an increase in the radial expansion because of the pole pitch. This means that the nacelle weight is almost three times heavier than the generator weight. If PMSG is applied to the 10 MW systems, the nacelle weight will exceed 750 tons. We concluded that an over 10 MW class wind turbine generator with PM has many challenging issues related to its size and weight. In addition to the physical challenges, the current market price of rare earth materials needed for PM is not stable.

Compared with the PMSG, all of the superconducting generators are potential candidates owing to their size and weight reduction characteristics. In the case of S-SCG, its diameter of 8.2 m is 37% smaller than that of PMSG, resulting in a reduction in the material weight of 100 tons to 164.4 tons, when compared to PMSG. On the other hand, the diameter of NS-SCG and FSCG is around 4.0 m. These values are almost a third of the PMSG diameter, which means that the generator weight may also be significantly reduced. In particular, the weight of FSCG is almost 60 tons, which is one-fifth that of PMSG. As the most lightweight and high power density machines, FSCG has the maximum advantages for 10 MW class wind turbine systems.

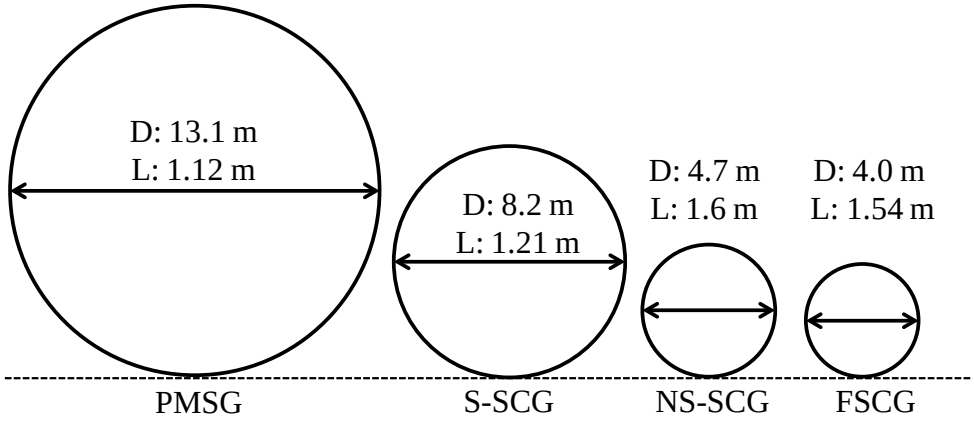

Fig. 7-1. Comparison of four wind turbine generator sizes

Table 7-1. Weights of four wind turbine generators

Weight	PMSG	S-SCG	NS-SCG	FSCG
Irons [tons]	198.7	121.4	85.6	58.2
Copper [tons]	19.9	12.1	11.4	N/A
YBCO [tons]	N/A	0.32	10.8	1.7
MgB_2 [tons]	N/A	N/A	N/A	3.7
Permanent magnet [tons]	13.1	N/A	N/A	N/A
Total weight [tons]	231.7	133.8	107.8	63.6

7-2. Length of Superconducting Wires

The number of HTS windings is related to the total cost of the superconducting wind turbine generator systems. Fig. 7-2 represents the length of YBCO and MgB_2 superconducting wires. For the case of NS-SCG, 1247 km of YBCO wires are required because of the air-cored structure and the large air gap of 100 mm. This value is not feasible for 10 MW class wind turbine generators. On the other hand, the use of S-SCG or FSCG can significantly reduce the YBCO wire length. FSCG can reduce the length to less than 200 km because of the shorter air gap of 80 mm, whereas S-SCG requires only 36.9 km of YBCO windings. This is because a lot of iron is used, and the lower air gap of 15 mm contributes to the reduction in wire length. As explained in the previous chapter, S-SCG is the largest and heaviest superconducting wind turbine generator of those considered. However, from an economical viewpoint, the S-SCG structure has the most advantages.

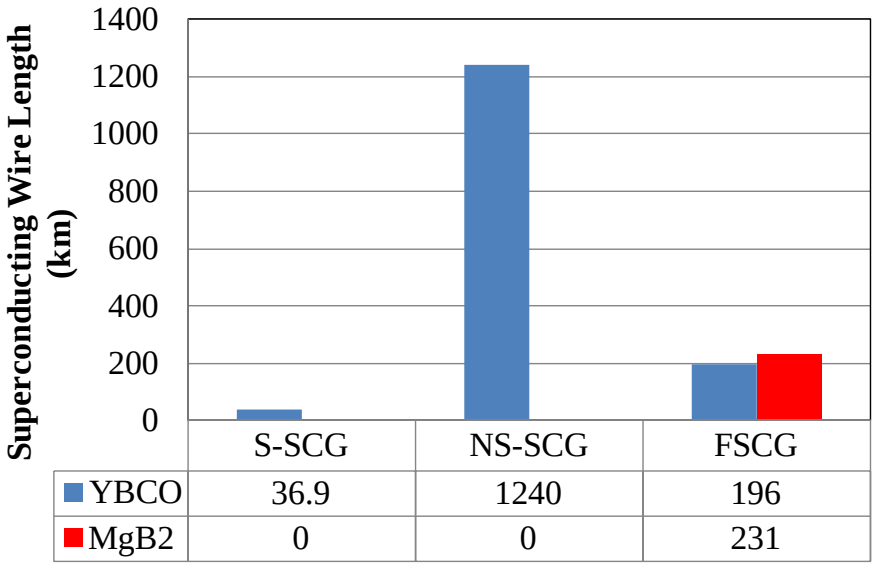

Fig. 7-2 Length of superconducting wires

7-3. Generator Losses

7-3-1. Full load losses

The copper and iron losses of PMSG in Table 7-2 indicate that at least 4.0% of the total output energy is lost. This generator will possess other losses, and the total generator efficiency is less than 90%. For the case of superconducting generators such as S-SCG and NS-SCG, the losses can be reduced, but these values of around 3.0% are still high, and should be reduced in order to bring about improvements in the total system efficiency. On the other hand, FSCG had no copper loss, but has an AC loss at the MgB_2 armature windings. If the COP of the cooling system and thermal insulation are assumed to be 0.01 and 100 kW, respectively, the total AC losses were estimated at 250–290 kW. These values would be almost 3.0% of the total outputs, and are not low values for entire systems. The difference between FSCG and the other systems was the operating time of the cooling system. The cooling system of FSCG has to work all of the time, whether or not FSCG is generating rated power. If FSCG is applied to 10 MW class wind turbine generator systems, AC losses that are smaller than the current values are desirable.

Table 7-2 Full load losses of four wind turbine generators

Losses	PMSG	S-SCG	NS-SCG	FSCG
Copper loss [kW]	386	235	226	N/A
AC loss [kW]	N/A	N/A	N/A	1.9
Iron loss [kW]	17.1	42.5	92.8	3.0

7-3-2. Partial load analysis

In general, the output power of wind turbine generators depends on wind speed conditions. In other words, the four wind turbine generators do not always generate an output power of 10 MW. This section evaluates the generator output in partial loads such as 10 MW (100%), 5.0 MW (50%), and 2.5 MW (25%), respectively. Table 7-3 shows analysis conditions for 10 MW class wind turbine generators. The blade diameter of a 10 MW class wind turbine is assumed to be 160 m. The rotation speed in three types of output, 10, 7.9, and 6.3 rpm, is estimated using the tip speed ratio, $\lambda = 6.92$.

Fig. 7-3 shows the partial load analysis results of four wind turbine generators. PMSG, S-SCG, and NS-SCG had lower iron and copper losses in partial load outputs. The ratio in the generator output was only 1%. On the other hand, FSCG consistently exhibited generator losses of approximately 2.0% because its cooling systems have to work all of the time whether or not it is generating an output of 10 MW. However, even for 5.0 or 2.5 MW, three superconducting wind turbine generators will have an efficiency of over 95%.

Table 7-3. Partial load analysis conditions for 10 MW class wind turbine generators

	10 MW (100%)	5.0 MW (50%)	2.5 MW (25%)
Blade diameter [m]	160	160	160
Tip speed ratio; λ	6.92	6.92	6.92
Rated speed [rpm]	10	7.9	6.3
Wind speed [m/s]	12.1	9.6	7.2
Circumferential velocity [rad/s]	83.8	66.2	52.8

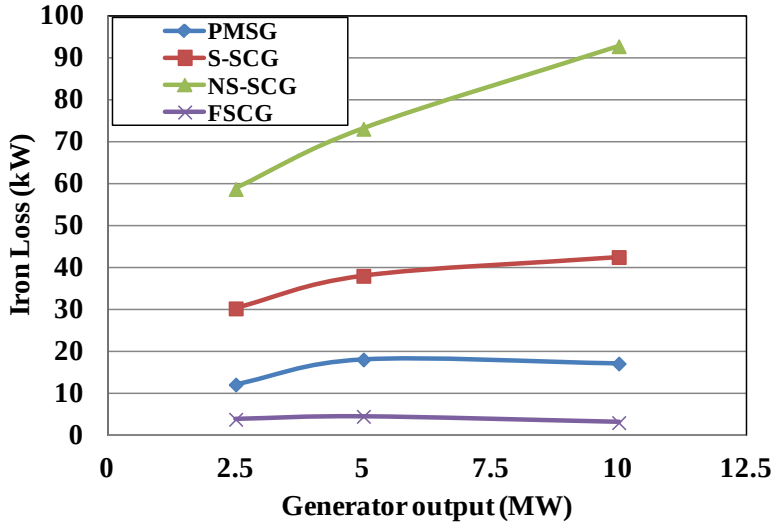

(a)

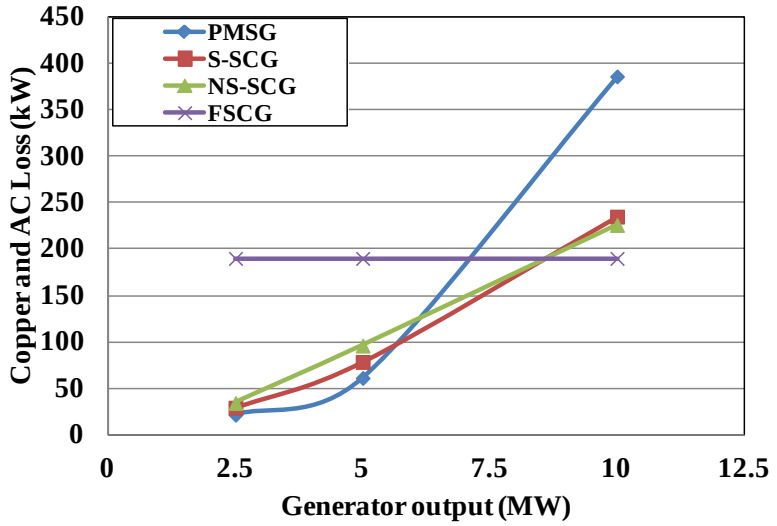

(b)

Fig. 7-3 Partial load losses of four wind turbine generators. (a) shows iron losses and (b) represents copper loss of three generators and AC loss of FSCG.

7-4. Summary of Chapter 7

We have compared the FEM analysis results of four 10 MW class wind turbine generators, and some of our observations are as follows:

- There are many challenging issues regarding the manufacture of such a generator with PM or other conventional technology because of the generator weight.
- Superconducting generators have a good potential for use in wind turbine systems. All of the superconducting generators can lead to a reduction in the size and weight of a 10 MW class. In particular, S-SCG and FSCG are considered to be good candidates.
- S-SCG has an economical merit owing to the reduction in the YBCO wire length, and requires only several tens of kilometers of wire length.
- Weight and size reduction is possible with the FSCG structure. This results in a lightweight and high power density generator.
- For the case of partial load operation, all four generators had good efficiency. Especially, the three of the superconducting wind turbine generators will have an efficiency of over 95% at 2.5 or 5.0 MW.

Chapter 8

Conclusions

8-1. Conclusions

This thesis focused on the electromagnetic design and FEM analysis for 10 MW class superconducting wind turbine generators. We proposed the world's first fully superconducting generator (FSCG) using YBCO and MgB_2 superconducting wire. We also investigated the electromagnetic characteristics using two other types of superconducting wind turbine generators, S-SCG and NS-SCG, and a conventional permanent magnet generator (PMSG) using FEM.

Chapter 1 had an introduction of this study.

Chapter 2 represented the design conditions for 10 MW class wind turbine generators. Four generator structures and their component design conditions were described in this chapter. Several design parameters were defined to allow the evaluation of these generators under uniform conditions.

Chapter 3 explained electromagnetic design of PMSGs. From the analysis results, we found that 14 tons of PMs were required for manufacturing. Considering today's unstable rare earth price, the cost of this generator is expected to be high. In addition, it will also be challenging to determine how to reduce the generator weight.

In Chapter 4, the electromagnetic design of salient pole-type superconducting generators (S-SCG) was investigated. The analysis results showed that the S-SCG structure required only several tens of kilometers of YBCO wire owing to the use of a large amount of iron. It was also possible to realize a smaller generator size and weight than PMSG. This generator may be a good candidate for 10 MW class superconducting wind turbine generators from the viewpoint of its economical merits. This structure was suitable for multipoles with larger diameters.

Chapter 5 showed the electromagnetic design using 2D FEM analysis of nonsalient pole-type superconducting generators (NS-SCG). Their generator characteristics showed that both NS-SCG structures had many technical challenges. In particular, from the viewpoint of cost, it was clear that S-SCG structures have many advantages. The NS-SCG structure required around 1000 km of YBCO wires, which was not feasible. In addition, the low synchronous reactance of this structure may introduce some risks.

In Chapter 6, the electromagnetic design of FSCGs had been investigated. Because of the reduction in the air gap length, the length of HTS wire was reduced in spite of its air-cored structure. While the required length of the HTS wire was less than 200 km, the generator size was 4.0 m. These values indicated that this structure had a balanced design from the perspective

of cost reduction and compactness of design. In addition, FSCG may be helpful from the perspective of the protection of the generator from accidents because the current limitation control with the *I–V* characteristics of MgB_2 armature windings was possible in short-circuit problems.

Chapter 7 compared the electromagnetic characteristics of four designed wind turbine generators in terms of generator diameter, weight, HTS wire length, generator loss, and so on. It was concluded that the design of an over 10 MW class wind turbine generator using PMs would be very challenging because its size and weight will exceed 10 m and 300 tons, respectively. On the other hand, S-SCG and FSCG may be good candidates. S-SCG can reduce the required number of YBCO windings, which would be more economical. Meanwhile, weight reduction was possible for FSCG, and would result in a more compact generator.

In summary, the results of this thesis were as follows:

- Superconducting generators may be a good solution for the development of 10 MW class lightweight and high output density wind turbine generators.
- FSCG may be a good candidate for superconducting wind turbine generators from the perspective of “compact” and “lightweight” machines.
- S-SCG will be the “least cost superconducting wind turbine generator” because it uses the least amount of YBCO superconducting wires.

8-2. Future Works

This thesis focused on the electromagnetic design for 10 MW class wind turbine generators with FEM. On the other hand, further analysis and design approaches are required to develop the generator. For example, the field coil shape was assumed to be rectangular. However, there are many design examples for the optimal design of the superconducting field coils [30]. The method used to design a mechanical supporting structure for superconducting field coils is also important. In addition to the mechanical approach, the thermal analysis of generators is also important. Finally, the 2D FEM analysis should be expanded to 3D analysis, and it may enable us to more precisely investigate the electromagnetic properties such as coil end effect.

I hope this thesis will contribute to the development of future superconducting wind turbine generators.

Bibliography

[1] Global Wind Energy Council (GWEC), *GLOBAL WIND* 2011 *REPORT*, 2012

[2] UpWind, Final Publication (http://www.ewea.org/fileadmin/ewea_documents/documents/upwind/21895_UpWind_Report_low_web.pdf), p.17, March, 2012

[3] NEDO, “風力発電導入ガイドブック”, 2008

[4] UpWind Finding design solutions for very large wind turbines, http://www.upwind.eu/

[5] 塚本修巳, 大崎博之, 福井聡, 長屋重夫, 鹿島直二, “超電導大容量風力発電の経済的検討”, 超電導応用電力機器研究会, ASC-10-28, 福岡, 2010年6月
O. Tsukamoto, H. Ohsaki, S. Fukui, S. Nagaya and N. Kashima, “Economic feasibility of large scale superconducting wind power generator”, *IEEJ technical meeting on Application of Superconductivity*, ASC-10-28, Fukuoka, June, 2010

[6] H. Li and Z. Chen, “Overview of different wind generator systems and their comparisons”, *IET Renew. Power Gener.* , Vol.2, pp.123-138, 2008

[7] 福井聡, “大型風力用発電機の技術動向と高温超伝導技術の適用可能性”, 低温工学, 第47巻, 6号, pp.362-369, 2012年6月
S. Fukui, “Technical Trends of Large-capacity Wind Turbine Generators and Feasibility of Application of High Temperature Superconducting Technology”, *TEION KOGAKU*, vol. 47, No. 6, pp.362-369, June, 2012 (*in Japanese*)

[8] Enercon HP, http://www.enercon.de/de-de/

[9] The European Wind Energy Direction (EWEA), *Articles on Wind directions*, 2007

[10] A.B. Abrahamsen, N. Mijatovic, E. Seiler, V. Zermeno, M.P. Sorensen, P.B. Norgard, N.F. Pedersen, J.C. Grivel, J. Ostergard, N.H. Andersen: “Superconducting wind turbine generators”, *Supercond. Sci. Technol.*, vol. 23, p.034019, 2010

[11] G. Snitchler, B. Gamble, C. King, and P. Winn, “10 MW Class Superconductor Wind Turbine Generators”, *IEEE Trans. on Applied Supercondcuctivity*, vol. 21, no. 3, pp.1089-1092, June, 2011

[12] juWi -Energy is here-, http://www.juwi.de/fileadmin/user_upload/de/PK_2011/juwi/Hintergrund%20Repowering%20Schneebergerhof%20E%20126.pdf, 2011 (*in German*)

[13] S. Fukui, J. Ogawa, T. Sato, O. Tsukamoto, N. Kashima, and S. Nagaya, “Study of 10 MW-Class Wind Turbine Synchronous Generators with HTS Field Windings”, *IEEE Trans. on Applied Supercondcuctivity*, vol. 21, no. 3, pp.1151-1154, June, 2011

[14] H.-J. Sung, G.-H. Kim, K.-M. Kim, M. Park, I.-K. Yu, Y.-G. Kim, H. Lee, “Conceptual design of a 10 MW class superconducting wind power generator considering weight issue”, 2012 Applied Superconductivity Conference (ASC2012), Portland, U.S.A., October, 2012

[15] 牧直樹, 篠原信行, 和泉充, “風力用突極型HTS発電機の電気設計検討”, 低温工学, 第47巻, 6号, pp.392-397, 2012年6月
N. Maki, N. Shinohara and M. Izumi, “Electrical Design Study of Salient-pole HTS Generators for Wind Power Systems”, *TEION KOGAKU*, vol. 47, No. 6, pp.392-397, June, 2012 (*in Japanese*)

[16] 牧直樹, 和泉充, “風力用突極型HTS発電機の電気性能とコスト検討”, 平成24年電気学会産業応用部門大会論文集, pp. III349-III354, 千葉, 2012年8月
N. Maki, N. Shinohara and M. Izumi, “Electrical Performance and Cost Study of Salient-pole HTS Generators for Wind Power Systems”, *Proceedings in 2012 IEEJ Industry Application Society Conference (JIASC2012)*, pp. III349-III354, Chiba, August, 2012 (*in Japanese*)

[17] Ruben Fair, “Superconductivity for Large Scale Wind Turbines”, DOE Report, DE-EE0005143, April, 2012

[18] 熊倉浩明, 許子萬, 戸叶一正, 松本明善, 和田仁, 木村薫, “拡散法による7芯MgB_2線材の作製とその超伝導特性”, 日本金属学会誌, 第74巻,7号, pp.439-443, 2010年
H. Kumakura, J. M. Hur, K. Togano, A. Matsumoto, H. Wada and K. Kimura, “Fabrication and Superconducting Properties of Diffusion Processed 7-Core MgB2 Wires”, *J. Japan Inst. Metals*, vol. 74, No. 7, pp.439-443, 2010 (*in Japanese*)

[19] Siemens, http://www.energy.siemens.com/hq/pool/hq/power-generation/renewables/wind-power/6_MW_Brochure_Jan.2012.pdf

[20] D.W. Hazelton, "2G HTS Applications Developments," Symposium on Superconducting Devices for Wind Energy, Barcelona, Spain, February, 2011.

[21] K Togano, J. Hur, A. Matsumoto, and H. Kumakura, "Microstructures and critical currents of single- and multi-filamentary MgB_2 superconducting wires fabricated by an internal Mg diffusion process", *Supercond. Sci. Technol.*,vol. 23, p.085002, 2010

[22] H. Li, Z. Chen, and H. Polinder, "Optimization of Multibrid Permanent-Magnet Wind Generator Systems", *IEEE Trans. on Energy Conversion*, vol. 24, no. 1, pp.82-92, March, 2009

[23] K. Sawatari, K. Sano and S. Shigeru, "Stator Frame Deformation Problem in Large Diameter Hydro-Generators", *IEEE Trans. on Energy Conversion*, EC-1, no. 1, pp.33-38, 1986

[24] K. Thorburn and M. Leijon, "Case study of upgrading potential for a small hydro power station", *Renewable Energy*, vol. 30, no. 7, pp. 1091-1099, 2005

[25] 猪狩武尚, 電気機械理論, p. 171, コロナ社, 1977

[26] JFE Steel Corporation, http://www.jfe-steel.co.jp/en/index.html

[27] C. P. Bean, "Magnetization of hard superconductors", *Phys. Rev. Lett.*, Vol. 8, pp. 250-253, 1962

[28] W. J. Carr, Jr., "AC Loss and Macroscopic Theory of Superconductors" Second Edition, *Taylor & Francis*, 2001

[29] Sumitomo Heavy Industries, Ltd., http://www.shicryogenics.com/

[30] S. Fukui, T. Kawai, M. Takahashi, J. Ogawa, T. Oka, T. Sato, O. Tsukamoto, “Numerical Study of Optimization Design of High Temperature Superconducting Field Winding in 20 MW Synchronous Motor for Ship Propulsion”, *IEEE Trans. on Applied Supercondcuctivity*, vol. 22, Issue. 3, p.5200504, June, 2012

Publication Lists

1. Journal Papers
Articles related to this thesis are 1-1 and 1-2.

1-1. **Y. Terao**, M. Sekino and H. Ohsaki: "Comparison of Conventional and Superconducting Generator Concepts for Offshore Wind Turbines", IEEE Transaction on Applied Superconductivity, to be published in 2013

1-2. **Y. Terao**, M. Sekino and H. Ohsaki: "Electromagnetic Design of 10 MW class Fully Superconducting Wind Turbine Generators", IEEE Transaction on Applied Superconductivity, Vol.22, Issue.3, Page(s) 5201904, 2012

1-3. **Y. Terao**, M. Sekino, H. Ohsaki, H. Teshima, and M. Morita: "Magnetic Shielding Characteristics of Multiple Bulk Superconductors for Higher Field Applications", IEEE Transaction on Applied Superconductivity, Vol.21, Issue.3, pp.1584-1587, 2011

1-4. H. Ohsaki, **Y. Terao**, and M. Sekino: "Wind Turbine Generators using Superconducting Coils and Bulks", IOP Publishing, Journal of Physics Conference Series, 234 032043, 2010

2. Conferences
2-1. International Conferences
Conferences related to this thesis are 2-1-a, 2-1-c and 2-1-f.

2-1-a. **Y. Terao**, M. Sekino and H. Ohsaki: "Comparison of Conventional and Superconducting Generator Concepts for Offshore Wind Turbines", 2012 Applied Superconductivity Conference (ASC 2012), Portland, U.S.A., October, 4LPG-08, 2012

2-1-b. H. Ohsaki, N. Okajima, **Y. Terao**, M. Sekino, H. Ohsaki, H. Teshima and M. Morita: "Magnetization characteristics of 140 mm diameter single-grained Gd-Ba-Cu-O bulk superconductors", 2012 Applied Superconductivity Conference (ASC 2012), Portland, U.S.A., October, 2MPN-03, 2012

2-1-c. **Y. Terao**, M. Sekino and H. Ohsaki: "Short-circuit characteristic analysis of 10 MW class superconducting wind turbine generators", 24th International Cryogenic Engineering Conference-International Cryogenic Materials Conference 2012 (ICEC 24-ICMC 2012), Fukuoka, Japan, May, 17P-P07-04, 2012

2-1-d. H. Teshima, M. Morita, N. Okajima, **Y. Terao**, M. Sekino, H. Ohsaki, A. Murakami: "Pr operties of Large Single-grained RE-Ba-Cu-O Bulk Superconductors 150 mm in diame ter fabricated using RE compositional gradient technique", 24th International Cryogenic Engineering Conference-International Cryogenic Materials Conference 2012 (ICEC 24-ICMC 2012), Fukuoka, Japan, May, 16P-P10-04, 2012

2-1-e. **Y. Terao**, N. Okajima, M. Sekino, H. Ohsaki, H. Teshima and M. Morita: "Magnetization Characteristics of Multiple Bulk Superconductors for Higher Field Applications", Superconductivity Centennial Conference (EUCAS-ISEC-ICMC 2011), Den Haag, Holland, September, A462, 2011

2-1-f. **Y. Terao**, M. Sekino and H. Ohsaki: "Electromagnetic Design of 10 MW class Fully Superconducting Wind Turbine Generators", International Conference on Magnet Technology (MT-22), Marseille, France, September, 4EP2-3, 2011

2-1-g. H. Ohsaki, **Y. Terao**, Rashidul M. Quddes and M. Sekino: "Electromagnetic Characteristics of 10 MW Class Superconducting Wind Turbine Generators", International Conference on Electrical Machines and Systems 2010 (ICEMS 2010), Incheon, Korea, October, 2010

2-1-h. **Y. Terao**, M. Sekino, H. Ohsaki, H. Teshima and M. Morita: "Magnetic Shielding Characteristics of Multiple Bulk Superconductors for Higher Field Applications", 2010 Applied Superconductivity Conference (ASC 2010), Washington, DC., U.S.A., August, 3LP3A-10, 2010

2-1-i. **Y. Terao**, M. Sekino and H. Ohsaki: "Design Study of Linear Synchronous Motors using Superconducting Coils and Bulks", International Power Electronics Conference (IPEC-Sapporo 2010), Sapporo, Japan, June, 23E2-4, 2010

2-1-j. **Y. Terao**, M. Sekino and H. Ohsaki: "Design Study of High-Thrust Superconducting Linear Motors", the 9th International Symposium on Linear Drives for Industry Applications (LDIA 2009), Incheon, Korea, September, PS3.4, 2009

2-1-k. H. Ohsaki, **Y. Terao** and, M. Sekino: Wind Turbine Generators using Superconducting Coils and Bulks, The 7th European Conference of Applied Superconductivity (EUCAS 2009), Dresden, Germany, September, P-77, 2009

2-1-l. H. Ohsaki, M. Sekino, T. Suzuki and **Y. Terao**: “Design Study of Wind Turbine Generators using Superconducting Coils and Bulks”, 2nd International Conference on Clean Electrical Power (ICCEP), Capri, Italy, June, 2009

2-2. Domestic Conferences

Conferences related to this thesis are 2-2-a and 2-2-c.

2-2-a. **寺尾 悠**, 大崎 博之: “構造の異なる10MW級超電導風力発電機の電磁特性の比較”, 第86回 2012年度秋季低温工学・超電導学会, いわて県民情報交流センター, 岩手県, 1P-p21, 2012年11月

2-2-b. 岡島 直輝, **寺尾 悠**, 関野 正樹, 大崎 博之, 手嶋英一, 森田 充: "大型Gd系バルク超電導体の捕捉磁場特性", 第24 回「電磁力関連のダイナミクス」シンポジウム in 富山（SEAD24 in 富山）, 富山国際会議場, 富山県, 18B2-4, 2012年5月

2-2-c. **寺尾 悠**, 関野 正樹, 大崎 博之: “10MW 級全超電導風力発電機の電磁特性”, 第85回 2011年度秋季低温工学・超電導学会, 金沢歌劇座, 石川県, 2P-p08, 2011年11月

2-2-d. **寺尾 悠**, 関野 正樹, 大崎 博之, 手嶋 英一, 森田 充: “複数積層させたタイル状バルクの着磁特性”, 第84回 2011年度春季低温工学・超電導学会, 物質材料研究機構, 茨城県, 2P-p33, 2011年5月

2-2-e. クッディス・モハンマッド・ラシド, **寺尾 悠**, 関野 正樹, 大崎 博之, 鹿島 直二, 長屋 重夫: “横方向磁束強化形超電導風力発電機の電磁設計”, 電気学会 超電導応用電力機器研究会, 福岡県, ASC-10-30, 2010年6月

2-2-f. **寺尾 悠**, 関野 正樹, 大崎 博之, 手嶋 英一, 森田 充: “高温超電導コイルとバルクを併用した風力発電機の出力特性の解析”, 第81回 2009年度秋季低温工学・超電導学会, 岡山大学, 岡山県, 2P-p30, 2009年11月

2-2-g. 大崎 博之, **寺尾 悠**, 長屋 重夫, 鹿島 直二: “風力発電用横方向磁束強化型超電導発電機の設計と特性解析”, 第81回 2009年度秋季低温工学・超電導学会, 岡山大学, 岡山県, 1B-p09, 2009年11月

2-2-h. 鈴木 達矢, **寺尾 悠**, 関野 正樹, 大崎 博之: “高温超電導コイルとバルク超電導磁気シールド材を併用した界磁を有する同期モータの研究”, 第21回「電磁力関連のダイナミクス」シンポジウム (SEAD21), メルパルク長野, 長野県, 21C1-2, 2009年5月

2-2-i. **寺尾 悠**, 関野 正樹, 大崎 博之: “高温超電導コイルとバルクを併用した界磁を有する風力発電機の検討”, 第80回 2009年度春季低温工学・超電導学会, 早稲田大学, 東京都, 2P-p30, 2009年5月

3. Columns

寺尾 悠, 服部 圭佑, 馬場 旬平: “Y系線材の開発最前線 -国際超電導産業技術研究センター (ISTEC)-”, 電気学会誌, Vol.132, No.5, pp.272-275, 2012

4. Award

2012年 低温工学・超電導学会 優良発表賞
“複 数 積 層 さ せ た タ イ ル 状 バ ル ク超電導体 の 着 磁 特 性”
(Magnetization Characteristics of Arrayed and Stacked Bulk Superconductors)

5. Grants

日本学術振興会特別研究員(DC2), 2012年4月1日-2013年3月31日

Research Fellow (DC2), Japan Society for the Promotion of Science, 4/1/2012-3/31/2013